Please cite this article in press as: Ma et al., Physical insights into single-component organic photovoltaics, Joule (2026), https://doi.org/10.1016/j.joule.2026.102397

Joule

CellPress

Review

Physical insights into single-component organic photovoltaics

Wenzhi Ma,[1,3] Liming Liu,[1,3] Jason A. Röhr,[2] Weitang Li,[1] Jun Zhu,[1] Zhigang Shuai,[1] and Jun Yan[1,*]
[1]Guangdong Basic Research Center of Excellence for Aggregate Science, School of Science and Engineering, The Chinese University of Hong Kong (Shenzhen), Longgang, Shenzhen 518172, Guangdong, P.R. China
[2]General Engineering, Tandon School of Engineering, New York University, Brooklyn, NY 11201, USA
[3]These authors contributed equally
*Correspondence: yanjun@cuhk.edu.cn
https://doi.org/10.1016/j.joule.2026.102397

CONTEXT & SCALE Organic photovoltaics provide a promising solution for solar energy harvesting. High-efficiency devices typically rely on a bulk-heterojunction architecture where donor and acceptor materials are physically blended. While yielding high performance, these blends are thermodynamically prone to degradation upon exposure to thermal and light stress. Single-component organic photovoltaics (SC-OPVs) address this instability by covalently bonding the donor and acceptor units within a single macromolecule. This integration restricts macroscopic phase separation and delivers exceptional morphological stability.
Despite superior stability, SC-OPVs exhibit lower power conversion efficiencies (PCEs) than blended devices. The covalent linkage alters nanoscale packing and limits the interfacial area required for exciton dissociation. As a result, these devices often face severe recombination losses and imbalanced charge transport. Overcoming this performance gap requires a deep understanding of photophysical bottlenecks, specifically how bound charge transfer states split into free carriers within a single-material range.
This review extracts and analyzes the key physical parameters governing exciton and charge dynamics across these systems. By diagnosing the mechanistic origins of efficiency loss, we identify targeted molecular design and morphological control strategies. Transitioning to physics-driven design allows researchers to optimize molecular conformation and transport networks. Overcoming these kinetic barriers will position SC-OPVs as a stable and efficient pathway to the commercialization of organic photovoltaics.

SUMMARY

Single-component organic photovoltaics (SC-OPVs) offer an innovative approach to the traditional bulk-heterojunction organic photovoltaics (BHJ-OPVs) by chemically bonding the donor and acceptor materials within a single molecule. This approach has the potential not only to reduce the manufacturing costs but also to stabilize the photoactive layer against common morphological degradation processes typically observed in BHJ-OPVs. However, SC-OPVs exhibit lower power conversion efficiencies (PCEs) compared with their BHJ counterparts, primarily due to suboptimal exciton splitting and charge-transport dynamics that have not been extensively discussed in the literature. This review aims to provide physical insights into these loss mechanisms, discuss the underlying scientific challenges, and finally propose suggestions that could potentially elevate the performance of SC-OPVs to meet or exceed that of BHJ-OPVs.

INTRODUCTION

Organic photovoltaics (OPVs) are promising contenders for the advancement of photovoltaic (PV) technologies. They offer potential for a range of applications, such as powering Internet of Things (IoT) devices with indoor light sources, integrating solar functionality into windows, and enhancing the sustainability of greenhouses.[1,2] Furthermore, OPVs are flexible and lightweight, which could unlock unprecedented opportunities for their incorporation into a myriad of portable and wearable devices and the development of electronic skin technologies.[3–6]

The operation of OPVs requires an external driving force to facilitate charge generation, a critical step toward solar energy-to-electricity conversion. This is primarily due to the small dielectric constant of organic semiconductors (typically 3–4); therefore, photogenerated excitons (known as Frenkel excitons) have large binding energies (several hundreds of milli-electron volts [meVs]) and cannot be easily separated at room

Please cite this article in press as: Ma et al., Physical insights into single-component organic photovoltaics, Joule (2026), https://doi.org/10.1016/j.joule.2026.102397

temperature.[7] To facilitate the separation of Frenkel excitons, the "bulk-heterojunction" (BHJ) approach, characterized by the physical blending of electron donors and acceptors (pi-conjugated molecules and/or polymer materials) within photoactive layers, was proposed, providing a driving force for exciton dissociation at donor-acceptor (D-A) interfaces with maximized interfacial area.[8,9] This methodology has become integral in the OPV field, setting a precedent for the design and fabrication of high-efficiency OPV devices.[10–13] The introduction and refinement of fused-ring electron acceptors (FREAs) (non-fullerene acceptor [NFAs]) have been pivotal in this context, propelling the power conversion efficiency (PCE) of BHJ-based OPVs (BHJ-OPVs) to surpass the 20% mark,[14–16] a feat that was once deemed unattainable.

Despite these advancements, BHJ-OPVs exhibit inherent vulnerability to degradation when subjected to thermal and light stressors, raising concerns regarding their long-term stability.[17] Over time, a transition toward self-aggregated domains occurs, which is thermodynamically favorable, leading to large-scale domains that hinder charge separation and transport.[18,19] In response to this challenge, the concept of "single-component organic photovoltaics" (SC-OPVs) has been brought back to the community's attention. This approach involves the covalent integration of donor and acceptor units, a strategy that has shown potential in enhancing the photo- and thermal-stability of SC-OPVs compared with their BHJ counterparts, thereby potentially reducing the rate of PV performance degradation.[20–23] While SC-OPVs present a promising candidate for maintaining stability, it is important to recognize that they are among several viable options being explored in this evolving field.[24,25]

Alongside SC-OPVs, several OPV architectures that target improved morphological stability have progressed rapidly in recent years. In layer-by-layer processed devices, the active layer is formed by sequential deposition of donor and acceptor films, and controlled interlayer diffusion can be used to tune intermixing at the interface while maintaining a vertically graded composition that supports charge generation and collection.[15,26,27] Homojunction OPVs take a different route, aiming to generate and separate charges within a single semiconductor by leveraging internal electrostatic or energetic gradients that can arise from controlled molecular orientation and packing.[28] SC-OPVs share similar stability motivation, but they are distinguished by integrating donor and acceptor moieties within one material, which can suppress macroscopic demixing while still allowing nanoscale organization that enables continuous transport pathways.

The initial exploration of SC-OPVs involved the use of a single chromophore (pristine donor or acceptor materials), which lacked the intricate intramolecular heterojunction structures necessary for efficient exciton dissociation, resulting in PCEs falling below the 0.1% threshold.[29] The adoption of the BHJ concept within single-component (SC) conjugated materials marked a significant step forward. By covalently linking electron-accepting and electron-withdrawing groups, researchers have developed materials featuring intramolecular heterojunction structures, such as small molecular (SM) materials, di-block copolymers (BCPs) (or called block copolymers), and double-cable polymers (DCPs). These materials are engineered for high-performance SC-OPVs, representing a leap forward in the quest for efficient and stable OPV technologies. Recent research demonstrates that the PCE of SC-OPVs is approaching 15%, showing their great promise.[30,31]

Despite substantial advancements over the past two decades, the pace of development and performance optimization of SC-OPVs has not kept up with the progress observed in BHJ-OPVs. This lag can be attributed to the incomplete understanding and exploration of the mechanisms behind exciton and charge-carrier dynamics in SC-OPVs. This review aims to first present an overview of recent developments in terms of structure design and performance; secondly, discuss the advantages in terms of photostability, thermal stability, and industrial viability; thirdly and most importantly, provide physical insights into the exciton and charge-carrier dynamics and discuss the main challenges currently facing SC-OPVs, including charge generation, recombination and energy loss, and charge transport; and finally, discuss possible methods to address those challenges, hoping to foster further advancements in SC-OPVs.

MATERIALS CATEGORY

In SC-OPVs, the structure of active materials is typically classified into SM and polymeric domains depending on their conjugation length. Within this classification, DCPs, along with molecular dyads and triads, align with the BHJ model. This model is characterized by inter-domain (through space) charge generation, as depicted in Figure 1A. Conversely, BCPs and homojunction (HJ) small molecules adhere to an HJ model, demonstrating intra-chain charge generation.[20,23,72–74] BHJ and HJ types are among the most studied structures in SC-OPVs.

Here, "BHJ model" refers to a charge generation pathway within SC systems and should not be conflated with conventional BHJ devices fabricated from physically blended donor and acceptor materials. For context, morphology development in conventional BHJ blends is briefly summarized below before returning to the constraints imposed by covalent D-A tethering in SC-OPVs. In BHJ OPVs, donor and acceptor exist as separate components, so film formation is largely governed by miscibility, phase separation during drying, and post treatments that often yield kinetically trapped mixed morphologies. These structures can later evolve through domain growth, reducing D-A interfacial area and weakening percolation pathways for charge extraction.[75] By contrast, SC-OPVs impose covalent connectivity between donor and acceptor segments, which constrains macroscopic demixing but still permits nanoscale organization through self-assembly and segment-specific packing.[46,49,76]

Early research on SC-OPVs started with SC chromophores, such as anthracene and copper phthalocyanine, but their limited efficiency in exciton dissociation and charge generation curtailed their potentials.[77–79] This preliminary observation sets the stage for a transition toward covalently linked D-A motifs, embracing the concept of intramolecular heterojunctions. This evolution signifies a paradigm shift from pristine donor or acceptor materials to more sophisticated D-A structures capable of efficient charge generation.

DCPs are distinguished by their unique architecture, featuring a polymeric donor backbone adorned with molecular

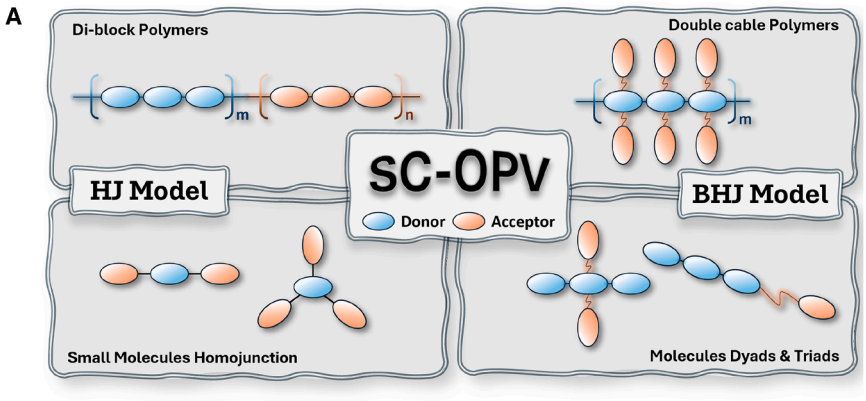

Figure 1. Structural schematic diagram of SC-OPVs and SC- and BHJ-OPVs efficiency development

(A) Diagrammatic representation of structural concepts based on SC-OPVs: double-cable (side-chain) polymers, di-block (in-chain) copolymers, and small molecules from the BHJ model and the HJ model.

(B) Efficiency evolution as a function of time (in years) for different types of OPV technologies. Data are collected from Tables 1, 2, 3, 4, and 5, and the certified PCEs of single-junction BHJ-OPVs were obtained from National Renewable Energy Laboratory (NREL).[71]

acceptor segments as lateral chains. This configuration facilitates dual-channel charge transport, which is paramount in enhancing the efficiency of SC-OPVs by mitigating bimolecular recombination.[80–82] Nonetheless, the intricacies of achieving optimal nanoscale separation and ambipolar charge transport in these polymers need to be considered, highlighting the criticality of the linker length between donor and acceptor components in modulating their excitonic, optical, and electronic properties.

In parallel, BCPs, which consist of donor and acceptor blocks along the same backbone, are notable for their ability to self-assemble into ordered, nanophase-separated structures that create continuous pathways for charge transport. Their synthesis and modification flexibility make them attractive for SC-OPV applications, as evidenced by a notable PCE of 14.89% in a BCP-based SC-OPV.[31] However, the limited variety of available polymer fragments for synthesis is a drawback, which highlights the need to expand the range of donor blocks and acceptor units to improve PV efficiency. In addition, the synthetic complexity is high, and challenges remain when it comes to the exact characterization of BCP structures, which is a common but major criticism of BCPs.[83]

In the realm of D-A SM architectures, analogous to polymeric structures, a bifurcation exists, delineating these entities into in-chain and side-chain variants. Within the in-chain classification, donor moieties are covalently bonded to acceptor units via extended conjugation, exemplified by fullerenes (C_{60}) and perylene bisimides (PBI).[50,70] The direct conjugation method often leads to poor phase segregation and reduced charge-transport efficiency. By contrast, the side-chain approach connects donor and acceptor domains using flexible and electrically insulating alkyl chains.[20,84] This configuration improves PV performance and enhances the structural stability of the devices.[85] Research highlights the importance of the physicochemical properties and dimensions of these flexible linkages in controlling nanoscale phase separation between donor and acceptor components, which is crucial for optimizing the functional performance of these materials.[20,84] However, significantly less attention has been drawn to small molecule-based SC materials, partially due to their poor efficiencies.[73]

Having defined the main SC-OPV material classes and their D-A connectivities, we note that BHJ-like SC-OPVs rely on donor-rich and acceptor-rich networks that simultaneously provide internal interfaces for charge generation and continuous pathways for charge extraction, whereas HJ-type architectures can generate charges at internal junctions that arise from sequence, packing, or orientation variations within a single material. We therefore move on in "PV performance" to show how these structural constraints set the balance between charge generation, charge collection, and recombination and how this balance ultimately determines short-circuit current density (J_{SC}), open-circuit voltage (V_{OC}), fill factor (FF), and PCE in SC-OPVs.

Please cite this article in press as: Ma et al., Physical insights into single-component organic photovoltaics, Joule (2026), https://doi.org/10.1016/j.joule.2026.102397

Table 1. PV performance of double-cable polymer-based SC-OPVs

No.	Year	AL	V_{oc} (V)	J_{SC} (mA · cm^{-2})	FF(%)	Bandgap (eV)	μ_h (cm^{2}s^{-1}V^{-1})	μ_e (cm^{2}s^{-1}V^{-1})	Energy loss (eV)	EQE_{max}	PCE (%)	Ref
1	2017	***BHJ_DC_1a***	0.55	3.12	30	1.45	–	–	0.9	0.12	0.51	Lai et al.[32]
2	2019	***BHJ_DC_6a***	0.74	2.28	39	1.39	1.09×10^{-3}	–	0.65	0.19	0.59	Liang et al.[33]
3	2018	***BHJ_DC_5c***	0.92	3.14	33	1.89	8.67×10^{-9}	6.94×10^{-8}	0.97	0.25	0.95	Yang et al.[34]
4	2017	***BHJ_DC_2***	0.74	4.26	33	1.47	3.40×10^{-2}	–	0.73	0.19	1.04	Li et al.[35]
5	2017	***BHJ_DC_1b***	0.57	7.03	41	1.41	–	–	0.84	0.27	1.64	Lai et al.[32]
6	2019	***BHJ_DC_6b***	0.63	6.14	43	1.45	1.54×10^{-3}	–	0.82	0.14	1.69	Liang et al.[33]
7	2019	***BHJ_DC_7***	0.74	6.54	36	1.93	1.16×10^{-5}	1.17×10^{-6}	1.19	0.45	1.72	Liang et al.[36]
8	2018	***BHJ_DC_5a***	1.01	5.76	33	1.89	1.08×10^{-7}	1.10×10^{-8}	0.88	0.40	1.92	Yang et al.[34]
9	2018	***BHJ_DC_5b***	0.94	5.86	37	1.89	4.36×10^{-9}	4.48×10^{-7}	0.95	0.43	2.01	Yang et al.[34]
10	2019	***BHJ_DC_6c***	0.60	8.03	44	1.42	7.85×10^{-3}	–	0.82	0.07	2.12	Liang et al.[33]
11	2017	***BHJ_DC_1c***	0.69	8.71	43	1.41	5.30×10^{-4}	2.10×10^{-6}	0.72	0.35	2.66	Lai et al.[32]
12	2017	***BHJ_DC_3a***	0.69	7.54	53	2.10	–	–	1.41	0.64	2.73	Feng et al.[37]
13	2019	***BHJ_DC_10a***	0.59	7.77	60	1.88	–	–	1.29	0.48	2.75	Lanzi and Pierini[38]
14	2019	***BHJ_DC_10c***	0.60	8.86	62	1.89	–	–	1.29	0.58	3.35	Lanzi and Pierini[38]
15	2019	***BHJ_DC_8***	0.80	9.32	46	1.81	1.40×10^{-2}	4.20×10^{-5}	1.01	0.51	3.43	Li et al.[39]
16	2017	***BHJ_DC_3b***	0.78	8.05	57	2.08	–	–	1.30	0.67	3.60	Feng et al.[37]
17	2022	***BHJ_DC_15a***	0.85	11.94	39	1.44	5.10×10^{-5}	1.10×10^{-4}	0.59	0.52	3.98	Liang et al.[40]
18	2019	***BHJ_DC_10b***	0.62	9.91	65	1.87	–	–	1.25	0.63	4.05	Lanzi and Pierini[38]
19	2017	***BHJ_DC_3c***	0.92	7.60	60	2.08	8.20×10^{-5}	2.40×10^{-6}	1.16	0.66	4.18	Feng et al.[37]
20	2019	***BHJ_DC_11a***	0.63	12.1	65	2.04	–	–	1.41	0.59	4.20	Lanzi et al.[41]
21	2019	***BHJ_DC_9***	1.05	8.31	50	1.90	1.47×10^{-4}	7.11×10^{-6}	0.85	0.63	4.34	Yang et al.[42]
22	2020	***BHJ_DC_14a***	1.00	8.20	62	1.87	1.00×10^{-3}	2.30×10^{-5}	0.87	0.55	5.06	Jiang et al.[43]
23	2017	***BHJ_DC_4***	0.68	13.30	62	–	8.40×10^{-4}	–	–	0.61	5.58	Pierini et al.[44]
24	2019	***BHJ_DC_11b***	0.68	13.50	71	1.83	–	–	1.15	0.68	5.80	Lanzi et al.[41]
25	2020	***BHJ_DC_13***	0.84	12.68	58	1.77	2.70×10^{-2}	2.10×10^{-5}	0.93	0.63	6.25	Yu et al.[45]
26	2019	***BHJ_DC_12***	0.90	10.80	65	1.84	2.60×10^{-1}	2.10×10^{-4}	0.94	0.67	6.30	Feng et al.[46]
27	2020	***BHJ_DC_14b***	0.94	12.81	69	1.85	2.70×10^{-4}	2.70×10^{-4}	0.91	0.76	8.40	Jiang et al.[43]
28	2023	***BHJ_DC_16A***	0.775	20.04	60	–	–	–	–	0.79	9.36	Zhang et al.[47]
29	2023	***BHJ_DC_16B***	0.812	19.08	63	–	–	–	–	0.77	9.77	Zhang et al.[47]
30	2022	***BHJ_DC_15b***	0.77	21.23	62	1.44	1.80×10^{-3}	9.90×10^{-4}	0.67	0.79	10.09	Liang et al.[40]
31	2023	***BHJ_DC_17***	0.90	22.24	65	1.43	4.79×10^{-3}	3.01×10^{-3}	0.53	0.80	13.02	Liang et al.[48]
32	2024	***BHJ_DC_18***	0.911	23.04	66	1.53	–	–	–	0.80	13.85	Li et al.[49]

PV PERFORMANCE

Figure 1B shows the PCE development as a function of time over the last two decades for SC-OPVs in comparison to BHJ-OPVs in single-junction configurations. The detailed parameters are listed in Tables 1, 2, 3, 4, and 5, containing V_{OC}, J_{SC}, FF, maximum external quantum efficiency (EQE_{max}), optical band gap (E_g), electron and hole mobilities (μ_e and μ_h), and PCE, which is determined via $PCE = \frac{V_{OC} J_{SC} FF}{P_{in}}$, where P_{in} is the incident power density. Among these parameters, J_{SC}, the short current density, represents the capacity to convert absorbed photons into electric charges.[86] V_{OC} is the open-circuit voltage, and the difference between the E_g and V_{OC} represents the voltage losses.[87] FF is the result of the competition between charge transport and recombination.[88,89] Additionally, four types of chemical structures matching to Tables 1, 2, 3, and 4 are provided in Schemes 1, 2, and 3. In less than 20 years, the PCE of SC-OPVs has increased by approximately two orders of magnitude (from 0.07% in 2006 to 14.89% in 2024; ≈2.1 × 10^4% increase), as summarized in Tables 1, 2, 3, and 4.[90] This remarkable progress is detailed in the development of SC-OPVs across four different systems. We note that we renamed all molecules for better presentations, and the full names can be found in Table S1.

Initially, research in double-cable polymer-based SC-OPVs (DCP-OPVs) employed fullerene and its derivatives as acceptors, much like the development seen in BHJ-OPVs. Notable examples include **BHJ_DC_4**, **BHJ_DC_10ABC**, and **BHJ_DC_**

Please cite this article in press as: Ma et al., Physical insights into single-component organic photovoltaics, Joule (2026), https://doi.org/10.1016/j.joule.2026.102397

Table 2. PV performance of di-block copolymer-based SC-OPVs

No.	Year	AL	V_{oc} (V)	J_{SC} (mA · cm^{-2})	FF (%)	Bandgap (eV)	μ_h (cm^{2}s^{-1}V^{-1})	μ_e (cm^{2}s^{-1}V^{-1})	Energy loss (eV)	EQE_{max}	PCE (%)	Ref
1	2006	***HJ_DB_1***	0.865	0.19	–	–	–	–	–	0.31	0.07	Narayanaswamy et al.[50]
2	2017	***HJ_DB_2a***	0.79	1.30	35	1.70	–	–	0.91	0.11	0.36	Lee et al.[51]
3	2017	***HJ_DB_3a***	0.46	5.25	51	–	–	–	–	0.40	1.23	Chen et al.[52]
4	2017	***HJ_DB_3b***	0.51	5.02	59	–	–	–	–	0.40	1.52	Chen et al.[52]
5	2017	***HJ_DB_2b***	0.79	4.04	48	1.69	–	–	0.90	0.26	1.54	Lee et al.[51]
6	2013	***HJ_DB_5***	1.22	5.30	47	2.00	–	–	0.78	0.31	3.10	Guo et al.[53]
7	2018	***HJ_DB_6***	0.93	8.26	50	1.80	–	–	0.87	0.51	3.87	Lee et al.[54]
8	2021	***HJ_DB_7a***	0.86	9.76	49	1.55	2.30×10^{-4}	2.00×10^{-4}	0.69	0.40	4.20	Li et al.[55]
9	2020	***HJ_DB_9***	0.89	10.76	65	1.58	5.33×10^{-6}	4.87×10^{-6}	0.69	0.60	6.22	Kwon et al.[56]
10	2020	***HJ_DB_10***	0.85	12.21	62	1.48	2.86×10^{-5}	2.51×10^{-5}	0.63	0.55	6.43	Park et al.[57]
11	2021	***HJ_DB_7b***	0.89	15.42	63	1.43	3.50×10^{-4}	2.50×10^{-4}	0.54	0.60	8.64	Li et al.[55]
12	2023	***HJ_DB_11a***	0.95	18.79	52	1.39	1.93×10^{-4}	5.90×10^{-4}	0.44	0.69	9.34	Liu et al.[58]
13	2022	***HJ_DB_12***	0.94	18.68	60	1.48	1.00×10^{-4}	7.00×10^{-5}	0.54	0.70	10.55	Phan et al.[59]
14	2021	***HJ_DB_8***	0.914	19.25	63	1.49	2.69×10^{-4}	1.51×10^{-4}	0.58	0.70	11.32	Wu et al.[60]
15	2023	***HJ_DB_11b***	0.95	17.62	70	1.38	3.58×10^{-4}	2.29×10^{-4}	0.43	0.62	11.78	Liu et al.[58]
16	2022	***HJ_DB_13***	0.895	20.57	68	–	3.64×10^{-4}	3.28×10^{-4}	–	0.75	12.60	Guo et al.[61]
17	2022	***HJ_DB_14***	0.92	21.87	66	1.422	4.33×10^{-4}	4.24×10^{-4}	0.502	0.69	13.28	Yang et al.[62]
18	2023	***HJ_DB_15***	0.957	20.95	67	1.45	1.95×10^{-4}	1.53×10^{-4}	0.493	0.77	13.40	Cheng et al.[22]
19	2022	***HJ_DB_16***	0.926	22.61	71	1.45	4.60×10^{-4}	2.90×10^{-4}	0.524	0.75	14.88	Wu et al.[30]
20	2024	***HJ_DB_17***	0.944	23.27	68	1.453	2.67×10^{-3}	2.57×10^{-3}	0.509	0.80	14.89	Cheng et al.[31]
21	2024	***HJ_DB_18***	0.888	23.84	71	1.59	4.8×10^{-4}	2.8×10^{-4}	–	0.85	15.02	Li et al.[63]

11AB, which demonstrated commendable performance (PCE ~5%) compared with contemporaneous NFA-based DCP-OPVs.[38,41,44] Fullerene acceptors offered several advantages. In particular, a triply degenerate lowest unoccupied molecular orbital (LUMO) can accommodate more electrons compared with a non-degenerate LUMO. This increases the electron-accepting capacity of the fullerene. Meanwhile, high electronegativity and electron affinity, isotropic electron transport, and a rigid molecular backbone could facilitate exciton separation and charge transfer (CT).[91] However, drawbacks such as high costs, complex purification processes, limited energy level tunability, low light absorption in a relatively insufficient wavelength range, and challenging chemical modifications led researchers to explore alternative materials.[92]

As researchers shifted focus toward NFAs, perylene diimide (PDI) emerged as a popular choice due to its excellent electron mobility, tunable LUMO level, and broad visible spectrum absorption.[93] Between 2017 and 2020, PDI-based DCP-OPVs achieved efficiencies around 6% (e.g., **BHJ_DC_12** and **BHJ_DC_13**). However, PDI tends to form aggregated crystalline domains, leading to excimer formation and exciton trapping.[94] Researchers addressed these issues by modifying PDI's active sites—bay, ortho, and N positions—to induce molecular twists and reduce aggregation. Through these adjustments, the related devices exhibited enhanced performance to varying degrees.[95–97] The discovery of FREAs, like 3,9-bis(2-methylene-(3-(1,1-dicyanomethylene)-indanone))-5,5,11,11-tetrakis(4-hexylphenyl)-dithieno[2,3-d:2',3'-d']-s-indaceno[1,2-b:5,6-b']dithiophene (ITIC) and 2,2'-((2Z,2'Z)-((12,13-bis(2-ethylhexyl)-3,9-diundecyl-12,13-dihydro-[1,2,5]thiadiazolo[3,4-e]thieno[2",3'':4',5']thieno[2',3':4,5]pyrrolo[3,2-g]thieno[2',3':4,5]-thieno[3,2-b]indole-2,10-diyl)bis(methanylylidene))bis(5,6-difluoro-3-oxo-2,3-dihydro-1H-indene-2,1-diylidene))dimalononitrile (Y6), significantly advanced BHJ-OPV efficiencies beyond 20%.[14–16] However, for commercial SC-OPVs aiming for low cost and high stability, FREAs may not be ideal. Thus, attention shifted to non-fused electron acceptors (NFREAs). Post-2022, the adoption of Thieno[3,4-c]pyrrole-4,6-dione (TPD)-based NFREAs replaced PDI, achieving PCEs exceeding 13% in examples such as **BHJ_DC_15AB**, **BHJ_DC_16AB**, and **BHJ_DC_17**.[40,47,48] TPD's crescent-shaped molecular geometry promoted tight molecular packing into a 3D network, simplifying morphological control and leading to efficient charge transport.[98]

BCP-based SC-OPVs (BCP-OPVs) have also made significant strides. Early BCP-OPV efficiencies were notably low—less than 0.1% (**HJ_DB_1**). Even by 2018, efficiencies remained below 5% (**HJ_DB_6**). In 2020, the design by Kwon et al. of **HJ_DB_9** marked a significant breakthrough, with a PCE of 6.22% under AM1.5G and 12.7% under indoor lighting conditions (500 lux), indicating substantial potential for indoor applications.[56] **HJ_DB_9**'s novel structure, $(A_1\text{-}D_1)\text{—}(A_2\text{-}D_2)$, where $(A_1\text{-}D_1)$ forms the donor block and $(A_2\text{-}D_2)$ forms the acceptor block, accelerated subsequent material developments. In 2021, Wu et al. synthesized **HJ_DB_8**, breaking the 11% PCE barrier and reigniting research enthusiasm for SC-OPVs by chemically

Please cite this article in press as: Ma et al., Physical insights into single-component organic photovoltaics, Joule (2026), https://doi.org/10.1016/j.joule.2026.102397

Table 3. PV performance of SC-OPVs based on BHJ model of small molecules

No.	Year	AL	V_{oc} (V)	J_{SC} (mA · cm^{-2})	FF (%)	Bandgap (eV)	μ_h (cm^{2}s^{-1}V^{-1})	μ_e (cm^{2}s^{-1}V^{-1})	Energy loss (eV)	EQE$_{max}$	PCE (%)	Ref
1	2019	***BHJ_SM_1***	0.78	5.05	28	–	2.30×10^{-5}	–	–	0.40	1.11	Labrunie et al.[64]
2	2013	***BHJ_SM_2b***	1.00	4.30	43	–	2.20×10^{-6}	1.50×10^{-5}	–	0.58	1.86	Qu et al.[65]
3	2013	***BHJ_SM_2c***	0.96	4.60	46	–	9.60×10^{-6}	4.60×10^{-6}	–	0.61	2.04	Qu et al.[65]
4	2013	***BHJ_SM_2a***	1.04	4.82	47	–	2.50×10^{-5}	9.10×10^{-6}	–	0.64	2.33	Qu et al.[65]
5	2017	***BHJ_SM_3***	0.97	7.02	36	1.84	1.03×10^{-6}	8.96×10^{-6}	0.87	0.46	2.44	Nguyen et al.[66]
6	2020	***BHJ_SM_4a***	0.80	8.64	41	1.55	–	–	0.75	0.41	2.80	Lucas et al.[67]
7	2019	***BHJ_SM_5***	0.98	7.50	44	1.81	1.78×10^{-3}	1.35×10^{-5}	0.83	0.43	3.22	Wang et al.[68]
8	2020	***BHJ_SM_4b***	0.81	9.94	43	1.54	–	–	0.73	0.40	3.37	Lucas et al.[67]
9	2020	***BHJ_SM_4c***	0.82	11.53	46	1.55	–	–	0.73	0.48	4.26	Lucas et al.[67]

bonding the backbone of PBDB-T and the Y-molecule.[60] Notably, they improved the performance of **HJ_DB_8**-based SC-OPVs using green solvents and adjusted the donor block's conjugation length, pushing the PCE from 11.32% (**HJ_DB_8**) to 12.6% (**HJ_DB_13**) and 13.28% (**HJ_DB_14**), respectively.[60–62] Following Wu's work, the introduction of PM6 as a donor block led to the design of **HJ_DB_16**, achieving a PCE of 14.88%.[30] Incorporating D18 as a donor block in **HJ_DB_15** provided new design insights. Chen et al. employed a "three-in-one strategy" with PM6 as donor block 1, D18 as donor block 2, and PYIT as the acceptor block and achieved precise control over block proportions, leading to enhanced light absorption, morphology control, and stability, and ultimately, one of the highest SC-OPV (**HJ_DB_17**) efficiencies of 14.89% was realized.[31]

On the other hand, small molecule-based SC-OPVs, regardless of whether they use the BHJ or HJ structural models, still show poorer efficiencies than their polymer counterparts and also gain less attention than DCP and BCP polymers. In such a structural design, electron acceptors that are derived from fullerenes have been frequently employed. For instance, in the SM dyad based on the HJ model (**HJ_SM_3**) developed by Singh et al., fullerene and diketopyrrolopyrrole (DPP) derivatives were covalently bonded; however, the fullerene's absorption did not complement **HJ_SM_3**'s absorption spectrum well enough, leading to a low Jsc of 6.71 mA·cm^{-2} and a PCE of 2.17%.[50] In the design of SM BHJ model structures, Woo et al. designed **BHJ_SM_3** by chemically bonding benzodiazepine-rhodanine (BDTRh) and [6,6]-phenyl-C_{61} butyric acid methyl ester (PCBM), leading to a PCE of 2.44% with a relatively low Jsc of 7.02 mA·cm^{-2}.[66] Inefficient charge generation seems to be the main obstacle for SM SC-OPVs, and more research efforts should be put into the design and development of SM materials, aligning with the pace of polymeric counterparts.

Overall, based on the collected data in Tables 1, 2, 3, and 4, the consistently enhanced J_{SC} and FF played a significant role in the recent achievements of SC-OPVs. Meanwhile, as shown in Figures 2A–2D, we perform a comparative analysis of the key performance parameters—J_{SC}, V_{OC}, FF, and PCE—for SC-OPV and BHJ-OPV devices against the Shockley-Queisser (SQ) limit.[99] From the comparison, it is clear that the performance gap is significant between SC-OPVs and BHJ-OPVs, primarily due to suboptimal J_{SC} and FF, which are related to charge generation and collection efficiencies. By evaluating these parameters, the study aims to provide insights into the operation of SC-OPVs in comparison to BHJ-OPVs, as discussed later.

POTENTIAL ADVANTAGES

Stability

The kinetically mixed donor and acceptor components in a BHJ typically lack thermodynamic stability, and unfavorable microstructural changes—phase separation or excessive mixing—may occur under external stresses like heat or light, resulting in microstructure-related performance degradation.[100,101] The creation of SC-OPVs—which, as previously shown, combine chemically bonded donor and acceptor moieties inside a single molecule or polymer—offers an effective solution to this instability

Table 4. PV performance of SC-OPVs based on HJ model of small molecules

No.	Year	AL	V_{oc} (V)	J_{SC} (mA · cm^{-2})	FF (%)	Bandgap (eV)	μ_h (cm^{2}s^{-1}V^{-1})	μ_e (cm^{2}s^{-1}V^{-1})	Energy loss (eV)	EQE$_{max}$	PCE (%)	Ref
1	2020	**HJ_SM_1a**	1.19	3.54	27	1.83	3.00×10^{-5}	3.10×10^{-5}	0.64	0.23	1.13	Mannanov et al.[69]
2	2020	**HJ_SM_1b**	1.08	3.71	27	1.80	–	–	0.72	0.21	1.13	Mannanov et al.[69]
3	2019	**HJ_SM_2a**	0.68	5.62	45	1.49	–	–	0.81	0.31	1.73	Xia et al.[70]
4	2019	**HJ_SM_2b**	0.83	6.08	40	1.47	–	–	0.64	0.30	2.04	Xia et al.[70]
5	2016	**HJ_SM_3**	0.66	6.70	49	1.72	1.30×10^{-4}	1.10×10^{-4}	1.03	0.38	2.17	Narayanaswamy et al.[50]
6	2019	**HJ_SM_2c**	0.73	8.03	43	1.48	–	–	0.75	0.39	2.52	Xia et al.[70]

Please cite this article in press as: Ma et al., Physical insights into single-component organic photovoltaics, Joule (2026), https://doi.org/10.1016/j.joule.2026.102397

Table 5. PV performance of selected single-junction BHJ-OPVs

No.	Year	AL	Bandgap (eV)	Energy loss (eV)	EQE_{max}	μ_h/μ_e	PCE (%)	Ref
1	2020	**PTB7-Th:IOTIC**	1.44	0.56	0.38	–	6.00	Karki et al.[188]
2	2020	**PTB7-Th:IOTIC-2F**	1.36	0.568	0.52	–	7.20	Karki et al.[188]
3	2020	**PE72:Y6**	1.37	0.535	0.60	0.58	9.74	Zhang et al.[189]
4	2020	**PM6:NOIC4**	1.62	0.68	0.68	0.44	10.10	Li et al.[190]
5	2020	**PTB7-Th:IOTIC-4F**	1.34	0.62	0.65	–	10.20	Karki et al.[188]
6	2018	**PffBT2T-TT:O-IDTBR**	1.60	0.55	0.68	–	10.40	Chen et al.[191]
7	2019	**J71:ITC6-IC**	1.67	0.72	0.69	–	10.41	Sun et al.[192]
8	2020	**PM6:NOIC**	1.62	0.73	0.77	1.40	11.40	Li et al.[190]
9	2019	**PBDB-T:IT4F:NMR-1**	1.53	0.76	0.81	–	11.47	Qin et al.[193]
10	2020	**PBDB-T:FOIC**	1.391	0.751	0.79	1.70	11.91	Wang et al.[194]
11	2020	**PE71:Y6**	1.37	0.545	0.70	0.81	12.03	Zhang et al.[189]
12	2019	**PM6:ITCPTC**	1.65	0.7	0.80	–	12.30	Luo et al.[195]
13	2020	**PM6:NOIC1**	1.46	0.6	0.75	0.96	12.50	Li et al.[190]
14	2019	**PM6:IT-4Cl**	1.56	0.76	0.78	–	12.70	Luo et al.[195]
15	2018	**PTB7-Th:IEICO-4F**	1.24	0.62	0.89	0.96	12.80	Song et al.[196]
16	2019	**PM6:IT-4F**	1.60	0.73	0.80	–	12.90	Luo et al.[195]
17	2018	**P2F-Ehp:IT-2F**	1.63	0.74	0.79	2.39	12.96	Fan et al.[197]
18	2017	**PBDB-T-SF:IT-4F**	1.54	0.66	0.83	0.75	13.10	Zhao et al.[198]
19	2018	**PFBDB-T:C8-ITIC**	1.54	0.60	0.86	0.85	13.20	Fei et al.[199]
20	2019	**PBDB-T:DOC2C6-2F**	1.42	0.57	0.78	0.71	13.24	Huang et al.[200]
21	2019	**PBDB-T:Y2**	1.40	0.57	0.74	12.45	13.40	Yuan et al.[201]
22	2019	**PBDB-T:Y1**	1.44	0.57	0.74	5.10	13.42	Yuan et al.[201]
23	2019	**PM6:ITC-2Cl**	1.58	0.67	0.79	–	13.60	Luo et al.[195]
24	2019	**BTR-Cl:Y6**	1.78	0.92	0.79	1.06	13.61	Chen et al.[202]
25	2020	**PBDB-T:H3**	1.31	0.55	0.83	0.80	13.75	He et al.[203]
26	2019	**L2:TTPT-T-4F**	1.576	0.721	0.81	5.04	14.00	Li et al.[204]
27	2020	**PBDB-T:H1**	1.41	0.66	0.82	1.49	14.06	Qin et al.[205]
28	2020	**PM6:NOIC2**	1.57	0.64	0.81	1.00	14.10	Li et al.[190]
29	2021	**PBDB-T:PYTT-2**	1.52	0.61	0.83	1.82	14.32	Wang et al.[206]
30	2019	**ZR1:Y6**	1.38	0.54	0.82	0.33	14.34	Zhou et al.[207]
31	2022	**PM6:BO5Cl**	1.48	0.522	0.79	1.12	15.02	He et al.[208]
32	2020	**PBDB-T:H2**	1.42	0.63	0.82	1.24	15.12	He et al.[203]
33	2020	**PM6:ABP4T-4F**	1.362	0.44	0.79	1.10	15.20	Gao et al.[209]
34	2020	**PM6:BTP-S1**	1.49	0.56	0.81	1.25	15.21	Li et al.[210]
35	2021	**PFBCPZ:IT-4F**	1.57	0.65	0.84	2.08	15.30	Wu et al.[211]
36	2019	**PM6:Y6**	1.42	0.58	0.81	1.67	15.40	Sun et al.[212]
37	2019	**PBDB-TF:BTP-4F**	1.407	0.573	0.84	–	15.60	Cui et al.[213]
38	2019	**PTQ10:Y6**	1.42	0.55	0.80	–	16.21	Sun et al.[214]
39	2020	**PM6:BTP-S2**	1.48	0.53	0.83	1.46	16.37	Li et al.[210]
40	2019	**PM6:BTP-4F-12**	1.40	0.55	0.85	–	16.40	Hong et al.[215]
41	2019	**S1:Y6**	1.41	0.54	0.81	1.58	16.42	Sun et al.[212]
42	2019	**PBDB-TF:BTP-4Cl**	1.4	0.53	0.84	–	16.50	Cui et al.[213]
43	2020	**PM6:BP5T-4F**	1.338	0.45	0.81	–	16.70	Gao et al.[209]
44	2021	**PNTB-2T:Y6**	1.407	0.535	0.83	0.71	16.72	Zhang et al.[216]
45	2021	**PM6:mBzS-4F**	1.25	0.446	0.87	1.28	17.02	Qi et al.[217]
46	2021	**PTQ10:BTP-Ph**	1.36	0.472	0.81	0.55	17.10	Chang et al.[218]
47	2020	**PM6:BP4T-4F**	1.329	0.49	0.83	–	17.10	Gao et al.[209]
48	2021	**PNTB-2T:Y6:PC71BM**	1.407	0.533	0.81	1.52	17.35	Zhang et al.[216]

(*Continued on next page*)

Please cite this article in press as: Ma et al., Physical insights into single-component organic photovoltaics, Joule (2026), https://doi.org/10.1016/j.joule.2026.102397

Table 5. Continued

No.	Year	AL	Bandgap (eV)	Energy loss (eV)	EQE_{max}	μ_h/μ_e	PCE (%)	Ref
49	2022	**PM6:Y6-HU**	1.37	0.50	0.85	1.17	17.40	Abbas et al.[219]
50	2020	**PM6:BTP-4F-12:MeIC**	1.389	0.526	0.8	1.29	17.40	Ma et al.[220]
51	2021	**PTQ10:m-BTP-C6Ph**	1.35	0.467	0.82	0.67	17.70	Chai et al.[221]
52	2021	**PM6:L8-BO**	1.42	0.55	0.85	1.62	18.32	Li et al.[222]
53	2022	**PM6:BO-4Cl:BO-5Cl**	1.37	0.496	0.86	0.51	18.36	He et al.[208]
54	2022	**D18:L8-BO**	1.46	0.542	0.85	1.06	19.05	Zhu et al.[223]
55	2022	**PBQx-TF:eC9-2Cl**	1.411	0.532	0.89	1.06	19.20	Wang et al.[224]
56	2022	**PM6:D18:L8-BO**	1.29	0.394	0.85	0.95	19.60	Zhu et al.[223]
57	2024	**PM6:eC9**	–	–	0.92	0.92	19.70	Yu et al.[225]
58	2024	**PBDB-TF:L8-BO:BTP-eC9**	–	–	0.93	–	20.17	Guan et al.[226]
59	2024	**D18:L8-BO(B6Cl)**	1.42	0.52	0.90	1.10	20.20	Sun et al.[227]
60	2025	**PM6:L8-BO-C4:L8-BO-C4-Br**	1.419	0.541	0.90	1.12	20.42	Li et al.[16]
61	2024	**D18-Cl:BTP-4F-P2EH**	–	–	0.90	1.13	20.80	Zhu et al.[15]
62	2025	**D18-Cl:N3:AT-β2O**	–	–	0.90	1.09	20.82	Chen et al.[14]

problem. Better morphological stability is provided by this chemically bonded structure, which stops the donor and acceptor from freely moving and developing into a large phase separation and unfavorable aggregation. Below, recent progress on photostability, thermal stability, and industrial viability is discussed.

Photostability

The DCP polymer **BHJ_DC_12**, reported by Li et al., exhibited remarkable photostability when used in SC-OPVs.[46] Following 300 h of continuous light exposure (under 1-sun illumination), as shown in Figure 3A, the J_{SC} of SC-OPVs remained nearly unchanged, while there was a minor decrease of 3%–5% in both the FF and the V_{OC}. As a result, there was an overall decline in the PCE of around 7%. This small drop in FF and V_{OC} may be caused by undesirable interfacial layers, such as zinc oxide (ZnO) and/or MoO_3, resulting in increased series resistance and decreased parallel resistance after exposure to light. Therefore, careful selection of interfacial layers is required for maintaining both efficiency and photostability. Building upon this work, Jiang et al. further developed **BHJ_DC_14A** and **BHJ_DC_14B**.[43] The SC-OPVs fabricated from **BHJ_DC_14A** and **BHJ_DC_14B** showed decent photostability in an inert N_2 environment, as depicted in Figures 3B–3E, with **BHJ_DC_14A**-based cells keeping nearly 100% of starting PCEs and **BHJ_DC_12**-based cells displaying around 94% of initial PCEs after 150 h, despite the fact that their PCEs did not match those of **BHJ_DC_12**. The phenomenon can be ascribed to the improved phase separation established between the backbones and the n-type semiconductor units (NDIs). Recently, Li et al. introduced two more novel DCP materials, **BHJ_DC_15A and BHJ_DC_15B**, utilizing distinct side chains (TPDIC), which demonstrated exceptional photostability, with **BHJ_DC_15B**-based SC-OPVs exhibiting mitigated FF loss (94% retention) without burn-in degradation after 1,000 h.[40] Compared with BHJ-mixture cells with a PCE reduction of 34%, the final PCE of **BHJ_DC_15B**-based devices only reduces by 14% as a result of these modifications (Figures 3F and 3G).

BCP polymers have also shown exceptional photostability due to the desired morphology created by the strong self-assembly of BCPs. **HJ_DC_10**, which was developed by Park et al. in 2020, gained recognition due to its utilization of eco-friendly solvents and remarkable morphological stability.[57] Tests conducted on the unencapsulated devices based on **HJ_DC_10**, compared with BHJ-mixture devices, showed that after a maximum storage time of 1,020 h, the **HJ_DC_10**-based solar cell maintained 90.1% of its initial PCE, while the blend-film-based devices only maintained 59.5% of their initial PCE (shown in Figures 4A and 4B). The **HJ_DB_11B** with a (D_1-A_1-A_2-A_3) structure was developed in 2021 by Guo et al.[58] By contrasting **HJ_DB_11B**-based SC-OPVs with BHJ structure cells of similar composition, they demonstrated that, primarily as a result of burn-in degradation of electrodes and interfaces,[55] the **HJ_DB_11B**-based devices showed a minor PCE decrease and retained approximately 90% of original PCEs after 1,000 h of storage in N_2 at three different test conditions, namely, room temperature and dark condition, continuous illumination condition, and 85°C heated condition (as shown in Figures 4C–4E, respectively). Later on, in 2024, Chen et al. employed a "triple-to-one strategy" and synthesized **HJ_DB_17** and achieved one of the highest device performances with a PCE of 14.89%.[31] In terms of maintaining photostability, although all three types of devices (comprising one, two, and three components of organic semiconducting material) exhibited a decrease compared with their initial PCE, SC-OPVs demonstrated superior photostability. Under continuous 1-sun-equivalent white light-emitting diode (LED) illumination for 520 min, SC-OPVs maintained 90.37% of their initial PCE, outperforming the other devices, which retained 87.25% and 87.12% of their initial PCE, respectively. Consequently, the final PCE of **HJ_DB_17** experiences a small reduction and keeps around 90% of the initial PCE (Figures 4F–4H).

Thermal stability

Thermal stability is another important factor to consider, as solar cells are heated when exposed to sunlight. This heat may induce stronger phase separation, leading to phase-segregated donor and acceptor domains, thereby damaging PV performances.

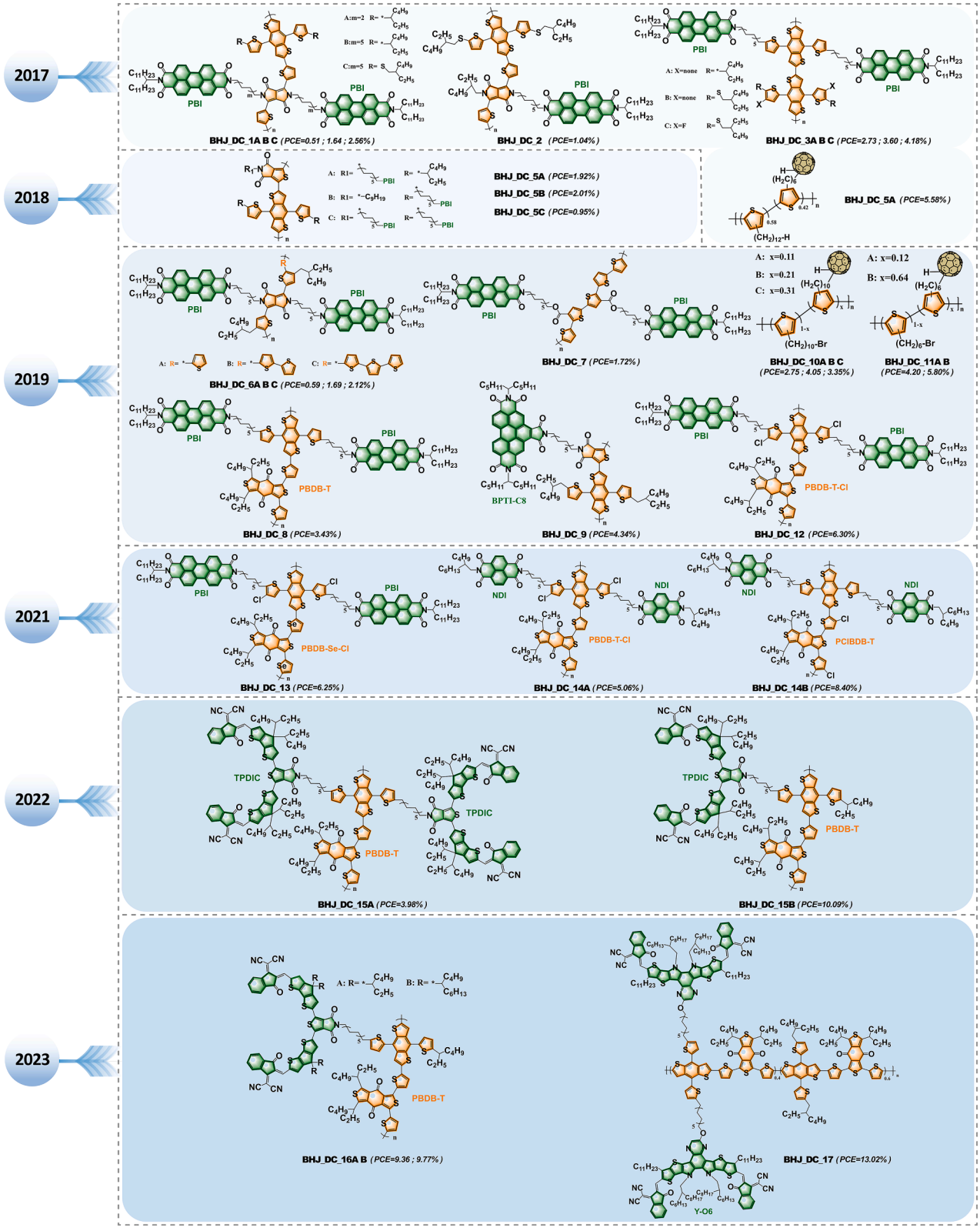

Scheme 1. Chemical structures of double-cable polymer-based SC-OPVs

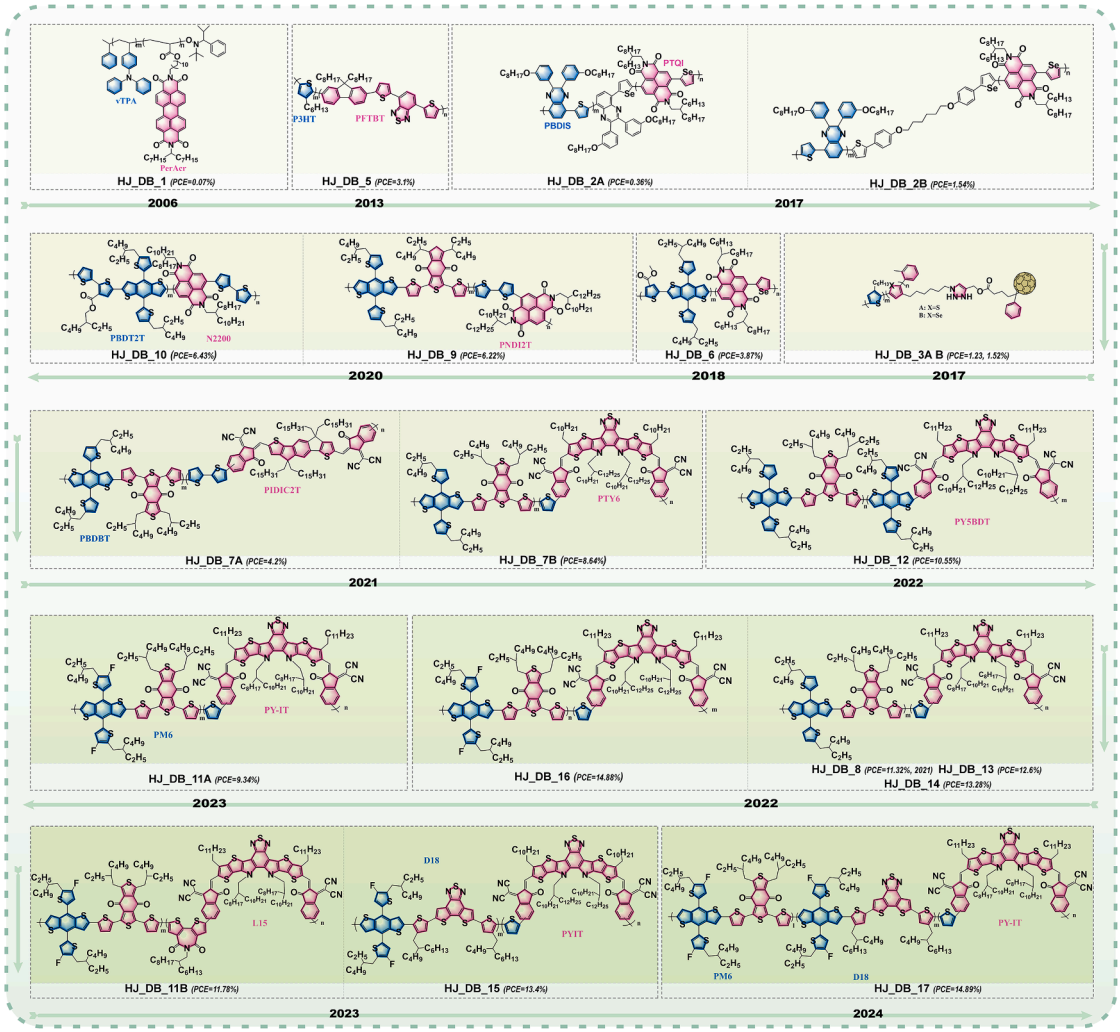

Scheme 2. Chemical structures of di-block copolymer-based SC-OPVs

Meanwhile, heated samples can lead to stronger electron-phonon coupling, since molecular vibration is strongly temperature dependent.[102] Promisingly, SC-OPVs generally demonstrate higher thermal stability in comparison to BHJ-OPVs manufactured from the same donor and acceptor materials. An exemplary example is the **BHJ_DC_17** polymer system, developed by Li and his team in 2023, which exhibited exceptional thermal stability throughout testing.[48] The SC-OPVs, which were based on **BHJ_DC_17**, retained 89% of their initial PCEs after being constantly heated at 85°C for 700 h in N_2. By contrast, BHJ-OPVs utilizing identical material thin films exhibited a mere 70% of their initial PCEs. In addition, the BCP polymer system **HJ_DB_16**, reported by Wu et al., exhibited exceptional thermal stability.[30] Remarkably, their investigation revealed that the thermal durability of SC-OPVs based on **HJ_DB_16** was enhanced even more when a Y6 additive was included. This resulted in a decrease in PCE deterioration from around 11% to roughly 7%. The performance of materials treated with certain additives is noteworthy, and the thermal stability of the device is greatly influenced by compositional ratios and the length of the linkers connecting the acceptor and donor.[38,62]

As discussed in "stability," in SC-OPVs, improved stability is often attributed to chemically bonding donor and acceptor motifs, which restricts D-A demixing and can therefore enhance morphological stability under external stress.[103] However, stability is also configuration dependent because linker length and flexibility, attachment geometry, the donor-to-acceptor block composition, and the size (length) of the side chains collectively determine solid-state packing, local free volume, and the extent of segmental motion that drives nanoscale reorganization during thermal or light exposure.[83] These packing changes directly translate into device responses, most notably mobility balance and recombination kinetics, which in turn govern voltage and FF losses during aging. In support of this link between configuration, packing, and operational stability, thermal annealing-induced ordering in double-cable polymers has been shown to reduce recombination and deliver strong retention of performance under continuous illumination.[46]

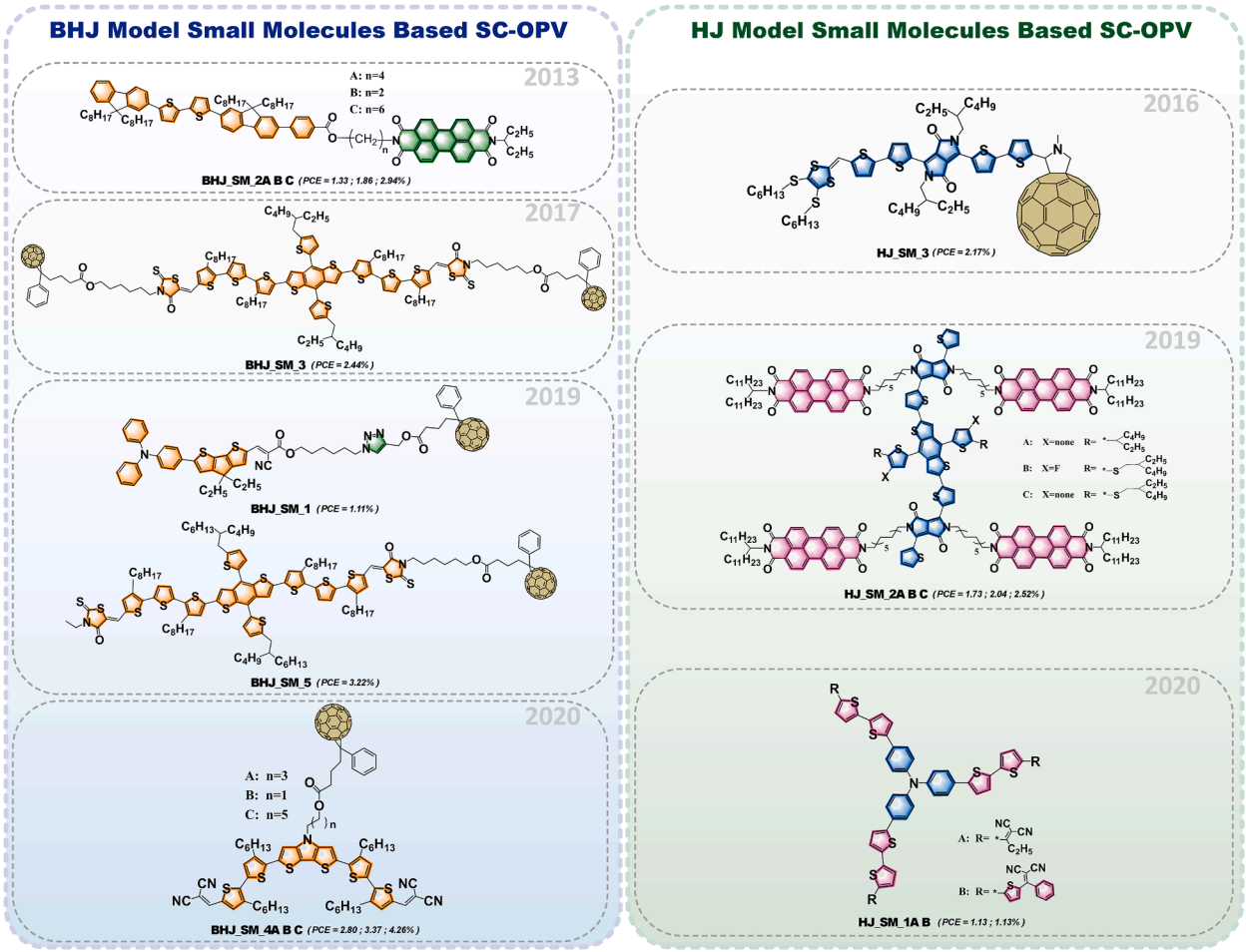

Scheme 3. Chemical structures of small molecules from BHJ and HJ model-based SC-OPVs

Industrial viability

Industrial viability concerns not only efficiency and stability but also synthetic complexity, as cost is a major factor when it comes to real-life demonstrations. To evaluate the industrial potential of SC-OPVs in comparison to BHJ-OPVs, He et al. developed an industrial figure of merit (i-FoM) as follows[103]:

$$\mathrm{i-FoM} = \frac{\mathrm{PCE} \times \mathrm{Photostability}}{\mathrm{Synthetic\ Complexity}}.$$

In the above equation, the PCE maintained under AM 1.5G light after 200 h of illumination is referred to as photostability, and the synthetic complexity was obtained from the following equation:

$$\mathrm{Synthetic\ Complexity} = 35\frac{NSS}{NSS_{max}} + 25\frac{\log(RY)}{\log(RY_{max})} + 15\frac{NUO}{NUO_{max}} + 15\frac{NCC}{NCC_{max}} + 15\frac{NHC}{NHC_{max}},$$

where *NSS* stands for the number of synthetic steps, *RY* represents the yields of the monomers, *NUO* refers to the number of unit operations, *NCC* denotes the number of column chromatography required for the purification of monomers, and *NHC*denotes the number of hazardous chemicals.

He et al. carried out a comprehensive evaluation of the i-FoM between SC-OPVs and BHJ-OPVs.[103] They examined the PCE, photostability, and the level of difficulty in synthesis for SC-OPVs and their corresponding BHJ-OPVs. The results indicated that SC-OPVs based on DCPs and small molecules had better i-FoM compared with the BHJ-OPV with relevant composition, as shown in Figure 5. Because of their improved performance and simpler synthesis, this study suggests that SC-OPVs using DCPs have great potential for future improvement, making them potentially the best candidates for widespread commercial and industrial applications. It is also worth noting that BCP materials based on Y-series acceptors and PBDB-T-based polymer donor blocks will be unlikely to exhibit good industrial viability due to their high synthetic complexity, although the most efficient SC-OPVs so far are mainly based on Y and PBDB-T blocks. Importantly, this also highlights a clear opportunity for BCP development, as future efforts could focus on synthetically streamlined molecular designs and more scalable routes while maintaining the optoelectronic

Please cite this article in press as: Ma et al., Physical insights into single-component organic photovoltaics, Joule (2026), https://doi.org/10.1016/j.joule.2026.102397

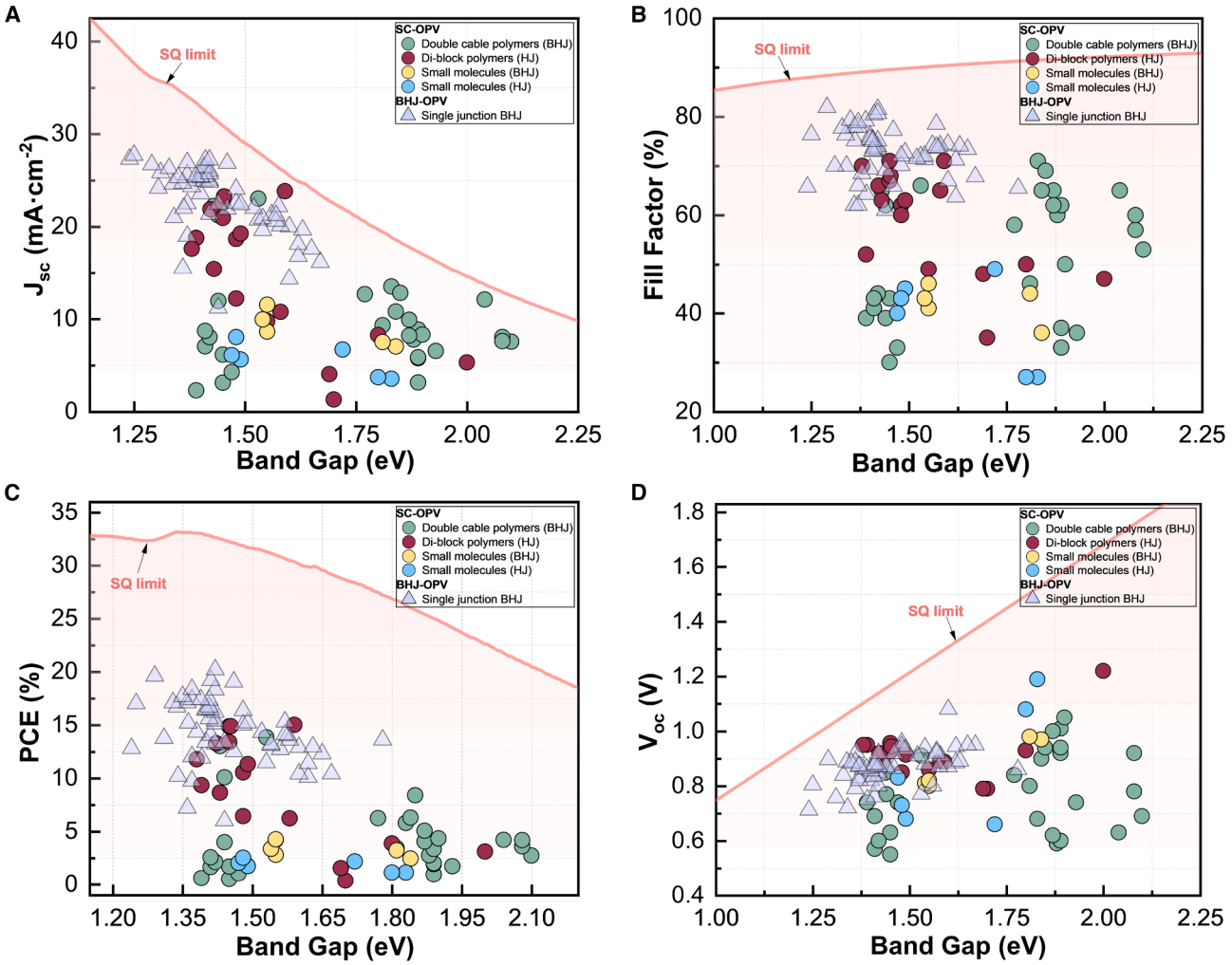

Figure 2. Comparison of PV parameters for SC-OPV and BHJ-OPV devices relative to the SQ limit

The respective parameters of (A) J_{SC}, (B) FF, (C) PCE, and (D) V_{OC} for both SC-OPV and BHJ-OPV devices are analyzed and compared against the Shockley-Queisser (SQ) limit, which is indicated in pink lines.

functionality and device performance required for high-efficiency SC-OPVs.

PHOTOPHYSICAL PROCESS IN SC-OPVs

We now provide a systematic review of the underlying photophysical processes in SC-OPVs to assess the factors limiting their performance. As outlined in Figure 6A, OPV operation proceeds through five key stages: (1) exciton creation via photoexcitation, (2) CT state formation, (3) CT exciton dissociation into free charge carriers, (4) charge-carrier transport, and (5) charge-carrier collection at the electrodes. Recombination, which reduces the current and voltage, occurs at all operational steps radiatively or non-radiatively (including via triplet states that are not shown in Figure 6A). Though the operational steps of SC-OPVs are the same as those of BHJ-OPVs, the CT process is slightly different, as shown in Figure 6B. In BHJ-OPVs, CT occurs intermolecularly between separated donor and acceptor domains, while it occurs intramolecularly through bonds or across flexible linkers in SC-OPVs. In this section, we compare these processes to those in conventional BHJ-OPVs, highlighting how the SC strategy alters the fundamental exciton and free charge dynamics, with attendant benefits and limitations.

Exciton generation and migration

Upon photoexcitation, a photon creates a tightly bound Frenkel exciton (Coulomb-bound electron-hole pair) rather than free carriers in organic semiconductors.[28] Exciton generation in SC-OPVs occurs in the conjugated segments (donor or acceptor units) of the single material, analogous to exciton creation in the donor or acceptor phase of a BHJ. These excitons must migrate (diffuse) to a D-A interface to initiate charge separation. In conventional BHJs, exciton diffusion is a critical bottleneck, as typical exciton diffusion lengths are only on the order of 5–20 nm. However, recent NFAs exhibit surprisingly long exciton diffusion

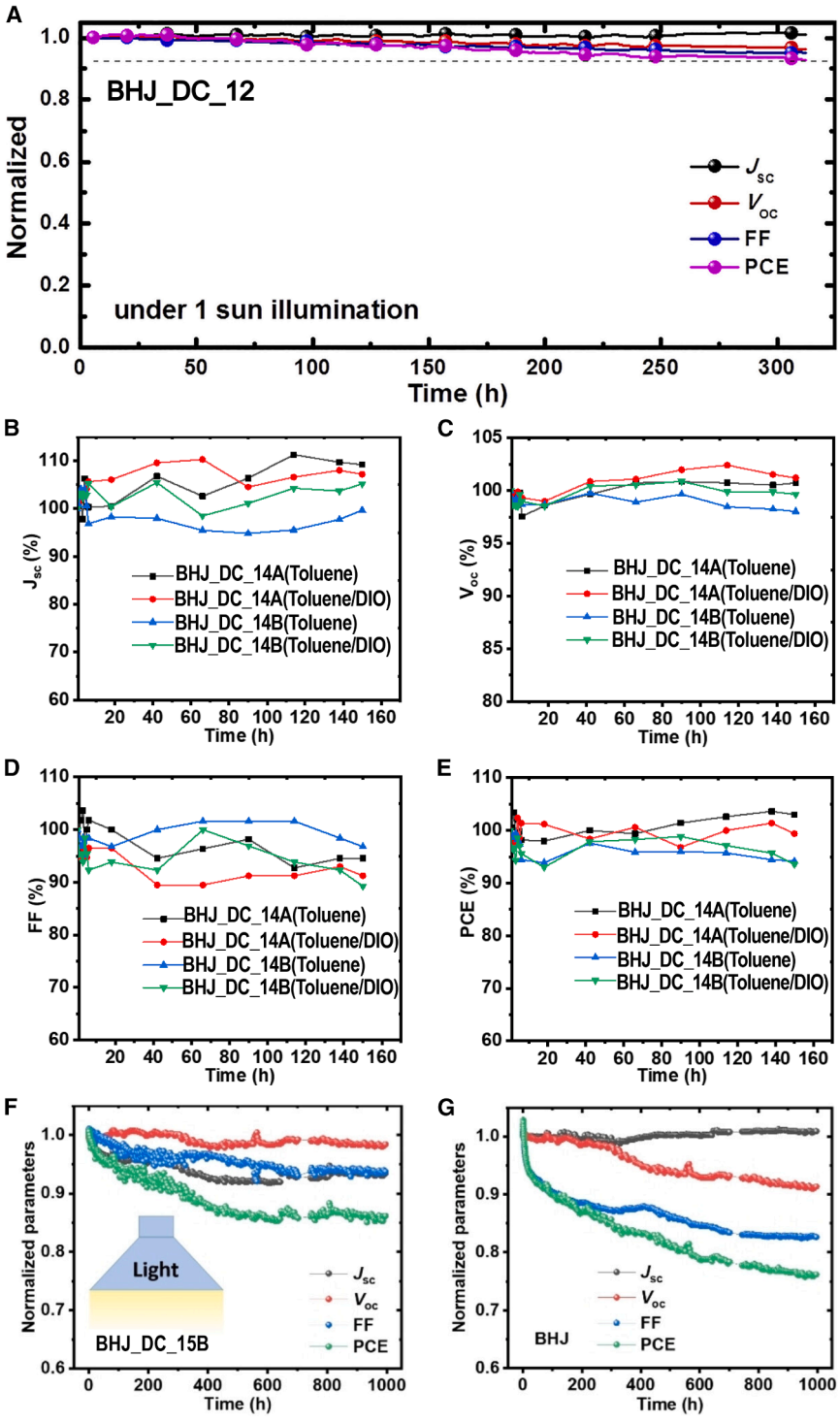

Figure 3. Stability evaluation of double-cable polymer-based SC-OPVs under varied aging conditions and device architectures

(A) The stability data of an optimized BHJ_DC_12 solar cell were measured for over 300 h under comparable one sun light.

(B–E) A stability test was conducted for SC-OPVs based on **BHJ_DC_14A and 14B**. The cells were kept in a glove box. **BHJ_DC_14A**-based cells showed nearly the same PCEs after 150 h, but **BHJ_DC_14B**-based cells showed 94% of the initial PCEs. The results also showed that the cells made from toluene, whether with or without 1,8-Diiodooctane (DIO), had comparable stability.

(F and G) Stability tests were conducted for cells under light based on different structures: (F) **BHJ_DC_15B**-based SC-OPV and (G) BHJ-OPV structure using the same materials. Adapted from Liang et al.,[40] Jiang et al.,[43], and Feng et al.[46]

of 20–47 nm.[104] Firdaus et al. demonstrated that several high-mobility NFAs have balanced ambipolar transport and highly delocalized excitons, enabling long-range exciton migration beyond typical limits.[104] Giannini et al. further showed a clear correlation between exciton diffusion constant and quantum delocalization: in materials like Y6, the exciton can transiently delocalize, significantly extending its diffusion range.[105] This means excitons in well-ordered SC-OPV materials can sample a larger volume before decay, increasing the likelihood of reaching a D-A interface (even a "hidden" one within the SC). Notably, modeling work has suggested that excitons might dissociate even tens of angstroms away from an interface, yielding partially separated electron-hole pairs that can more easily overcome Coulomb attraction.[106] Such long-range exciton dissociation was predicted to be quite common in polymer:-fullerene BHJs, implying that an exciton need not be exactly at a D-A contact to begin charge separation.

In SC-OPVs, the D and A moieties are inherently in proximity (either as covalently linked blocks or pendant side groups). This architecture can facilitate exciton harvesting by ensuring that an acceptor is never far from an excited donor (and vice versa). For DCP architectures with fullerene or NFA side-chain acceptors, the donor backbone provides the exciton source while pendant acceptors furnish proximate electron-accepting sites. This intramolecular capture proceeds on ultrafast (sub-ps) timescales, obviating long-range exciton diffusion and reducing encounter-limited loss.[37,43,107] By analogy, in a BCP, the covalent D-A junctions along a single chain provide similarly short capture distances: in the fully conjugated (F8-TBT)-b-P3HT system, intrachain CT excitons form within 40 fs of excitation, with pronounced quenching of P3HT photoluminescence even at the single-chain level.[82] This sub-50 fs timescale is much faster than typical

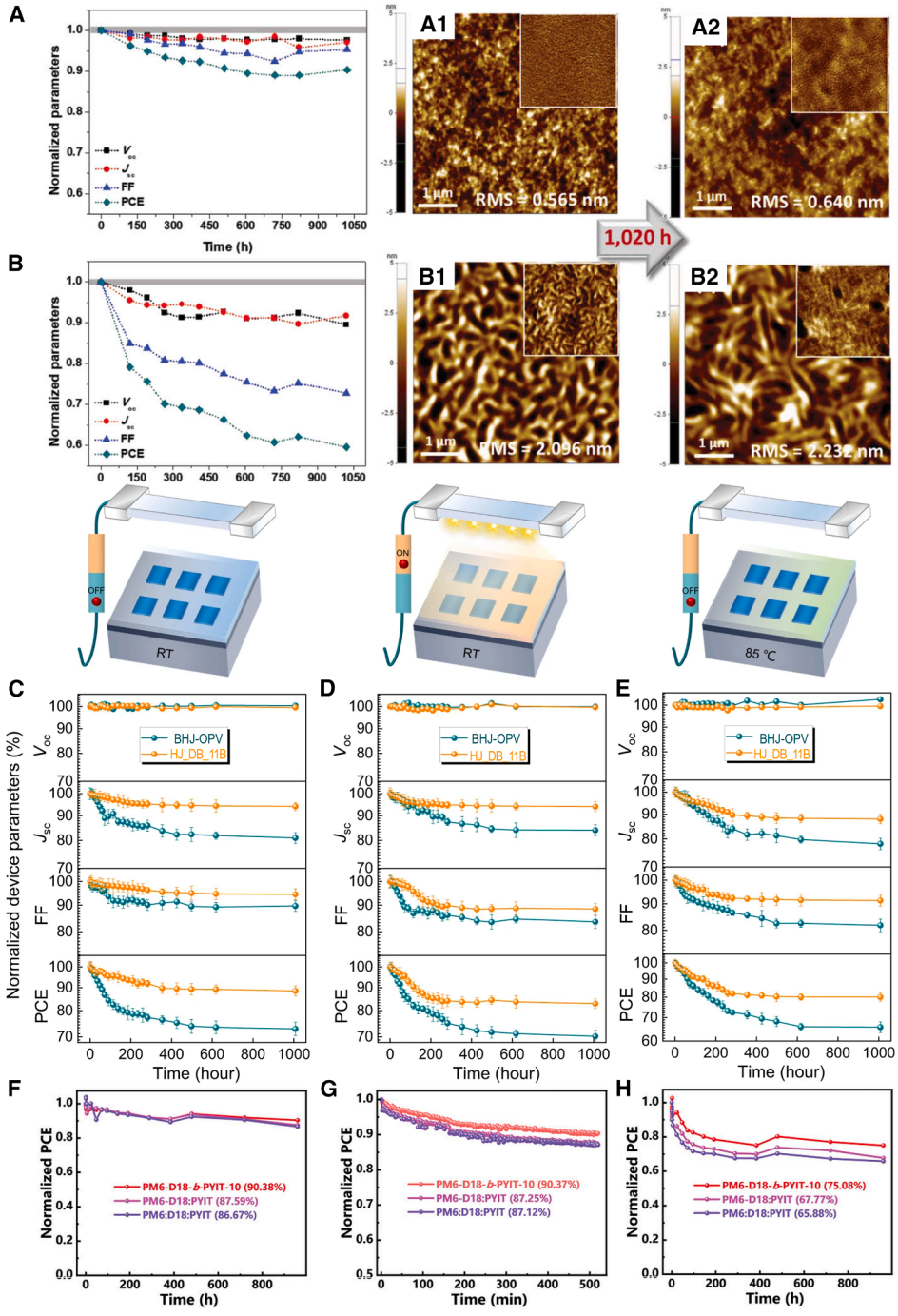

Figure 4. Comprehensive stability evaluation of SC-OPVs and BHJ-OPVs based on di-block polymers under diverse environmental and operational stressors

(A and B) An assessment was conducted to determine the stability of SC-OPV performance under ambient circumstances for a storage period of up to 1,020 h. The evaluation was carried out for two different structures with the same materials: (A) **HJ_DB_10** and **(B) HJ_DB_10** blend BHJ-OPVs. The atomic force microscopy (AFM) height photos depict the **(A_1 and A_2) HJ_DB_10** film and **(B_1 and B_2)** blend film.

(C–E) The PV characteristics of the optimized blend system **HJ_DB_11B**-based BHJ-OPVs and **HJ_DB_11B**-based SC-OPVs were studied for a storage period of up to 1,008 h in a nitrogen gas environment. The evolution of these parameters was investigated under the following three different conditions: (C) under room temperature and dark conditions, (D) continuous illumination conditions, and (E) 85°C heated conditions.

(F–H) Evolution of PV parameters of the PM6-D18-b-PYIT-10 (**HJ_DB_17**), PM6-D18:PYIT, and PM6:D18:PYIT-based OPV in a nitrogen atmosphere: (F) under dark conditions and at room temperature, (G) under continuous illumination conditions, and (H) under 85°C heated conditions. Adapted from Cheng et al.,[31] Park et al.,[57] and Liu et al.[58]

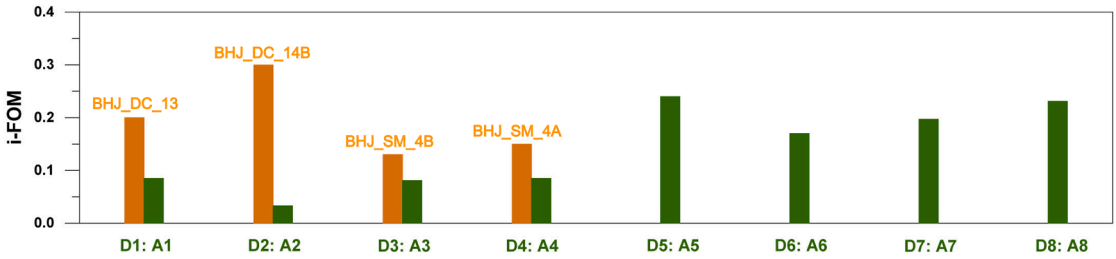

Figure 5. Comparison of i-FoM for SC-OPVs and BHJ-OPVs

The orange columns represent SC-OPVs, and the green ones indicate BHJ-OPVs. Adapted from He et al.[103]

exciton diffusion times, indicating that excitons are being captured almost immediately by nearby intrachain D-A interfaces. A similar study noted that these intrachain exciton dissociations were efficient at creating CT states (with a notable quenching of P3HT photoluminescence), even in isolated single chains.[76] Also, in BCPs with well-defined microphase-separated domains, exciton migration will occur within the donor-rich domain until the exciton reaches a donor/acceptor domain interface. If domain sizes are comparable to or smaller than the exciton diffusion length (~10 nm), most excitons can reach an interface before decaying. P3HT-b-PPerAc*r* exemplifies the influence of morphology: finely intermixed, disordered D-A nanoscale domains (e.g., achieved by certain processing conditions or lower molecular weight) led to substantial steady-state photoluminescence (PL) quenching and ultrafast (~1 ps) photoinduced CT, reflecting exciton dissociation at numerous small D-A sites.[108] By contrast, the same BCP processed to have larger, more phase-separated domains showed slower exciton dissociation kinetics. Thus, controlling exciton migration in SC-OPVs involves tuning the internal morphology: a higher density of D-A contacts (either via molecularly intermixed phases or via intramolecular contacts) increases the likelihood that an exciton will encounter an interface before decay.

It is worth noting that some emerging organic semiconductors blur the line between needing a heterojunction and behaving more like inorganic absorbers in terms of exciton dissociation. For instance, Y6 has a relatively low exciton binding energy due to its high polarizability (high dielectric constant) and extended conjugation. Remarkably, SC Y6 films can generate a large fraction of free charge carriers directly upon photoexcitation, without any second phase: at solar illumination intensities, an estimated 60%–90% of Y6 excitons dissociate into free charges intrinsically.[109] This behavior is highly unusual for organic absorbers and is attributed to strong coupling between the local exciton and CT states in Y6 aggregates, as well as an intermolecular polarization pattern that aids exciton ionization. While Y6 by itself still suffers from significant recombination losses (discussed later), its ability to generate free charge carriers from excitons in an SC film highlights the potential for efficient exciton harvesting in carefully designed organic semiconductors.

SC-OPVs are generally designed to maximize exciton migration to an internal D-A interface, either by bringing the interface to the exciton (via intrachain acceptors) or by controlling domain sizes, thereby mitigating the diffusion bottleneck present in traditional BHJs. Also, the interfacial distance or domain size of SC-OPVs in principle should be better controlled than that in BHJ-OPVs, since donors and acceptors are covalently bonded. Therefore, via proper chemical design, SC-OPV is likely to present excellent exciton migration and CT efficiencies, which are, however, still one of the challenges, as discussed later.

CT state formation and evolution

When an exciton reaches a D-A interface (whether an intermolecular interface or an intramolecular junction), electrons can transfer from the donor to the acceptor, or holes can transfer from the acceptor to the donor, forming a CT state. This CT state is essentially a Coulombically bound e-h pair (electron on the acceptor, hole on the donor) that can be thought of as an interfacial exciton with partial charge separation. The properties and fate of the CT state are pivotal for free-charge generation. In BHJ systems, though electrons and holes are spatially separated, CT states are still tightly bound in energy—for example, at a planar organic donor/acceptor interface, CT excitons can be bound by 0.1–0.4 eV depending on their quantum state.[110] The lowest-energy (relaxed) CT exciton often has a large binding energy (~0.4 eV in one measured case), which would ordinarily prevent it from dissociating into free charges.[110] While the exact mechanism for CT excitons to dissociate into free charges is still unknown in BHJ-OPVs, considerable attention has been drawn to the discussions of "exciton delocalization," "hot CT states," and "entropy-driven dissociation." Strong delocalization leads to spatially separated electron and hole pairs that can easily dissociate into free charge carriers,[111] while hot CT states—higher-energy CT excitons with extra vibrational or electronic energy—can form and be more readily split into free carriers before relaxing into the tightly bound state.[110] On the other hand, entropy may also play an important role by reducing barrier height at the D-A interfaces, which will facilitate exciton dissociation.[111]

In SC-OPVs, CT-state formation can follow different pathways depending on the molecular architecture. This CT state often occurs intra-molecularly (e.g., along a double-cable polymer chain) or at the interface of D/A microdomains in a BCP (Figure 6B). The initial separation distance in such a geminate intrachain CT pair may be small (on the order of a single covalent bond or a few nanometers along the chain), which can lead to a strongly bound CT state. Early studies on fully conjugated D-A BCPs indeed found that CT states would form readily but often remained Coulomb-bound (and eventually recombined) rather than

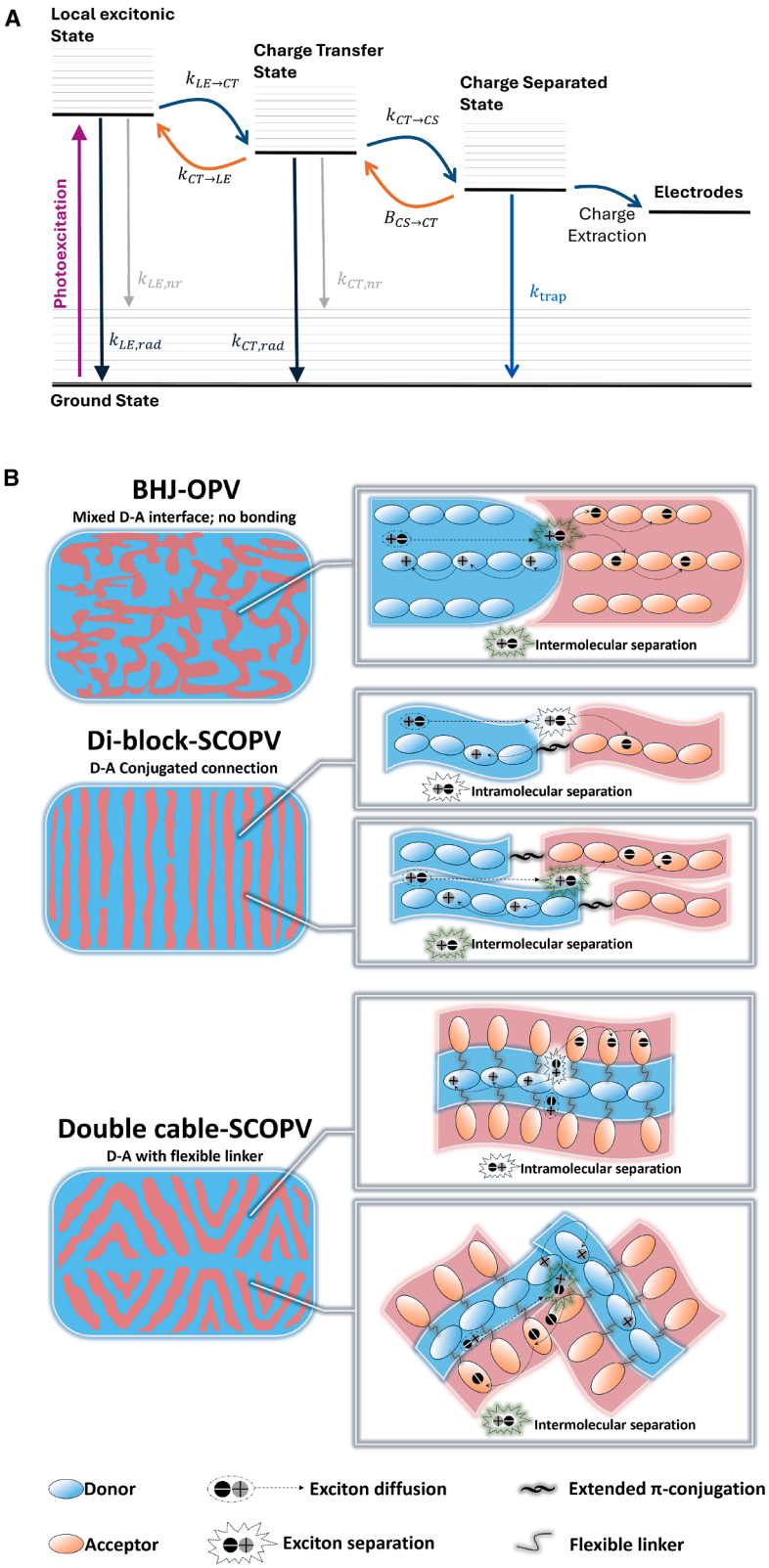

Figure 6. Jablonski diagram of OPV operating mechanisms and comparative CT processes in BHJ- and SC-OPVs

(A) Jablonski diagram of the operation mechanism of a typical OPV device. $k_{LE\rightarrow CT}$ refers to the rate constant from LE to CT transition, $k_{CT\rightarrow LE}$ is the back transfer rate constant from CT to LE, $k_{CT\rightarrow CS}$ is the rate constant of CT to CS transition, and $B_{CS\rightarrow CT}$ is the bimolecular recombination coefficient, in which process one electron and a hole form a CT exciton. $k_{LE,rad(nr)}$ and $k_{CT,rad(nr)}$ are the radiative (non-radiative) recombination rate constants for LE and CT, respectively. k_{trap} represents the recombination rate constant due to trap-assisted recombination. Note here that the diagram is the simplest form, where triplet states are not considered.

(B) Illustration of the difference in the CT process between BHJ-OPVs and SC-OPVs.

Please cite this article in press as: Ma et al., Physical insights into single-component organic photovoltaics, Joule (2026), https://doi.org/10.1016/j.joule.2026.102397

producing free charges.[76,82,112] For example, in the (F8-TBT)-b-P3HT BCP mentioned above, ultrafast spectroscopy (US) revealed that interfacial CT excitons formed rapidly (<40 fs) upon excitation, but these CT states possessed unusually large oscillator strength and mostly failed to dissociate further into free carriers.[82] Rather, the CT exciton recombined radiatively or non-radiatively, contributing little to photocurrent—a behavior attributed to the strong binding and perhaps insufficient driving force for separation in that particular intrachain D-A pair. Interestingly, when the same donor and acceptor components (P3HT and F8TBT) were simply blended as separate polymers, much improved charge generation was observed, whereas the covalently linked version showed a suppressed yield of free charge carriers.[82] This highlighted an early challenge in SC-OPVs: although bringing donor and acceptor units into the same molecule guarantees CT formation, it does not guarantee CT dissociation.

Specifically, in SC-OPVs, donor and acceptor motifs are covalently integrated within a single material, which keeps them in close proximity and can facilitate the formation of CT states upon photoexcitation, but photocurrent generation requires that the resulting CT pair escape Coulomb binding and evolve into spatially separated, extractable charges before geminate loss occurs.[20,103,113] Accordingly, the decisive step is therefore CT dissociation rather than CT formation[114]: delocalization over ordered aggregates and enhanced dielectric screening can reduce the effective binding and facilitate separation,[115,116] whereas strong electronic coupling and energetic disorder can stabilize bound polaron-pair-like intermediates that relax back through radiative or non-radiative pathways.[117,118] This framing also clarifies why design strategies in SC-OPVs emphasize (1) promoting nanoscale packing motifs that support charge delocalization and connectivity and (2) molecular design choices that tune wave function overlap and screening, for example, via spacer and side-chain engineering and the use of more polarizable motifs.[103,119]

The evolution of the CT state, i.e., whether it proceeds to split into free charges or relaxes and recombines, is thus a critical step. Several molecular and morphological strategies have been developed to promote favorable CT evolution in SC-OPVs. One strategy is to delocalize the charges in the CT state. Recent studies suggest that delocalization and molecular ordering are crucial: Zhang et al. found that the high-efficiency acceptor Y6 packs into π-π stacks that create delocalized, emissive excitons and electron wave functions, which (1) minimize the electron-hole binding in the interfacial CT state and (2) yield small non-radiative voltage losses.[98] In other words, a CT state formed at a Y6-based D/A junction is less tightly bound, because the charge density spreads over multiple molecules, reducing Coulomb attraction. Similarly, intramolecular CT along a single conjugated chain can be extremely fast and efficient. Li et al. employed transient absorption (TA) spectroscopy on a D-A BCP and observed ultrafast CT-state formation—on the order of hundreds of femtoseconds—accompanied by prompt exciton dissociation.[63] The directly synthesized BCP (with well-controlled interfaces) showed higher intrachain CT efficiency than a randomly synthesized analog, highlighting that precise covalent connectivity and sequence regularity can suppress kinetic barriers to CT formation. Theoretical advances also reinforce these observations: Kassal and coworkers modeled charge generation with a delocalized kinetic Monte Carlo (KMC) approach and found that exciton-CT hybrid states can form even in the *bulk* of a single-phase material, enabling excitons to dissociate without a traditional heterojunction driving force.[120] Their simulations show that when exciton and charge wave functions hybridize into "mixed" states, charges can hop out to longer distances, dramatically boosting separation kinetics. Designing polymers that promote such delocalized CT states (for instance, by aligning energy levels of D and A units and using flexible spacers) is therefore a key strategy. Indeed, a recent perspective emphasizes that optimizing the donor/acceptor interface at the molecular level, aligning D, A, and linker units, is crucial to suppress unfavorable couplings and create CT states that readily convert to free charges.[103]

Applying these insights to SC-OPVs, researchers have designed SC systems to favor CT states that are weakly bound and short-lived (quickly splitting). For example, PBDB-T-b-PTY6, a D-A BCP combining a PBDB-T donor block (a high-performance polymer donor) with a Y6-derivative acceptor block (PTY6), has demonstrated highly efficient intrachain CT.[63]

Charge separation mechanisms

The conversion of a bound CT exciton into free charge carriers is a pivotal step in OPVs. In BHJ cells, charge separation is facilitated by the existence of two separate phases: after a CT state forms at a donor/acceptor interface, the electron can delocalize into the acceptor domain and the hole into the donor domain, reducing their Coulomb attraction. Thermal energy, entropy, and the built-in electric field all assist in overcoming the Coulomb binding in these multi-component systems, as mentioned above. In SC systems, achieving the same outcome requires clever molecular and morphological design, since initially the electron and hole may reside on the same macromolecule. Here. we discuss several different charge separation pathways and mechanisms for SC-OPVs.

Intra-to-intermolecular separation

Following intramolecular CT, one of the charges hops to a neighboring molecule, creating an intermolecular CT exciton that has a larger electron-hole distance, hence lowering the binding energy. For instance, in a DCP polymer where an electron is on a fullerene side chain, and the hole is on the polymer backbone, the electron can hop from that side-chain acceptor to another acceptor unit on an adjacent side chain, thereby placing the electron and hole on different molecules.[43,46] This process effectively converts an intramolecular CT into an intermolecular CT spanning two chains, greatly reducing Coulomb binding.[32] The efficiency of this step depends on the packing and phase segregation of the acceptor moieties. If the acceptor side groups (e.g., C60, perylene diimide, etc.) aggregate into clusters or percolating pathways, an electron can migrate through those clustered acceptors, leaving behind the hole on the original chain. Thermal annealing is often employed to induce a partial phase separation of this kind. A good example is the case of a DCP polymer that, as-cast, exhibited limited performance (PCE ~2%–3%), but after a thermal treatment to drive nanophase segregation of donor and acceptor sub-domains, its efficiency jumped to ~6%.[46]

Please cite this article in press as: Ma et al., Physical insights into single-component organic photovoltaics, Joule (2026), https://doi.org/10.1016/j.joule.2026.102397

Similarly, Jiang et al. achieved >8% efficiency by using a miscibility-tailored DCP polymer: after high-temperature annealing, the polymer self-assembled into purer donor and acceptor phases, which reduced the interfacial Coulomb attraction and doubled the CT state's lifetime (the CT-to-ground recombination rate in the optimized polymer was half that of a more mixed analog).[43] The result was a much higher probability of CT states splitting into long-lived charge carriers. Thus, by allowing the covalently bound D and A to sort into interpenetrating networks (while still chemically tethered), one can mimic the charge separation mechanisms of a BHJ where the charges are effectively in different phases after separation, even though no distinct second material was added.

Delocalization and entropy-driven separation

Even without pronounced phase separation, charge separation can be aided by delocalization of charge carriers and entropic considerations. In DCP polymers, a photogenerated hole or electron may delocalize along the polymer backbone or over several repeat units of an acceptor side chain. This delocalization reduces the Coulomb attraction by spreading the charge and increasing the distance between the electron and hole. For instance, Li et al. developed a DCP polymer with randomly distributed acceptor side chains (as opposed to perfectly alternating "regular" placement), enabling efficient charge separation with a PCE of 13%.[48] This random architecture tends to produce optimized nanophase separation and interpenetrating networks that improve ambipolar transport, which also suggests easier charge separation. In a BCP polymer, for example, the hole could delocalize along the donor block while the electron resides on an acceptor block, providing a larger separation than the initial CT interface. Additionally, if each separated charge has multiple energy sites to occupy (e.g., an electron could reside on any of many acceptor units on other chains), the entropy of dissociation is enhanced and could potentially facilitate charge separation—a concept often invoked in BHJ systems and still relevant in SC systems. Recent reviews note that through optimized molecular design (e.g., incorporating NFA units with extended conjugation), SC-OPVs now achieve charge separation yields approaching those of BHJs, with overall internal quantum efficiencies steadily improving into the 80%–90% range in the latest systems.[83,107]

Field-assisted separation

In BHJ-OPVs, interfacial energetics together with the built-in/external field set the early-time fate of photogenerated excitons. Fields preferentially lower the escape barrier of interfacial CT excitons rather than tightly bound singlet excitons, as evidenced by field/temperature-dependent PL quenching in PTB7:PCBM.[121] In addition, time-delayed collection field (TDCF) and field/temperature-dependent photocurrent and PL studies show a monotonic rise of free charge-carrier yield with enhanced electrical field in polymer:fullerene blends, consistent with Onsager-type polaron-pair dissociation and microscopic field-assisted tunneling.[122,123] On the other hand, US studies show that, once created at the D/A interface, charge carriers can separate over several nanometers on sub-ps time scales, outpacing geminate recombination. The electric field then primarily serves a sweep-out role that competes with bimolecular losses.[124,125] Quantitatively, in the prototypical PCDTBT:PCBM blend, ~89% of photo-excitations produce free carriers on ultrafast timescales, with only ~11% forming CT states that recombine geminately on the ns scale.[126] We note that field-independent free-charge generation has also been demonstrated in several high-performing BHJs, where excess energy/delocalization or interfacial order enables barrierless (or low-activation) separation.[115,127]

In SC-OPVs, intrinsic D-A heterojunctions (covalent D-A linkages or HJ electrostatics) could create hybrid exciton/CT manifolds capable of efficient, often endothermic separation with small driving forces. In these chemically uniform films, the internal field—set by contact boundary conditions and space charge—mainly governs drift/extraction rather than being a prerequisite for charge creation.[128,129] Consistently, for BCP-based SC-OPVs (e.g., PBDB-T-b-PTY6/-PYIT), TA resolves sub-ps exciton-to-CT conversion, and rapid charge carriers can escape at intrachain D-A junctions, supporting efficient pre-diffusive exciton separation. However, systematic field dependence at the device level remains under-studied in SC BCPs, and further experiments are needed to quantify the balance between field-assisted sweep-out and bimolecular loss.[130] Finally, both architectures reach high efficiency when sub-ps exciton separation outpaces geminate loss and the internal electrical field extracts carriers before encounter-limited recombination. Whether the initial driver is interfacial excess energy/delocalization (BHJ) or intramolecular coupling/entropy (SC-OPV), further experimental or computational evidence is needed.[124,129]

Charge transport and extraction

From a device-equation standpoint, the internal field (x) in thin-film OPVs is set by contact boundary conditions and space charge via Poisson-continuity, and the operating photocurrent is the kinetic outcome of drift-assisted extraction competing with bimolecular recombination, and this is formalized by a recent unified diode equation for low-mobility thin-film PVs and is material-agnostic (thus applicable to SC-OPVs as well as BHJs).[128,131] In BHJ devices, efficient transport requires a bicontinuous D/A network with near-balanced mobilities. Quantitative drift-diffusion/experiment studies show that mobility imbalance steepens space-charge buildup and depresses the FF, while encounter-limited recombination is mitigated by appropriate phase separation (i.e., reduced Langevin factor).[131–134] Vertical composition profiles further modulate extraction barriers and series resistance—favorable gradients improve carrier selectivity and current delivery, whereas unfavorable or uniform profiles can throttle extraction.[135]

In SC structures, percolation still matters but is encoded by chemistry. Carrier mobility is therefore dictated by how effectively the covalently integrated donor and acceptor motifs can organize into continuous, compositionally enriched transport pathways in the solid film. D-A BCPs microphase-separate into donor- and acceptor-rich lanes that are covalently tethered, supplying dual, interpenetrating highways for holes and electrons. Wu et al. show that such BCPs can sustain thick layers with balanced μ_e and μ_h and >11% PCE.[60] Historical counter-examples (e.g., P3HT-b-PPerAcr) illustrate the importance of domain orientation: in-plane lamellae lengthen the hop sequence to contacts and

Please cite this article in press as: Ma et al., Physical insights into single-component organic photovoltaics, Joule (2026), https://doi.org/10.1016/j.joule.2026.102397

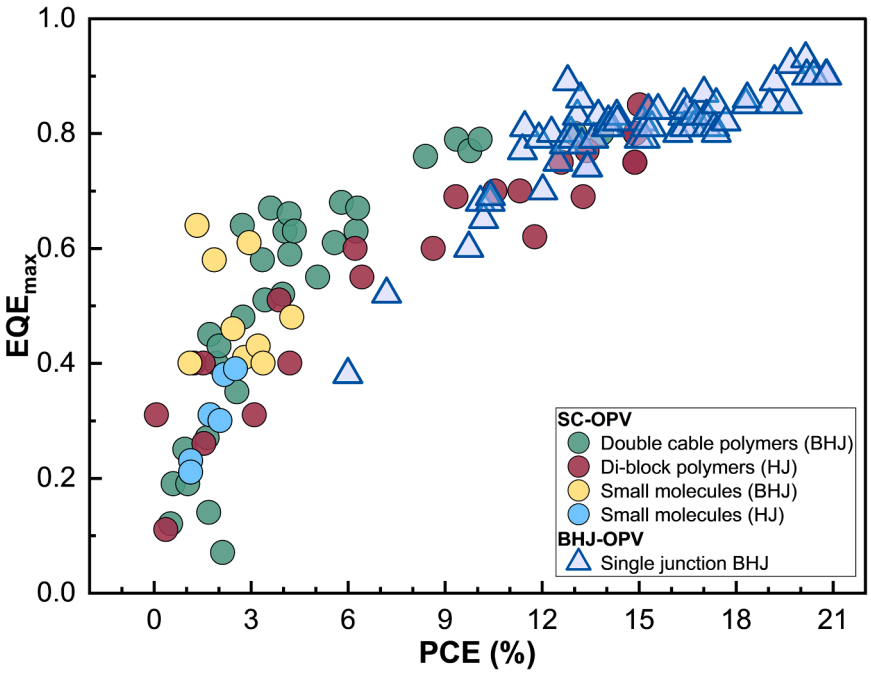

Figure 7. Correlation between EQE_{max} and PCE for various SC-OPV and single-junction BHJ-OPV material systems

Maximum external quantum efficiency (EQE_{max}) as a function of power conversion efficiency (PCE) for various material structures in SC-OPVs, in comparison to single-junction BHJ-OPVs. Data are collected from Tables 1, 2, 3, 4, and 5.

undermine extraction despite long-lived charges—underscoring that geometry, not only purity, governs transport.[108] For double-cable polymers, a π-conjugated donor backbone typically provides the primary channel for hole transport, whereas electron transport hinges on whether the pendant acceptor units assemble into sufficiently connected aggregates. Linker geometry and side-chain sterics can thus directly set electron percolation and, in turn, the degree of mobility balance.[37] Processing that promotes nanoscale ordering, for example, thermal annealing or additive-assisted organization, often improves extraction while also reducing recombination losses, underscoring that packing control affects transport through both morphology and kinetics.[46] Side-chain engineering is a particularly practical handle in this context, since transport can be mediated by a dense network of close interchain contacts rather than by a single dominant packing motif.[32] Early C_{60}-pendant designs suffered "islanded" transport, but Y-series side chains and random-architecture strategies now yield ambipolar networks and record 13% SC-OPV efficiencies with improved ordering and clear mobility gains.[48]

"Photophysical process in SC-OPVs" provides a systematic analysis of the photophysical processes in SC-OPVs and clarifies that, in many cases, they proceed through the same operational stages as BHJ-OPVs, including exciton generation, CT-state formation at internal donor-rich and acceptor-rich contacts, separation into free charges, and carrier extraction. The key distinction is that, in SC-OPVs, covalent D/A integration constrains the extent of phase separation and therefore limits the accessible interfacial area and the characteristic length scales over which charges separate and percolate, so that macroscopic demixing is suppressed while nanoscale donor-rich and acceptor-rich organization can still emerge as functional separation sites and continuous transport pathways. Importantly, intramolecular CT often serves as an early, local capture step that populates short-range CT configurations, particularly in covalently linked dyads and triads based on SC-OPVs, whereas high free-charge generation efficiency typically requires subsequent intermolecular charge delocalization and hopping within extended donor-rich and acceptor-rich aggregates. This increases the separation between the electron and the hole and lowers the effective Coulomb binding, so the CT to free-carrier conversion is strongly governed by solid-state packing and local connectivity. Accordingly, in SC-OPVs the transport landscape is more directly encoded by molecular architecture and self-assembly: dyads and triads rely on solid-state packing to sustain electronically coupled, ambipolar networks, and double-cable systems support hole transport primarily along the conjugated backbone, while electron transport depends on the formation and continuity of percolating aggregates of the acceptor side units, and BCPs can microphase-separate into donor-rich and acceptor-rich domains whose orientation and connectivity set the effective mobility balance and extraction distance, which together control the FF.

CHALLENGES AND SUGGESTIONS

In this section, we discuss the remaining challenges in terms of performance and provide suggestions to tackle those issues, with Tables 1, 2, 3, 4, and 5 summarizing representative device-relevant parameters for SC- and BHJ-OPVs. In parallel, we note that several commonly used experimental characterization and analysis protocols are subject to debate. As a result, extracted parameter values may deviate substantially from their true magnitudes. We therefore provide a critical appraisal of these methods and offer practical suggestions to improve the measurement fidelity and interpretability. Together, these analyses establish a device-physics-level and practical guideline for materials design, characterization, and data interpretation.

Charge-carrier generation

Figure 7 indicates that most high-PCE BHJ-OPVs reach *EQEmax* values above 80%, whereas many SC-OPVs remain around 60%–70%, pointing to persistent losses during charge generation and a low proportion of free charges (as mentioned in "exciton generation and migration," "CT state formation and evolution," and "charge separation mechanisms"). Here, we concentrate on the experimental observables and

Please cite this article in press as: Ma et al., Physical insights into single-component organic photovoltaics, Joule (2026), https://doi.org/10.1016/j.joule.2026.102397

complementary measurements needed to unambiguously assign the dominant EQE loss channel within a given SC-OPV architecture.

The US offers a valuable tool for probing the early-time evolution of local and CT excitons in SC-OPV. This technique can identify key limitations during exciton dissociation, facilitating a deeper understanding of the relationship between D-A network structures and exciton dissociation processes. TA spectroscopy (TAS) is an effective method for capturing the dynamic changes in exciton and free charge populations over time.[136] These capabilities make TAS one of the most powerful and widely used techniques for elucidating charge generation and recombination dynamics in OPVs. For example, Woo et al. used TAS to study the exciton and charge generation and recombination dynamics in **BHJ_SM_3**.[66] By comparing the results with those from a blend system (BHJ-OPV) of the same composition, they found that in **BHJ_SM_3**, the electron transfer time is only 300 fs, and the polaron lifetime (3.5 ns) is an order of magnitude longer than in the blend structure. Similarly, Guo et al. employed TAS to investigate the differences in hole transfer kinetics between SC-OPV and BHJ-OPV in **HJ_DB_11B**.[58]

Nevertheless, the application and analysis of TAS and related techniques in SC-OPVs remain relatively limited compared with their use in BHJ-OPVs. Charge generation mechanisms in SC-OPVs are still not well understood. Therefore, future research and applications of TAS in SC-OPVs hold great promise. Advanced TAS methodologies could provide more detailed temporal and spatial resolution, offering a comprehensive understanding of exciton and charge-carrier dynamics. Integrating TAS with other spectroscopic techniques, such as time-resolved photoluminescence (TRPL) and terahertz spectroscopy, could offer complementary insights into the electronic and structural properties of SC-OPVs. Such combined approaches would enable a more holistic view of charge generation processes, leading to the development of optimal SC materials. Leveraging these advanced techniques, researchers can systematically explore the fundamental mechanisms governing SC-OPVs, paving the way for innovative strategies in material design. This will enhance the efficiency and stability of SC-OPVs and accelerate the transition toward more sustainable and commercially viable OPV technologies, providing chemists with essential insights and guidance for the precise design of highly efficient and stable SC materials.

Charge recombination and energy losses

One of the primary challenges affecting the efficiency of SC-OPVs is recombination, which leads to significant energy losses. Understanding and identifying the different forms and mechanisms of recombination in OPVs have been subjects of considerable debate due to their complex and diverse nature. The complexity of these processes makes it difficult to reach a consensus on their interpretation. Consequently, varying interpretations of recombination can directly or indirectly influence researchers' conclusions regarding the nature of recombination in both BHJ-OPVs and SC-OPVs. This ongoing debate highlights the need for further detailed studies to elucidate the underlying recombination mechanisms and their impact on the performance of OPVs. Prior to elucidating these concepts, it is necessary to clarify various forms of recombination, which are often categorized as geminate recombination and non-geminate recombination. Geminate recombination refers to recombination that happens prior to exciton separation, i.e., direct decay of local excitons or CT excitons, while non-geminate recombination usually means bimolecular or trap-assisted recombination.[137,138]

Intramolecular charge recombination describes the early-time geminate loss, i.e., the decay of the initially generated exciton of the local excitonic state and/or the ensuing intramolecular CT (bound polaron-pair) state before the electron-hole pair escapes into spatially separated, extractable charges.[49] In SC-OPVs, donor and acceptor segments are covalently connected, and the primary CT pair is formed at short range due to strong electronic coupling (H_{AB}),[139,140] which can also facilitate back electron transfer to the local excitonic (LE) state followed by decay to the ground state or directly decay to the ground state unless the solid-state (thin-film microstructure) packing rapidly promotes charge delocalization and separation into distinct, percolating electron and hole transport networks. In practice, incomplete nanoscale segregation and locally mixed regions can further increase the probability of geminate loss, which has been discussed as a key limitation for SC-OPVs. Once free charges are generated, recombination proceeds predominantly through bimolecular and trap-assisted recombination, i.e., non-geminate pathways, which remain sensitive to energetic disorder and to imbalanced μ_e and μ_h.[141]

Bimolecular recombination is commonly considered a crucial component that restricts the performance of OPVs and requires thorough investigation.[142–144] Measurements of photocurrent density (J_{ph}) as a function of light intensity (I) are frequently employed to characterize bimolecular recombination in OPV devices, in which the connection between J_{ph} and I may be expressed as $J_{ph} \propto I^{\alpha}$. It is often interpreted that in the presence of dominating monomolecular recombination or trap-assisted recombination, α approaches unity and thereafter declines monotonically when bimolecular recombination increases.[145,146] However, this hypothesis is debatable, as many studies have clearly demonstrated that it is difficult to determine recombination types using such a method. As an example, Deibel and Wagenpfahl stated that intensity-dependent photocurrent is not substantially associated with loss mechanisms since recombination is generally negligible at short-circuit conditions.[147] Würfel et al. showed that J_{ph} vs. I (power-law) could not be used to distinguish bimolecular and trap-assisted recombination.[144] Recently, Kirchartz et al. suggested that trap-assisted recombination could lead to a J_{ph} *vs.* I relationship that is sublinear in thin devices (100 nm thickness of active layer) without space charge effects.[148] This relationship, however, is often mistakenly characterized as bimolecular recombination in the literature. In addition, they challenged the common interpretation that a sublinear trend seen in thin devices at low light intensities eliminates the possibility of recombination through deep traps as the primary recombination process. Nonetheless, direct and deep-trap recombination still have the potential to result in a highly linear correlation, although significant losses through tail states that are independent of absorber thickness may not. Overall, it is desirable for researchers to embrace more precise models or employ numerical models to thoroughly ascertain recombination

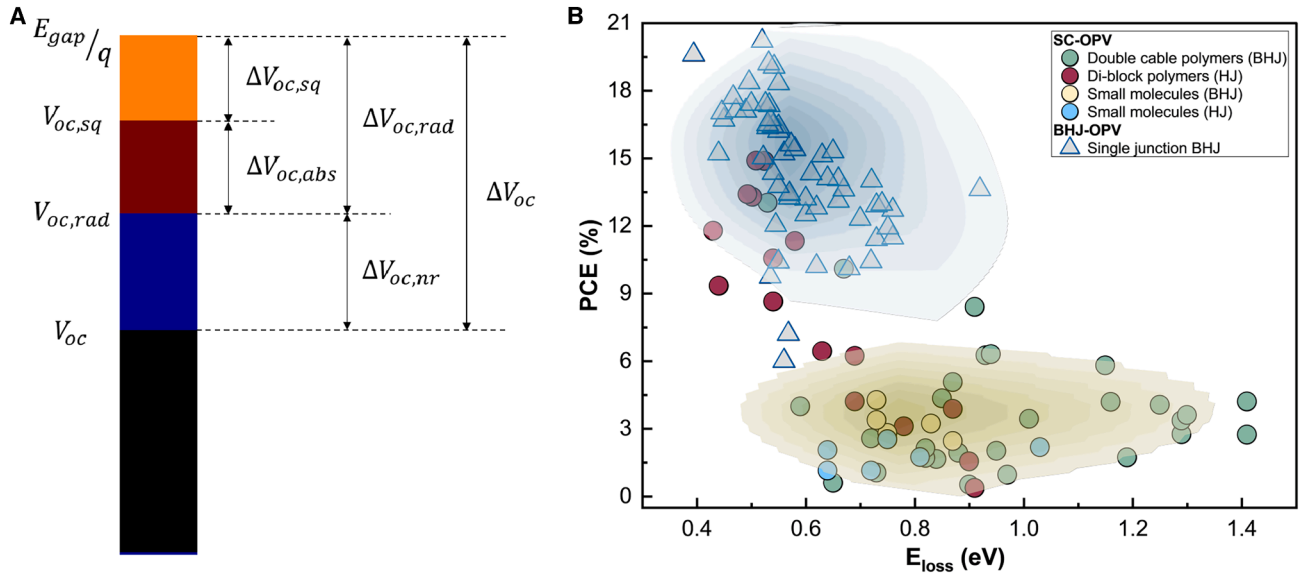

Figure 8. Energy loss analysis and its relationship with PCE for various OPV structures

(A) Decomposition of energy/voltage losses.

(B) Power conversion efficiency (PCE) as a function of total energy losses (E_{loss}) for various OPV technologies.

mechanisms, instead of just depending on a single model using the J_{ph} vs. I relationship.

Recombination can also be divided into radiative and non-radiative pathways. Radiative recombination, stemming from the reciprocity between absorption and spontaneous emission, is an unavoidable process as described by Shockley and Queisser.[149] Non-radiative recombination, often triggered by trap states in inorganic semiconductors, is further exacerbated by strong molecular vibrations in organic materials characterized by carbon and carbon double bonds, which facilitate quantum tunneling between vibronic modes from excited states to ground states, predominantly through CT states.[87,118,150] This loss pathway leads to intrinsically larger non-radiative energy losses in OPVs compared with inorganic counterparts (e.g., silicon and GaAs) and perovskite PVs.[151,152] Therefore, energy loss, defined as $E_{loss} = E_g - qV_{oc}$, where q is the elementary charge and E_g is the E_g of photoactive materials, represents a major issue in OPVs and can also further be detailed as $E_{loss} = q(\Delta V_{oc,sq} + \Delta V_{oc,rad} + \Delta V_{oc,nr})$, where $\Delta V_{oc,sq}$ is the SQ limit of radiative voltage loss, $\Delta V_{oc,rad}$ arises from absorption of sub-band gap or tail states, and $\Delta V_{oc,nr}$ is attributed to non-radiative recombination, as illustrated in Figure 8A.[153,154] The physical details behind voltage loss analysis can be found elsewhere.[87,118] Although there is a lack of sufficient data for a rigorous analysis of radiative and non-radiative voltage losses in SC-OPVs, collected data on the total energy loss could provide an idea of the gaps between SC-OPVs and BHJ-OPVs, as shown in Figure 8B.

Historically, energy losses from 0.7 eV to 1.0 eV are typical for fullerene-acceptor-based BHJ-OPVs,[155] which means almost half of the photon energy is lost during power conversion, which restricts the PCE to roughly 12%. Nevertheless, BHJ-OPVs that utilize FREAs often exhibit reduced energy losses, often below 0.5 eV, as demonstrated in Figure 8B. This is believed to arise from a combined effect of state hybridization[156,157] and thermal repopulation[158] due to reduced offset between LE and CT states. For SC-OPVs, although BCP-based systems have shown promising efficiency improvements in recent years, substantial energy loss (> 0.7 eV) for other types of SC-OPVs remains a limiting factor, as shown in Figure 8B.

It's worth mentioning that, in traditional BHJ-OPVs, which mix donor and acceptor materials, disorder is inevitable and contributes significantly to non-radiative recombination and associated energy losses.[118,150] By contrast, SC systems, where donor and acceptor units are covalently bonded, have the potential to exhibit more controlled phase separation and reduced energetic disorder. However, as depicted in Figure 8B, these systems still experience significant energy losses that have not yet reached satisfactory levels. Various models to quantify energy losses in BHJ-OPVs have been proposed but are yet to be extended to SC-OPVs.[118,150,152,156–158] An in-depth investigation of energy losses in SC-OPVs is crucial for the development of novel materials with reduced energy losses and could greatly contribute to the progress of SC-OPV technology as a whole.

Charge transport

Charge transport also remains a big problem in SC-OPVs, in which balanced and dual-channel transport for electrons and holes is generally missing. Compared with SC-OPVs, the majority of high-efficiency BHJ-OPV devices exhibit relatively balanced hole and electron mobilities, with μ_h/μ_e approaching unity. This balance is likely attributed to the "dual-channel" structure of BHJs, which facilitates carrier transport by providing distinct pathways for both types of charge carriers, i.e., holes and electrons travel through the donor and acceptor domains, respectively. While earlier SC-OPV devices generally exhibited

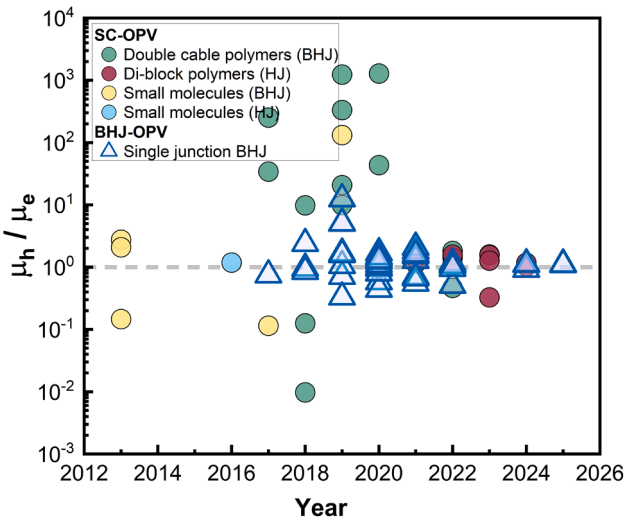

Figure 9. Evolution of mobility balance in SC- and BHJ-OPVs over publication years

Logarithm of the ratio of hole and electron mobility as a function of publication year for various SC-OPVs and BHJ-OPVs.

imbalanced carrier mobilities, recent advancements, particularly with BCP-based OPVs, have led to more balanced carrier mobilities, as highlighted in Figure 9. However, the limited data on carrier mobilities in SC-OPV devices poses a significant challenge, hindering a comprehensive analysis of the carrier transport properties in these systems. This gap in understanding remains a critical issue for ongoing research efforts. To resolve such an issue, quantifying charge-transport mobility is crucial, yet still a major difficulty in OPV research at large, primarily because of the intrinsic energetic disorder in organic materials and the complexity of data analysis.

Space-charge-limited current (SCLC),[159] organic field-effect transistor (OFET),[160] and time-of-flight (ToF)[161] measurements are commonly used techniques to measure carrier mobility in organic semiconductors. ToF experiments typically necessitate film thickness exceeding 1 micron, which is difficult to achieve in practice and therefore not suitable for standard OPV mobility testing. OFET operates under a "high injection condition" that is fundamentally distinct from the operating state of OPVs. Under high injection conditions, the defect states are easily filled up, thereby hindering the acquisition of critical parameters like trap state distribution. Consequently, OFET is not the optimal experimental method for OPV mobility testing. By contrast, the SCLC method does not require thick films, and the measurements operate under a relatively "low injection condition" that closely emulates the charge injection conditions of OPVs. Therefore, the SCLC approach is widely utilized as the primary mobility testing technique in the field of OPVs.

Nevertheless, studies on SCLC experiments in existing literature in both BHJ-OPVs and SC-OPVs frequently utilize the idealized Mott-Gurney (MG) model. This model assumes the following conditions: (1) the material is defect-free and lacks energetic disorder, (2) the concentration of the intrinsic carrier is insignificant during current flow, (3) the current density is solely determined by drift, and (4) both injection and extraction contacts are Ohmic. However, those conditions are rarely met in OPVs. Therefore, adopting the MG law without careful consideration might lead to significant mistakes in the values of mobilities.[162] As a solution, using a numerical drift-diffusion model based on the multiple trapping and release framework, Nelson and their team analyzed experimental SCLC data across various thicknesses and temperatures, providing insights into non-ideal factors such as defect state distribution.[89,163] They also observed that the injection barrier and trap combination can both produce a current density to voltage slope of 2 on a double logarithmic scale, in which case mobility values could be wrong if analyzed using the MG law.[162] Their approach allowed for a more nuanced understanding of these factors, rather than presenting absolute conclusions. Similar models are also frequently used in the literature, such as the Gaussian disorder model by Kemerink et al.[164] Although SCLC is experimentally accessible, it typically yields an effective mobility that can be distorted by non-ohmic or asymmetric contacts, injection barriers, unintentional doping, trap filling, series resistance, and thickness-dependent field profiles, so single-slope fits can misrepresent both absolute values and trends.[165] We therefore recommend that mobility measurements report the full fitting assumptions (contact and trap models, treatment of field dependence) together with key device conditions such as contact selectivity, injection barriers, thickness regime, and series resistance. Whenever possible, SCLC results should be benchmarked against at least one complementary approach that probes transport under varying charge-carrier densities, such as impedance-based transport resistance, transient measurements, or drift-diffusion model verification.[166]

Theoretical investigations into the mechanisms of charge transport in SC-OPVs are extremely lacking, partially due to the complicated nature of donor and acceptor networks as well as the limited research attention on SC-OPVs. Currently, theoretical methods employed in organic semiconductors include transient localization theory (TLT) hopping based on Marcus theory using KMC, the Kubo formula solved by finite temperature time-dependent density matrix renormalization group (TD-DMRG), and quantum Monte Carlo techniques (QMCs).[167] Recently, a foundational understanding of the impact of transfer integrals, reorganization energy, and dynamic disorder on carrier mobility in organic semiconductors has been established.[168] A high transfer integral facilitates band-like transport and enhances carrier mobility. The influence of reorganization energy and dynamic disorder on carrier mobility presents a more complex scenario. Specifically, if the reorganization of energy is high, dynamic disorder can enhance mobility due to phonon-assisted current. Conversely, when the reorganization energy is low or moderate, dynamic disorder emerges as a constraining factor for charge transport, with the carrier diffusion occurring via transient localization. Overall, it is preferred to reduce both reorganization energy and dynamic disorder. Additional determining factors of carrier mobility include the topology of the carrier transport network, the relative phase of the transfer integral for different molecule pairs, and the magnitude of static disorder.[167] Recent studies have also shown that charge transport in crystalline and ordered organic semiconductors is likely enhanced by the "transient delocalization" of charge carriers but could also be significantly slowed down due to large disorder

Please cite this article in press as: Ma et al., Physical insights into single-component organic photovoltaics, Joule (2026), https://doi.org/10.1016/j.joule.2026.102397

in electrostatics in organic thin films.[163,169] Those studies provide a solid foundation for the understanding of charge-transport mechanisms in organic semiconductors yet remain to be explored in SC materials, in which donor and acceptor networks are extremely complicated. A tightly integrated experimental and theoretical investigation into the mechanisms of charge transport in SC materials is desirable for the further development of SC-OPVs.

OUTLOOK

We have demonstrated that SC-OPVs offer a fundamental advantage in operational stability, owing to the covalent bonding between donor and acceptor units, as compared with their BHJ counterparts. However, the broader adoption of this promising technology has been limited by its comparatively lower performance. In the following discussion, we outline several strategic pathways to achieve this goal, including molecular design, morphology control, and advanced characterization, all aimed at unlocking the full potential of SC-OPV devices.

Molecular design

To make the rapidly expanding SC-OPV materials space translate into predictive design rules, we begin by identifying the dominant charge generation pathway and classifying systems accordingly. This framing naturally separates two archetypes. In BHJ-like SC-OPV (dyads, triads, and many double-cable polymers), the covalent connection suppresses macroscopic demixing, but efficient devices still require donor-enriched and acceptor-enriched regions that provide sufficient D/A interfacial area and continuous pathways for both carriers.[46] Moreover, future design progress is more reliable when linker rigidity reduces conformational disorder, yet steric design prevents over-coplanar stacking, and when optimization is benchmarked against device-relevant metrics such as CT-state disorder, recombination and extraction kinetics, and non-radiative voltage losses rather than PCE alone.[39,43,88,118] In turn, for the HJ-type picture, which is particularly relevant to conjugated BCPs and HJ small molecules, the decisive step is charge separation across internal junctions within an SC film (e.g., between domains with distinct packing or orientation), where packing- and orientation-dependent electrostatic potential offsets can lower the effective barrier for CT dissociation.[28]

Within either archetype, backbone and side chains play different yet complementary roles. The backbone largely defines the electronic structure and energetics that govern absorption and charge generation, namely the E_g, the energy, and the delocalization of the CT state. It also sets the strength of electronic coupling along and between chains that ultimately limits charge transport. For this reason, backbone engineering is often essential when the aim is to suppress voltage losses and increase charge generation.[170,171] Side chains, by contrast, frequently provide the most practical leverage in SC-OPV because they simultaneously regulate solubility and solution-state aggregation, steer the crystallization and molecular orientation, and tune the balance between D/A segregation and interfacial mixing that governs between free-charge generation and recombination.[84,172]

The efficiencies now reached by SC-OPVs (reported in this review) justify a more predictive molecular design direction, where further improvements are expected from polar and suitable branched side chains that regulate D/A segregation and strengthen dielectric screening of the Coulomb interaction, from backbone planarization and conformational restraint that raise carrier mobilities without promoting excessive crystallinity in a single segment, and from steric plus local dipolar engineering at the covalently linked D/A junction that increases free-charge generation efficiency while suppressing aggregation-driven non-radiative recombination.

Morphology control

In SC-OPVs, morphology control is less about suppressing macroscopic demixing and more about steering self-assembly toward a nanoscale donor/acceptor network that is continuous for both carriers and remains stable under thermal, photo, and bias stress. The morphological target is the simultaneous satisfaction of sufficient internal D-A interfacial area for charge generation, transport pathways for charge extraction, and kinetic stability of that network.

For BHJ-like SC-OPVs such as double-cable polymers, thermal annealing and solvent vapor treatments remain effective because they tune backbone ordering while allowing pendant acceptors to reorganize, thereby adjusting nanophase separation, transport, and non-geminate recombination in a chemically tethered morphology.[21,33,46] A more predictive processing strategy is to connect processing variables to measurable descriptors, such as backbone crystalline coherence, acceptor aggregate size/distribution, and vertical composition gradients that influence contact selectivity rather than relying on empirical optimization alone.[173,174] At the same time, controlling solution-state aggregation and solvent selectivity is a direct route to forming desirable nanostructures prior to solidification, which can then be partially retained because covalent linkage reduces the driving force for large-scale reorganization after film formation.[46,175]

For conjugated BCP SC-OPVs, microphase separation provides a built-in route to covalently linked donor-rich and acceptor-rich transport pathways, making morphology tuning more systematic. Here, block ratio, molecular weight, and dispersity directly set domain spacing and connectivity, and a domain dimension comparable to exciton diffusion lengths is repeatedly identified as a key constraint for efficient charge generation.[53,176] Accordingly, "chemical precision" (here referring to well-defined block lengths and dispersity, high end-group fidelity, and minimized structural/compositional defects) is best treated as a morphology tool because it stabilizes the intended microphase-separated solid-state structure and reduces connectivity bottlenecks that, otherwise, elevate recombination under operating conditions.[83,177]

Advanced characterization

Accurate characterization of exciton and charge dynamics is at the heart of advancing the performance of SC-OPVs. As we discussed above, the early-time dynamics of photogenerated excitons are essential for efficient charge generation, followed by efficient charge transport along continuous transporting pathways. Future research should be focused on properly

characterizing the dynamics of exciton and charge dynamics, assisted by theoretical and computational modeling.

At early times, the US should be used to separate two questions that are often conflated: how rapidly photoexcited excitons evolve into interfacial CT excitons, and on what timescale those CT excitons separate into free charges that contribute to photocurrent.[117] Conventional pump-probe TA and TRPL remain essential to track exciton decay and the emergence of CT-like signatures, but TA amplitudes alone should not be taken as a quantitative free-charge generation efficiency because CT state and free charge spectral responses can overlap, especially in optimized devices where charge separation is efficient.[178] A more discriminating approach is therefore to pair TA/TRPL with pump-push photocurrent or pump-push photoluminescence and related multi-pulse schemes that directly perturb bound populations and read out their contribution to device response so that the role of bound CT states can be isolated rather than inferred indirectly.[179,180] Temperature- and field-dependent variants of these measurements can then be used to test whether charge generation is limited by CT dissociation (or by the thermal accessibility of delocalized configurations) rather than by the initial formation of CT character, which is particularly relevant for low-offset, low-voltage-loss designs.[117] In parallel, ultrafast results should be co-reported with a quantitative descriptor of CT-state energetic disorder, because increasing static disorder of the CT manifold has been shown to increase non-radiative voltage losses and reduce the radiative V_{OC}, making CT disorder a concrete target for simultaneously improving Voc and efficiency.[118]

On the transport side, the characterization priority in SC-OPVs is not "the mobility" as a single number, but identifying which element of the tethered transport network limits transport at the operating point: the hole-conducting pathway, the electron-conducting pathway, a bottleneck at internal boundaries, or imperfect contact that promotes interfacial recombination.[88,181] SCLC methods can be informative when implemented carefully, but mobility extraction is only reliable when injection barriers, contact asymmetry, and field-dependent transport are explicitly considered and when the conclusions are cross-checked against drift-diffusion modeling rather than a single analytic fit.[166,182,183] A forward-looking addition is to quantify bias- and light-dependent "transport resistance" or collection losses and to connect them with trap formation and microstructural bottlenecks because these effects can dominate FF losses and accelerate degradation even when voltage losses are already suppressed.[184]

Finally, recombination dynamics should be parameterized under operating conditions and interpreted together with carrier-density-dependent characteristics, rather than inferred from a single open-circuit transient that may not map onto the recombination pathways near the maximum power piont.[88] In practice, modifications to transient photovoltage decay are also recommended to directly probe the free charge lifetime.[185] As the transient photovoltage (TPV) decay constant is a small-perturbation effective lifetime, which can be influenced by charge redistribution, capacitive effects, and transport bottlenecks when collection is not ideal, therefore, interpretation may benefit from drift-diffusion modeling that treats extraction and recombination within one consistent framework.[186,187] Establishing a standard characterization package that includes morphology descriptors, bound-state selective ultrafast kinetics, transport under bias, and recombination parameters extracted at matched carrier density would make structure-to-function iteration more predictive and accelerate progress across SC-OPV material families.

CONCLUSION

In this review, we have outlined the recent progress and key challenges in terms of performance in SC-OPVs. We discussed different molecular structures and their unique potential in enhancing device stability. We highlighted the efficiency gap between SC-OPVs and traditional BHJ-OPVs and provided detailed physical insights into the operation of SC-OPVs and suggestions on how to tackle those challenges. Future work should be focused on precise molecular control of the complicated and large molecular structures of SC materials. Together with advanced experimental probes and computational frameworks, one should aim to establish a proper structure-property relationship that can help future efficiency development. While this review is primarily focused on the physical insights into the device's performance, additional work is also needed to enhance its operational stability and to reduce its synthetic complexity.

ACKNOWLEDGMENTS

J.Y. acknowledges funding support from the National Natural Science Foundation of China (nos. 62404191 and 62574175), the Guangdong Basic and Applied Basic Research Foundation (nos. 2023A1515111140 and 2024A1515012318), the Guangdong Provincial Program (no. 2023QN10C144), the Shenzhen Science and Technology Program (nos. KQTD20240729102028011 and JCYJ20240813113553067), and the Guangdong Basic Research Center of Excellence for Aggregate Science. The authors thank Jenny Nelson and Jolanda Muller for fruitful discussions.

AUTHOR CONTRIBUTIONS

W.M. and L.L. contributed equally to this work. W.M., L.L., and J.Y. prepared the manuscript. All authors contributed to the revision of the manuscript. J.Y. supervised this work.

DECLARATION OF INTERESTS

The authors declare no competing interests.

SUPPLEMENTAL INFORMATION

Supplemental information can be found online at https://doi.org/10.1016/j.joule.2026.102397.

REFERENCES

1. Yan, N., Zhao, C., You, S., Zhang, Y., and Li, W. (2020). Recent progress of thin-film photovoltaics for indoor application. Chin. Chem. Lett. *31*, 643–653. https://doi.org/10.1016/j.cclet.2019.08.022.
2. Needell, D.R., Phelan, M.E., Hartlove, J.T., and Atwater, H.A. (2021). Solar power windows: Connecting scientific advances to market signals. Energy *219*, 119567. https://doi.org/10.1016/j.energy.2020.119567.
3. Gao, W., Ota, H., Kiriya, D., Takei, K., and Javey, A. (2019). Flexible Electronics toward Wearable Sensing. Acc. Chem. Res. *52*, 523–533. https://doi.org/10.1021/acs.accounts.8b00500.

4. Qin, J., Lan, L., Chen, S., Huang, F., Shi, H., Chen, W., Xia, H., Sun, K., and Yang, C. (2020). Recent Progress in Flexible and Stretchable Organic Solar Cells. Adv. Funct. Mater. *30*, 2002529. https://doi.org/10.1002/adfm.202002529.

5. Zhang, L., He, Y., Deng, W., Guo, X., Bi, Z., Zeng, J., Huang, H., Zhang, G., Xie, C., Zhang, Y., et al. (2024). High-efficiency flexible organic solar cells with a polymer-incorporated pseudo-planar heterojunction. Discov. Nano *19*, 39. https://doi.org/10.1186/s11671-024-03982-1.

6. Zhang, M., Zhang, C., Yang, Y., Ren, H., Zhang, J., Zhao, X., Tong, Y., Tang, Q., and Liu, Y. (2021). Highly Stable Nonhydroxyl Antisolvent Polymer Dielectric: A New Strategy towards High-Performance Low-Temperature Solution-Processed Ultraflexible Organic Transistors for Skin-Inspired Electronics. Research (Wash DC) *2021*, 9897353. https://doi.org/10.34133/2021/9897353.

7. Forrest, S.R. (2004). The path to ubiquitous and low-cost organic electronic appliances on plastic. Nature *428*, 911–918. https://doi.org/10.1038/nature02498.

8. Halls, J.J.M., Walsh, C.A., Greenham, N.C., Marseglia, E.A., Friend, R.H., Moratti, S.C., and Holmes, A.B. (1995). Efficient photodiodes from interpenetrating polymer networks. Nature *376*, 498–500. https://doi.org/10.1038/376498a0.

9. Yu, G., Gao, J., Hummelen, J.C., Wudl, F., and Heeger, A.J. (1995). Polymer Photovoltaic Cells: Enhanced Efficiencies via a Network of Internal Donor-Acceptor Heterojunctions. Science *270*, 1789–1791. https://doi.org/10.1126/science.270.5243.1789.

10. Cui, Y., Yao, H., Zhang, J., Xian, K., Zhang, T., Hong, L., Wang, Y., Xu, Y., Ma, K., An, C., et al. (2020). Single-Junction Organic Photovoltaic Cells with Approaching 18% Efficiency. Adv. Mater. *32*, e1908205. https://doi.org/10.1002/adma.201908205.

11. Fan, B., Zhang, D., Li, M., Zhong, W., Zeng, Z., Ying, L., Huang, F., and Cao, Y. (2019). Achieving over 16% efficiency for single-junction organic solar cells. Sci. China Chem. *62*, 746–752. https://doi.org/10.1007/s11426-019-9457-5.

12. Lin, Y., Firdaus, Y., Nugraha, M.I., Liu, F., Karuthedath, S., Emwas, A.-H., Zhang, W., Seitkhan, A., Neophytou, M., Faber, H., et al. (2020). 17.1% Efficient Single-Junction Organic Solar Cells Enabled by n-Type Doping of the Bulk-Heterojunction. Adv. Sci. (Weinh) *7*, 1903419. https://doi.org/10.1002/advs.201903419.

13. Cui, Y., Xu, Y., Yao, H., Bi, P., Hong, L., Zhang, J., Zu, Y., Zhang, T., Qin, J., Ren, J., et al. (2021). Single-Junction Organic Photovoltaic Cell with 19% Efficiency. Adv. Mater. *33*, e2102420. https://doi.org/10.1002/adma.202102420.

14. Chen, H., Huang, Y., Zhang, R., Mou, H., Ding, J., Zhou, J., Wang, Z., Li, H., Chen, W., Zhu, J., et al. (2025). Organic solar cells with 20.82% efficiency and high tolerance of active layer thickness through crystallization sequence manipulation. Nat. Mater. *24*, 444–453. https://doi.org/10.1038/s41563-024-02062-0.

15. Zhu, L., Zhang, M., Zhou, G., Wang, Z., Zhong, W., Zhuang, J., Zhou, Z., Gao, X., Kan, L., Hao, B., et al. (2024). Achieving 20.8% organic solar cells via additive-assisted layer-by-layer fabrication with bulk p-i-n structure and improved optical management. Joule *8*, 3153–3168. https://doi.org/10.1016/j.joule.2024.08.001.

16. Li, C., Song, J., Lai, H., Zhang, H., Zhou, R., Xu, J., Huang, H., Liu, L., Gao, J., Li, Y., et al. (2025). Non-fullerene acceptors with high crystallinity and photoluminescence quantum yield enable >20% efficiency organic solar cells. Nat. Mater. *24*, 433–443. https://doi.org/10.1038/s41563-024-02087-5.

17. Tarique, W.B., and Uddin, A. (2023). A review of progress and challenges in the research developments on organic solar cells. Mater. Sci. Semicond. Process. *163*, 107541. https://doi.org/10.1016/j.mssp.2023.107541.

18. Wang, Y., Lee, J., Hou, X., Labanti, C., Yan, J., Mazzolini, E., Parhar, A., Nelson, J., Kim, J.-S., and Li, Z. (2021). Recent Progress and Challenges toward Highly Stable Nonfullerene Acceptor-Based Organic Solar Cells. Adv. Energy Mater. *11*, 2003002. https://doi.org/10.1002/aenm.202003002.

19. Song, J., Zhang, M., Hao, T., Yan, J., Zhu, L., Zhou, G., Zeng, R., Zhong, W., Xu, J., Zhou, Z., et al. (2022). Design Rules of the Mixing Phase and Impacts on Device Performance in High-Efficiency Organic Photovoltaics. Research (Wash DC) *2022*, 9817267. https://doi.org/10.34133/2022/9817267.

20. Roncali, J., and Grosu, I. (2019). The Dawn of Single Material Organic Solar Cells. Adv. Sci. (Weinh) *6*, 1801026. https://doi.org/10.1002/advs.201801026.

21. He, Y., Heumüller, T., Lai, W., Feng, G., Classen, A., Du, X., Liu, C., Li, W., Li, N., and Brabec, C.J. (2019). Evidencing Excellent Thermal- and Photostability for Single-Component Organic Solar Cells with Inherently Built-In Microstructure. Adv. Energy Mater. *9*, 1900409. https://doi.org/10.1002/aenm.201900409.

22. Cheng, Y., Mao, Q., Zhou, C., Huang, X., Liu, J., Deng, J., Sun, Z., Jeong, S., Cho, Y., Zhang, Y., et al. (2023). Regulating the Sequence Structure of Conjugated Block Copolymers Enables Large-Area Single-Component Organic Solar Cells with High Efficiency and Stability. Angew. Chem. Int. Ed. *62*, e202308267. https://doi.org/10.1002/anie.202308267.

23. He, Y., Li, N., and Brabec, C.J. (2021). Single-Component Organic Solar Cells with Competitive Performance. Org. Mater. *03*, 228–244. https://doi.org/10.1055/s-0041-1727234.

24. Luke, J., Yang, E.J., Labanti, C., Park, S.Y., and Kim, J.-S. (2023). Key molecular perspectives for high stability in organic photovoltaics. Nat. Rev. Mater. *8*, 839–852. https://doi.org/10.1038/s41578-023-00606-5.

25. Wu, M., Ma, B., Li, S., Han, J., and Zhao, W. (2023). Powering the Future: A Critical Review of Research Progress in Enhancing Stability of High-Efficiency Organic Solar Cells. Adv. Funct. Mater. *33*, 2305445. https://doi.org/10.1002/adfm.202305445.

26. Sun, R., Wu, Q., Guo, J., Wang, T., Wu, Y., Qiu, B., Luo, Z., Yang, W., Hu, Z., Guo, J., et al. (2020). A Layer-by-Layer Architecture for Printable Organic Solar Cells Overcoming the Scaling Lag of Module Efficiency. Joule *4*, 407–419. https://doi.org/10.1016/j.joule.2019.12.004.

27. Zhou, W., Dai, X., Fan, B., Li, H., Xu, X., Wu, Y., and Peng, Q. (2025). Solvent vapor diffusion–driven multiscale pre-aggregation of non-fullerene acceptors enables high-performance organic solar cells. Nat. Commun. *16*, 11188. https://doi.org/10.1038/s41467-025-66199-5.

28. Dong, Y., Nikolis, V.C., Talnack, F., Chin, Y.-C., Benduhn, J., Londi, G., Kublitski, J., Zheng, X., Mannsfeld, S.C.B., Spoltore, D., et al. (2020). Orientation dependent molecular electrostatics drives efficient charge generation in homojunction organic solar cells. Nat. Commun. *11*, 4617. https://doi.org/10.1038/s41467-020-18439-z.

29. Eckert, J.-F., Nicoud, J.-F., Nierengarten, J.-F., Liu, S.-G., Echegoyen, L., Barigelletti, F., Armaroli, N., Ouali, L., Krasnikov, V., and Hadziioannou, G. (2000). Fullerene−Oligophenylenevinylene Hybrids: Synthesis, Electronic Properties, and Incorporation in Photovoltaic Devices. J. Am. Chem. Soc. *122*, 7467–7479. https://doi.org/10.1021/ja9941072.

30. Wu, Y., Fan, Q., Fan, B., Qi, F., Wu, Z., Lin, F.R., Li, Y., Lee, C.-S., Woo, H.Y., Yip, H.-L., et al. (2022). Non-Fullerene Acceptor Doped Block Copolymer for Efficient and Stable Organic Solar Cells. ACS Energy Lett. *7*, 2196–2202. https://doi.org/10.1021/acsenergylett.2c01082.

31. Cheng, Y., Huang, B., Mao, Q., Huang, X., Liu, J., Zhou, C., Zhou, W., Ren, X., Kim, S., Kim, W., et al. (2024). Three-in-One Strategy Enables Single-Component Organic Solar Cells with Record Efficiency and High Stability. Adv. Mater. *36*, e2312938. https://doi.org/10.1002/adma.202312938.

32. Lai, W., Li, C., Zhang, J., Yang, F., Colberts, F.J.M., Guo, B., Wang, Q.M., Li, M., Zhang, A., Janssen, R.A.J., et al. (2017). Diketopyrrolopyrrole-Based Conjugated Polymers with Perylene Bisimide Side Chains for Single-Component Organic Solar Cells. Chem. Mater. *29*, 7073–7077. https://doi.org/10.1021/acs.chemmater.7b02534.

33. Liang, S., Xu, Y., Jiang, X., Li, C., and Li, W. (2019). Correlating crystallinity to photovoltaic performance in single-component organic solar cells via conjugated backbone engineering. Dyes Pigments *170*, 107575. https://doi.org/10.1016/j.dyepig.2019.107575.

34. Yang, F., Wang, X., Feng, G., Ma, J., Li, C., Li, J., Ma, W., and Li, W. (2018). A new strategy for designing polymer electron acceptorsc: electronrich conjugated backbone with electron-deficient side units. Sci. China Chem. *61*, 824–829. https://doi.org/10.1007/s11426-018-9241-0.

35. Li, C., Yu, C., Lai, W., Liang, S., Jiang, X., Feng, G., Zhang, J., Xu, Y., and Li, W. (2018). Multifunctional Diketopyrrolopyrrole-Based Conjugated Polymers with Perylene Bisimide Side Chains. Macromol. Rapid Commun. *39*, e1700611. https://doi.org/10.1002/marc.201700611.

36. Liang, S., Xu, Y., Li, C., Li, J., Wang, D., and Li, W. (2019). Realizing lamellar nanophase separation in a double-cable conjugated polymer via a solvent annealing process. Polym. Chem. *10*, 4584–4592. https://doi.org/10.1039/C9PY00765B.

37. Feng, G., Li, J., Colberts, F.J.M., Li, M., Zhang, J., Yang, F., Jin, Y., Zhang, F., Janssen, R.A.J., Li, C., et al. (2017). "Double-Cable" Conjugated Polymers with Linear Backbone toward High Quantum Efficiencies in Single-Component Polymer Solar Cells. J. Am. Chem. Soc. *139*, 18647–18656. https://doi.org/10.1021/jacs.7b10499.

38. Lanzi, M., and Pierini, F. (2019). Effect of Electron-Acceptor Content on the Efficiency of Regioregular Double-Cable Thiophene Copolymers in Single-Material Organic Solar Cells. ACS Omega *4*, 19863–19874. https://doi.org/10.1021/acsomega.9b02790.

39. Li, C., Wu, X., Sui, X., Wu, H., Wang, C., Feng, G., Wu, Y., Liu, F., Liu, X., Tang, Z., et al. (2019). Crystalline Cooperativity of Donor and Acceptor Segments in Double-Cable Conjugated Polymers toward Efficient Single-Component Organic Solar Cells. Angew. Chem. Int. Ed. *131*, 15678–15686. https://doi.org/10.1002/ange.201910489.

40. Liang, S., Liu, B., Karuthedath, S., Wang, J., He, Y., Tan, W.L., Li, H., Xu, Y., Li, N., Hou, J., et al. (2022). Double-Cable Conjugated Polymers with Pendent Near-Infrared Electron Acceptors for Single-Component Organic Solar Cells. Angew. Chem. Int. Ed. *61*, e202209316. https://doi.org/10.1002/anie.202209316.

41. Lanzi, M., Salatelli, E., Marinelli, M., and Pierini, F. (2020). Effect of Photocrosslinking of D-A Thiophene Copolymers on the Performance of Single-Material Solar Cells. Macromol. Chem. Phys. *221*, 1900433. https://doi.org/10.1002/macp.201900433.

42. Yang, F., Li, J., Li, C., and Li, W. (2019). Improving Electron Transport in a Double-Cable Conjugated Polymer via Parallel Perylenetriimide Design. Macromolecules *52*, 3689–3696. https://doi.org/10.1021/acs.macromol.9b00495.

43. Jiang, X., Yang, J., Karuthedath, S., Li, J., Lai, W., Li, C., Xiao, C., Ye, L., Ma, Z., Tang, Z., et al. (2020). Miscibility-Controlled Phase Separation in Double-Cable Conjugated Polymers for Single-Component Organic Solar Cells with Efficiencies over 8 %. Angew. Chem. Int. Ed. *132*, 21867–21876. https://doi.org/10.1002/ange.202009272.

44. Pierini, F., Lanzi, M., Nakielski, P., Pawłowska, S., Urbanek, O., Zembrzycki, K., and Kowalewski, T.A. (2017). Single-Material Organic Solar Cells Based on Electrospun Fullerene-Grafted Polythiophene Nanofibers. Macromolecules *50*, 4972–4981. https://doi.org/10.1021/acs.macromol.7b00857.

45. Yu, P., Feng, G., Li, J., Li, C., Xu, Y., Xiao, C., and Li, W. (2020). A selenophene substituted double-cable conjugated polymer enables efficient single-component organic solar cells. J. Mater. Chem. C *8*, 2790–2797. https://doi.org/10.1039/C9TC06667E.

46. Feng, G., Li, J., He, Y., Zheng, W., Wang, J., Li, C., Tang, Z., Osvet, A., Li, N., Brabec, C.J., et al. (2019). Thermal-Driven Phase Separation of Double-Cable Polymers Enables Efficient Single-Component Organic Solar Cells. Joule *3*, 1765–1781. https://doi.org/10.1016/j.joule.2019.05.008.

47. Zhang, Z., Wang, J., Hu, Z., Xiao, C., Chen, Q., Tang, Z., and Li, W. (2023). Low temperature, non-halogen solvent processed single-component organic solar cells with 10% efficiency. Chin. Chem. Lett. *34*, 108527. https://doi.org/10.1016/j.cclet.2023.108527.

48. Liang, S., Xiao, C., Xie, C., Liu, B., Fang, H., and Li, W. (2023). 13% Single-Component Organic Solar Cells based on Double-Cable Conjugated Polymers with Pendent Y-Series Acceptors. Adv. Mater. *35*, e2300629. https://doi.org/10.1002/adma.202300629.

49. Li, Y., Pacalaj, R.A., Luo, Y., Ai, K., Hai, Y., Liang, S., Fan, K., Sergeev, A.A., Ma, R., Dela Peña, T.A., et al. (2025). Molecular Control of the Donor/Acceptor Interface Suppresses Charge Recombination Enabling High-Efficiency Single-Component Organic Solar Cells. Adv. Mater. *37*, e2409212. https://doi.org/10.1002/adma.202409212.

50. Narayanaswamy, K., Venkateswararao, A., Nagarjuna, P., Bishnoi, S., Gupta, V., Chand, S., and Singh, S.P. (2016). An Organic Dyad Composed of Diathiafulvalene-Functionalized Diketopyrrolopyrrole–Fullerene for Single-Component High-Efficiency Organic Solar Cells. Angew. Chem. Int. Ed. *55*, 12334–12337. https://doi.org/10.1002/anie.201602969.

51. Lee, D.H., Lee, J.H., Kim, H.J., Choi, S., Park, G.E., Cho, M.J., and Choi, D.H. (2017). (D)n–σ–(A)m type partially conjugated block copolymer and its performance in single-component polymer solar cells. J. Mater. Chem. A *5*, 9745–9751. https://doi.org/10.1039/C7TA01819C.

52. Chen, P., Nakano, K., Suzuki, K., Hashimoto, K., Kikitsu, T., Hashizume, D., Koganezawa, T., and Tajima, K. (2017). Organic Solar Cells with Controlled Nanostructures Based on Microphase Separation of Fullerene-Attached Thiophene-Selenophene Heteroblock Copolymers. ACS Appl. Mater. Interfaces *9*, 4758–4768. https://doi.org/10.1021/acsami.6b14629.

53. Guo, C., Lin, Y.-H., Witman, M.D., Smith, K.A., Wang, C., Hexemer, A., Strzalka, J., Gomez, E.D., and Verduzco, R. (2013). Conjugated Block Copolymer Photovoltaics with near 3% Efficiency through Microphase Separation. Nano Lett. *13*, 2957–2963. https://doi.org/10.1021/nl401420s.

54. Lee, J.H., Park, C.G., Kim, A., Kim, H.J., Kim, Y., Park, S., Cho, M.J., and Choi, D.H. (2018). High-Performance Polymer Solar Cell with Single Active Material of Fully Conjugated Block Copolymer Composed of Wide-Band gap Donor and Narrow-Band gap Acceptor Blocks. ACS Appl. Mater. Interfaces *10*, 18974–18983. https://doi.org/10.1021/acsami.8b03580.

55. Li, S., Yuan, X., Zhang, Q., Li, B., Li, Y., Sun, J., Feng, Y., Zhang, X., Wu, Z., Wei, H., et al. (2021). Narrow-Bandgap Single-Component Polymer Solar Cells with Approaching 9% Efficiency. Adv. Mater. *33*, e2101295. https://doi.org/10.1002/adma.202101295.

56. Kwon, N.Y., Park, S.H., Kang, H., Takaloo, A.V., Harit, A.K., Woo, H.Y., Kim, T.G., Yoon, H.J., Cho, M.J., and Choi, D.H. (2020). Rational design of a main chain conjugated copolymer having donor–acceptor heterojunctions and its application in indoor photovoltaic cells. J. Mater. Chem. A *8*, 20091–20100. https://doi.org/10.1039/D0TA06420C.

57. Park, S.H., Kim, Y., Kwon, N.Y., Lee, Y.W., Woo, H.Y., Chae, W.-S., Park, S., Cho, M.J., and Choi, D.H. (2020). Significantly Improved Morphology and Efficiency of Nonhalogenated Solvent-Processed Solar Cells Derived from a Conjugated Donor–Acceptor Block Copolymer. Adv. Sci. (Weinh) *7*, 1902470. https://doi.org/10.1002/advs.201902470.

58. Liu, B., Sun, H., Lee, J.-W., Jiang, Z., Qiao, J., Wang, J., Yang, J., Feng, K., Liao, Q., An, M., et al. (2023). Efficient and stable organic solar cells enabled by multicomponent photoactive layer based on one-pot polymerization. Nat. Commun. *14*, 967. https://doi.org/10.1038/s41467-023-36413-3.

59. Phan, T.N.-L., Lee, J.-W., Oh, E.S., Lee, S., Lee, C., Kim, T.-S., Li, S., and Kim, B.J. (2022). Efficient and Nonhalogenated Solvent-Processed Organic Solar Cells Enabled by Conjugated Donor–Acceptor Block Copolymers Containing the Same Benzodithiophene Unit. ACS Appl. Mater. Interfaces *14*, 57070–57081. https://doi.org/10.1021/acsami.2c16908.

60. Wu, Y., Guo, J., Wang, W., Chen, Z., Chen, Z., Sun, R., Wu, Q., Wang, T., Hao, X., Zhu, H., et al. (2021). A conjugated donor-acceptor block

copolymer enables over 11% efficiency for single-component polymer solar cells. Joule *5*, 1800–1815. https://doi.org/10.1016/j.joule.2021.05.002.

61. Guo, J., Wu, Y., Wang, W., Wang, T., and Min, J. (2022). Achieving 12.6% Efficiency in Single-Component Organic Solar Cells Processed from Nonhalogenated Solvents. Sol. RRL *6*, 2101024. https://doi.org/10.1002/solr.202101024.

62. Yang, X., Wu, Y., Gao, Y., Guo, J., Wang, W., and Min, J. (2023). Over 13% Efficient Single-Component Organic Solar Cells Enabled by Adjusting the Conjugated-Length of Intermediate PBDB-T Block. Adv. Funct. Mater. *33*, 2208412. https://doi.org/10.1002/adfm.202208412.

63. Li, B., Kong, Y., Li, T., Li, H., Zhao, H., Cheng, P., and Yuan, J. (2024). Enhanced Intramolecular Hole Transfer in Block Copolymer Enables >15% and Operational Stable Single-Material–Organic Solar Cells. Adv. Mater. *36*, e2408988. https://doi.org/10.1002/adma.202408988.

64. Labrunie, A., Habibi, A.H., Dabos-Seignon, S., Blanchard, P., and Cabanetos, C. (2019). Exploration of the structure-property relationship of push-pull based dyads for single-molecule organic solar cells. Dyes Pigments *170*, 107632. https://doi.org/10.1016/j.dyepig.2019.107632.

65. Qu, J., Gao, B., Tian, H., Zhang, X., Wang, Y., Xie, Z., Wang, H., Geng, Y., and Wang, F. (2014). Donor–spacer–acceptor monodisperse conjugated co-oligomers for efficient single-molecule photovoltaic cells based on non-fullerene acceptors. J. Mater. Chem. A *2*, 3632–3640. https://doi.org/10.1039/C3TA14701K.

66. Nguyen, T.L., Lee, T.H., Gautam, B., Park, S.Y., Gundogdu, K., Kim, J.Y., and Woo, H.Y. (2017). Single Component Organic Solar Cells Based on Oligothiophene-Fullerene Conjugate. Adv. Funct. Mater. *27*, 1702474. https://doi.org/10.1002/adfm.201702474.

67. Lucas, S., Kammerer, J., Pfannmöller, M., Schröder, R.R., He, Y., Li, N., Brabec, C.J., Leydecker, T., Samorì, P., Marszalek, T., et al. (2021). Molecular Donor–Acceptor Dyads for Efficient Single-Material Organic Solar Cells. Sol. RRL *5*, 2000653. https://doi.org/10.1002/solr.202000653.

68. Wang, W., Sun, R., Guo, J., Guo, J., and Min, J. (2019). An Oligothiophene–Fullerene Molecule with a Balanced Donor–Acceptor Backbone for High-Performance Single-Component Organic Solar Cells. Angew. Chem. Int. Ed. *58*, 14556–14561. https://doi.org/10.1002/anie.201908232.

69. Mannanov, A.L., Savchenko, P.S., Luponosov, Y.N., Solodukhin, A.N., Ponomarenko, S.A., and Paraschuk, D.Yu. (2020). Charge photogeneration and recombination in single-material organic solar cells and photodetectors based on conjugated star-shaped donor-acceptor oligomers. Org. Electron. *78*, 105588. https://doi.org/10.1016/j.orgel.2019.105588.

70. Xia, D., Yang, F., Li, J., Li, C., and Li, W. (2019). Conjugated molecular dyads with diketopyrrolopyrrole-based conjugated backbones for single-component organic solar cells. Mater. Chem. Front. *3*, 1565–1573. https://doi.org/10.1039/C9QM00238C.

71. NERL. (2025). Best Research-Cell Efficiency Chart. Photovoltaic Research. https://www.nrel.gov/pv/cell-efficiency.html.

72. Nakayama, K.I., Okura, T., Okuda, Y., Matsui, J., Masuhara, A., Yoshida, T., White, M.S., Yumusak, C., Stadler, P., Scharber, M., et al. (2021). Single-Component Organic Solar Cells Based on Intramolecular Charge Transfer Photoabsorption. Materials (Basel) *14*, 1200. https://doi.org/10.3390/ma14051200.

73. Roncali, J. (2021). Single-Material Organic Solar Cells Based on Small Molecule Homojunctions: An Outdated Concept or a New Challenge for the Chemistry and Physics of Organic Photovoltaics? Adv. Energy Mater. *11*, 2102987. https://doi.org/10.1002/aenm.202102987.

74. Roncali, J. (2011). Single Material Solar Cells: the Next Frontier for Organic Photovoltaics? Adv. Energy Mater. *1*, 147–160. https://doi.org/10.1002/aenm.201000008.

75. Nam, M., Cha, M., Lee, H.H., Hur, K., Lee, K.-T., Yoo, J., Han, I.K., Kwon, S.J., and Ko, D.-H. (2017). Long-term efficient organic photovoltaics based on quaternary bulk heterojunctions. Nat. Commun. *8*, 14068. https://doi.org/10.1038/ncomms14068.

76. Aplan, M.P., Grieco, C., Lee, Y., Munro, J.M., Lee, W., Gray, J.L., Seibers, Z.D., Kuei, B., Litofsky, J.H., Kilbey, S.M., et al. (2019). Conjugated Block Copolymers as Model Systems to Examine Mechanisms of Charge Generation in Donor–Acceptor Materials. Adv. Funct. Mater. *29*, 1804858. https://doi.org/10.1002/adfm.201804858.

77. Chamberlain, G.A., Cooney, P.J., and Dennison, S. (1981). Photovoltaic properties of merocyanine solid-state photocells. Nature *289*, 45–47. https://doi.org/10.1038/289045a0.

78. Chamberlain, G.A., and Cooney, P.J. (1979). Photoelectric properties of aluminium/copper phthalocyanine/gold photovoltaic cells. Chem. Phys. Lett. *66*, 88–94. https://doi.org/10.1016/0009-2614(79)80374-7.

79. Kallmann, H., and Pope, M. (1959). Photovoltaic effect in organic crystals. J. Chem. Phys. *30*, 585–586. https://doi.org/10.1063/1.1729992.

80. Mok, J.W., Lin, Y.-H., Yager, K.G., Mohite, A.D., Nie, W., Darling, S.B., Lee, Y., Gomez, E., Gosztola, D., Schaller, R.D., et al. (2015). Linking Group Influences Charge Separation and Recombination in All-Conjugated Block Copolymer Photovoltaics. Adv. Funct. Mater. *25*, 5578–5585. https://doi.org/10.1002/adfm.201502623.

81. Yu, C., Xu, Y., Li, C., Feng, G., Yang, F., Li, J., and Li, W. (2018). An Isoindigo-Based "Double-Cable" Conjugated Polymer for Single- Component Polymer Solar Cells. Chin. J. Chem. *36*, 515–518. https://doi.org/10.1002/cjoc.201800009.

82. Johnson, K., Huang, Y.-S., Huettner, S., Sommer, M., Brinkmann, M., Mulherin, R., Niedzialek, D., Beljonne, D., Clark, J., Huck, W.T.S., et al. (2013). Control of Intrachain Charge Transfer in Model Systems for Block Copolymer Photovoltaic Materials. J. Am. Chem. Soc. *135*, 5074–5083. https://doi.org/10.1021/ja3121247.

83. Theunissen, D., Smeets, S., and Maes, W. (2023). Single-component organic solar cells—Perspective on the importance of chemical precision in conjugated block copolymers. Front. Chem. *11*, 1326131. https://doi.org/10.3389/fchem.2023.1326131.

84. Luo, Z., Xu, T., Zhang, C., and Yang, C. (2023). Side-chain engineering of nonfullerene small-molecule acceptors for organic solar cells. Energy Environ. Sci. *16*, 2732–2758. https://doi.org/10.1039/D3EE00908D.

85. Bai, Y., Zhang, Z., Zhou, Q., Geng, H., Chen, Q., Kim, S., Zhang, R., Zhang, C., Chang, B., Li, S., et al. (2023). Geometry design of tethered small-molecule acceptor enables highly stable and efficient polymer solar cells. Nat. Commun. *14*, 2926. https://doi.org/10.1038/s41467-023-38673-5.

86. Baran, D., Gasparini, N., Wadsworth, A., Tan, C.H., Wehbe, N., Song, X., Hamid, Z., Zhang, W., Neophytou, M., Kirchartz, T., et al. (2018). Robust nonfullerene solar cells approaching unity external quantum efficiency enabled by suppression of geminate recombination. Nat. Commun. *9*, 2059. https://doi.org/10.1038/s41467-018-04502-3.

87. Yao, J., Kirchartz, T., Vezie, M.S., Faist, M.A., Gong, W., He, Z., Wu, H., Troughton, J., Watson, T., Bryant, D., et al. (2015). Quantifying Losses in Open-Circuit Voltage in Solution-Processable Solar Cells. Phys. Rev. Appl. *4*, 014020. https://doi.org/10.1103/PhysRevApplied.4.014020.

88. Bartesaghi, D., Pérez, I.D.C., Kniepert, J., Roland, S., Turbiez, M., Neher, D., and Koster, L.J.A. (2015). Competition between recombination and extraction of free charges determines the fill factor of organic solar cells. Nat. Commun. *6*, 7083. https://doi.org/10.1038/ncomms8083.

89. Xiao, B., Calado, P., MacKenzie, R.C.I., Kirchartz, T., Yan, J., and Nelson, J. (2020). Relationship between Fill Factor and Light Intensity in Solar Cells Based on Organic Disordered Semiconductors: The Role of Tail States. Phys. Rev. Appl. *14*, 024034. https://doi.org/10.1103/PhysRevApplied.14.024034.

90. Li, B., Yang, X., Li, S., and Yuan, J. (2023). Stable block copolymer single-material organic solar cells: progress and perspective. Energy Environ. Sci. *16*, 723–744. https://doi.org/10.1039/D2EE03082A.

91. Nielsen, C.B., Holliday, S., Chen, H.-Y., Cryer, S.J., and McCulloch, I. (2015). Non-Fullerene Electron Acceptors for Use in Organic Solar Cells. Acc. Chem. Res. *48*, 2803–2812. https://doi.org/10.1021/acs.accounts.5b00199.

92. Li, S., Liu, W., Li, C.-Z., Liu, F., Zhang, Y., Shi, M., Chen, H., and Russell, T.P. (2016). A simple perylene diimide derivative with a highly twisted geometry as an electron acceptor for efficient organic solar cells. J. Mater. Chem. A *4*, 10659–10665. https://doi.org/10.1039/C6TA04232E.

93. Cao, J., and Yang, S. (2022). Progress in perylene diimides for organic solar cell applications. RSC Adv. *12*, 6966–6973. https://doi.org/10.1039/D1RA08484D.

94. Chen, Y., Zhang, X., Zhan, C., and Yao, J. (2015). In-depth understanding of photocurrent enhancement in solution-processed small-molecule: perylene diimide non-fullerene organic solar cells. Phys. Status Solidi A. *212*, 1961–1968. https://doi.org/10.1002/pssa.201532102.

95. Schaack, C., Evans, A.M., Ng, F., Steigerwald, M.L., and Nuckolls, C. (2022). High-Performance Organic Electronic Materials by Contorting Perylene Diimides. J. Am. Chem. Soc. *144*, 42–51. https://doi.org/10.1021/jacs.1c11544.

96. Liu, Z., Wu, Y., Zhang, Q., and Gao, X. (2016). Non-fullerene small molecule acceptors based on perylene diimides. J. Mater. Chem. A *4*, 17604–17622. https://doi.org/10.1039/C6TA06978A.

97. Park, G.E., Kim, H.J., Choi, S., Lee, D.H., Uddin, M.A., Woo, H.Y., Cho, M.J., and Choi, D.H. (2016). New M- and V-shaped perylene diimide small molecules for high-performance nonfullerene polymer solar cells. Chem. Commun. *52*, 8873–8876. https://doi.org/10.1039/C6CC04229E.

98. Zhang, G., Chen, X.-K., Xiao, J., Chow, P.C.Y., Ren, M., Kupgan, G., Jiao, X., Chan, C.C.S., Du, X., Xia, R., et al. (2020). Delocalization of exciton and electron wavefunction in non-fullerene acceptor molecules enables efficient organic solar cells. Nat. Commun. *11*, 3943. https://doi.org/10.1038/s41467-020-17867-1.

99. Shockley, W., and Queisser, H.J. (1961). Detailed Balance Limit of Efficiency of p-n Junction Solar Cells. J. Appl. Phys. *32*, 510–519. https://doi.org/10.1063/1.1736034.

100. Heumueller, T., Mateker, W.R., Sachs-Quintana, I.T., Vandewal, K., Bartelt, J.A., Burke, T.M., Ameri, T., Brabec, C.J., and McGehee, M.D. (2014). Reducing burn-in voltage loss in polymer solar cells by increasing the polymer crystallinity. Energy Environ. Sci. *7*, 2974–2980. https://doi.org/10.1039/C4EE01842G.

101. Fraga Domínguez, I., Distler, A., and Lüer, L. (2017). Stability of Organic Solar Cells: The Influence of Nanostructured Carbon Materials. Adv. Energy Mater. *7*, 1601320. https://doi.org/10.1002/aenm.201601320.

102. Panhans, M., Hutsch, S., Benduhn, J., Schellhammer, K.S., Nikolis, V.C., Vangerven, T., Vandewal, K., and Ortmann, F. (2020). Molecular vibrations reduce the maximum achievable photovoltage in organic solar cells. Nat. Commun. *11*, 1488. https://doi.org/10.1038/s41467-020-15215-x.

103. He, Y., Li, N., Heumüller, T., Wortmann, J., Hanisch, B., Aubele, A., Lucas, S., Feng, G., Jiang, X., Li, W., et al. (2022). Industrial viability of single-component organic solar cells. Joule *6*, 1160–1171. https://doi.org/10.1016/j.joule.2022.05.008.

104. Firdaus, Y., Le Corre, V.M., Karuthedath, S., Liu, W., Markina, A., Huang, W., Chattopadhyay, S., Nahid, M.M., Nugraha, M.I., Lin, Y., et al. (2020). Long-range exciton diffusion in molecular non-fullerene acceptors. Nat. Commun. *11*, 5220. https://doi.org/10.1038/s41467-020-19029-9.

105. Giannini, S., Peng, W.-T., Cupellini, L., Padula, D., Carof, A., and Blumberger, J. (2022). Exciton transport in molecular organic semiconductors boosted by transient quantum delocalization. Nat. Commun. *13*, 2755. https://doi.org/10.1038/s41467-022-30308-5.

106. Caruso, D., and Troisi, A. (2012). Long-range exciton dissociation in organic solar cells. Proc. Natl. Acad. Sci. USA *109*, 13498–13502. https://doi.org/10.1073/pnas.1206172109.

107. He, Y., Wang, B., Lüer, L., Feng, G., Osvet, A., Heumüller, T., Liu, C., Li, W., Guldi, D.M., Li, N., et al. (2022). Unraveling the Charge-Carrier Dynamics from the Femtosecond to the Microsecond Time Scale in Double-Cable Polymer-Based Single-Component Organic Solar Cells. Adv. Energy Mater. *12*, 2103406. https://doi.org/10.1002/aenm.202103406.

108. Huettner, S., Hodgkiss, J.M., Sommer, M., Friend, R.H., Steiner, U., and Thelakkat, M. (2012). Morphology-Dependent Charge Photogeneration in Donor–Acceptor Block Copolymer Films Based on Poly(3-hexylthiophene)-block-Poly(perylene bisimide acrylate). J. Phys. Chem. B *116*, 10070–10078. https://doi.org/10.1021/jp301966p.

109. Price, M.B., Hume, P.A., Ilina, A., Wagner, I., Tamming, R.R., Thorn, K.E., Jiao, W., Goldingay, A., Conaghan, P.J., Lakhwani, G., et al. (2022). Free charge photogeneration in a single component high photovoltaic efficiency organic semiconductor. Nat. Commun. *13*, 2827. https://doi.org/10.1038/s41467-022-30127-8.

110. Muntwiler, M., Yang, Q., Tisdale, W.A., and Zhu, X.Y. (2008). Coulomb Barrier for Charge Separation at an Organic Semiconductor Interface. Phys. Rev. Lett. *101*, 196403. https://doi.org/10.1103/PhysRevLett.101.196403.

111. Tamura, H., and Burghardt, I. (2013). Ultrafast Charge Separation in Organic Photovoltaics Enhanced by Charge Delocalization and Vibronically Hot Exciton Dissociation. J. Am. Chem. Soc. *135*, 16364–16367. https://doi.org/10.1021/ja4093874.

112. Hu, H., Mu, X., Li, B., Gui, R., Shi, R., Chen, T., Liu, J., Yuan, J., Ma, J., Gao, K., et al. (2023). Desirable Uniformity and Reproducibility of Electron Transport in Single-Component Organic Solar Cells. Adv. Sci. (Weinh) *10*, e2205040. https://doi.org/10.1002/advs.202205040.

113. Vandewal, K., Albrecht, S., Hoke, E.T., Graham, K.R., Widmer, J., Douglas, J.D., Schubert, M., Mateker, W.R., Bloking, J.T., Burkhard, G.F., et al. (2014). Efficient charge generation by relaxed charge-transfer states at organic interfaces. Nat. Mater. *13*, 63–68. https://doi.org/10.1038/nmat3807.

114. Nakano, K., Chen, Y., Xiao, B., Han, W., Huang, J., Yoshida, H., Zhou, E., and Tajima, K. (2019). Anatomy of the energetic driving force for charge generation in organic solar cells. Nat. Commun. *10*, 2520. https://doi.org/10.1038/s41467-019-10434-3.

115. Perdigón-Toro, L., Zhang, H., Markina, A., Yuan, J., Hosseini, S.M., Wolff, C.M., Zuo, G., Stolterfoht, M., Zou, Y., Gao, F., et al. (2020). Barrierless Free Charge Generation in the High-Performance PM6:Y6 Bulk Heterojunction Non-Fullerene Solar Cell. Adv. Mater. *32*, e1906763. https://doi.org/10.1002/adma.201906763.

116. Bernardo, B., Cheyns, D., Verreet, B., Schaller, R.D., Rand, B.P., and Giebink, N.C. (2014). Delocalization and dielectric screening of charge transfer states in organic photovoltaic cells. Nat. Commun. *5*, 3245. https://doi.org/10.1038/ncomms4245.

117. Hinrichsen, T.F., Chan, C.C.S., Ma, C., Paleček, D., Gillett, A., Chen, S., Zou, X., Zhang, G., Yip, H.-L., Wong, K.S., et al. (2020). Long-lived and disorder-free charge transfer states enable endothermic charge separation in efficient non-fullerene organic solar cells. Nat. Commun. *11*, 5617. https://doi.org/10.1038/s41467-020-19332-5.

118. Yan, J., Rezasoltani, E., Azzouzi, M., Eisner, F., and Nelson, J. (2021). Influence of static disorder of charge transfer state on voltage loss in organic photovoltaics. Nat. Commun. *12*, 3642. https://doi.org/10.1038/s41467-021-23975-3.

119. Liang, S., Jiang, X., Xiao, C., Li, C., Chen, Q., and Li, W. (2021). Double-Cable Conjugated Polymers with Pendant Rylene Diimides for Single-Component Organic Solar Cells. Acc. Chem. Res. *54*, 2227–2237. https://doi.org/10.1021/acs.accounts.1c00070.

120. Balzer, D., and Kassal, I. (2024). Delocalisation enables efficient charge generation in organic photovoltaics, even with little to no energetic offset. Chem. Sci. *15*, 4779–4789. https://doi.org/10.1039/D3SC05409H.

121. Gerhard, M., Arndt, A.P., Bilal, M., Lemmer, U., Koch, M., and Howard, I.A. (2017). Field-induced exciton dissociation in PTB7-based organic

solar cells. Phys. Rev., B *95*, 195301. https://doi.org/10.1103/PhysRevB.95.195301.

122. Petersen, A., Ojala, A., Kirchartz, T., Wagner, T.A., Würthner, F., and Rau, U. (2012). Field-dependent exciton dissociation in organic heterojunction solar cells. Phys. Rev., B *85*, 245208. https://doi.org/10.1103/PhysRevB.85.245208.

123. Mihailetchi, V.D., Koster, L.J., Hummelen, J.C., and Blom, P.W. (2004). Photocurrent Generation in Polymer-Fullerene Bulk Heterojunctions. Phys. Rev. Lett. *93*, 216601. https://doi.org/10.1103/PhysRevLett.93.216601.

124. Gélinas, S., Rao, A., Kumar, A., Smith, S.L., Chin, A.W., Clark, J., van der Poll, T.S., Bazan, G.C., and Friend, R.H. (2014). Ultrafast Long-Range Charge Separation in Organic Semiconductor Photovoltaic Diodes. Science *343*, 512–516. https://doi.org/10.1126/science.1246249.

125. Amarasinghe Vithanage, D.A., Devižis, A., Abramavičius, V., Infahsaeng, Y., Abramavičius, D., MacKenzie, R.C.I., Keivanidis, P.E., Yartsev, A., Hertel, D., Nelson, J., et al. (2013). Visualizing charge separation in bulk heterojunction organic solar cells. Nat. Commun. *4*, 2334. https://doi.org/10.1038/ncomms3334.

126. Etzold, F., Howard, I.A., Mauer, R., Meister, M., Kim, T.-D., Lee, K.-S., Baek, N.S., and Laquai, F. (2011). Ultrafast Exciton Dissociation Followed by Nongeminate Charge Recombination in PCDTBT:PCBM Photovoltaic Blends. J. Am. Chem. Soc. *133*, 9469–9479. https://doi.org/10.1021/ja201837e.

127. Kurpiers, J., Ferron, T., Roland, S., Jakoby, M., Thiede, T., Jaiser, F., Albrecht, S., Janietz, S., Collins, B.A., Howard, I.A., et al. (2018). Probing the pathways of free charge generation in organic bulk heterojunction solar cells. Nat. Commun. *9*, 2038. https://doi.org/10.1038/s41467-018-04386-3.

128. Sandberg, O.J., and Armin, A. (2024). Diode Equation for Sandwich-Type Thin-Film Photovoltaic Devices Limited by Bimolecular Recombination. PRX Energy *3*, 023008. https://doi.org/10.1103/PRXEnergy.3.023008.

129. Monahan, N.R., Williams, K.W., Kumar, B., Nuckolls, C., and Zhu, X.Y. (2015). Direct Observation of Entropy-Driven Electron-Hole Pair Separation at an Organic Semiconductor Interface. Phys. Rev. Lett. *114*, 247003. https://doi.org/10.1103/PhysRevLett.114.247003.

130. Li, T., Li, B., Zhou, H., Wang, J., Ni, G., Ma, W., Sheng, C., Yuan, J., and Zhao, H. (2024). Ultrafast Exciton Dissociation in Block Copolymer toward Efficient Single Material Organic Solar Cells. Adv. Funct. Mater. *34*, 2311798. https://doi.org/10.1002/adfm.202311798.

131. Amorim, D.R.B., Coutinho, D.J., Miranda, P.B., and Faria, R.M. (2020). Analytical Model for Photocurrent in Organic Solar Cells as a Function of the Charge-Transport Figure of Merit Including Second-Order Recombination. Phys. Rev. Appl. *14*, 034046. https://doi.org/10.1103/PhysRevApplied.14.034046.

132. Scheunemann, D., Wilken, S., Sandberg, O.J., Österbacka, R., and Schiek, M. (2019). Effect of Imbalanced Charge Transport on the Interplay of Surface and Bulk Recombination in Organic Solar Cells. Phys. Rev. Appl. *11*, 054090'. https://doi.org/10.1103/PhysRevApplied.11.054090.

133. Heiber, M.C., Baumbach, C., Dyakonov, V., and Deibel, C. (2015). Encounter-Limited Charge-Carrier Recombination in Phase-Separated Organic Semiconductor Blends. Phys. Rev. Lett. *114*, 136602. https://doi.org/10.1103/PhysRevLett.114.136602.

134. Deibel, C., Wagenpfahl, A., and Dyakonov, V. (2009). Origin of reduced polaron recombination in organic semiconductor devices. Phys. Rev., B *80*, 075203. https://doi.org/10.1103/PhysRevB.80.075203.

135. Bi, S., Ouyang, Z., Shaik, S., and Li, D. (2018). Effect of Donor-Acceptor Vertical Composition Profile on Performance of Organic Bulk Heterojunction Solar Cells. Sci. Rep. *8*, 9574. https://doi.org/10.1038/s41598-018-27868-2.

136. Tamai, Y., Murata, Y., Natsuda, S., and Sakamoto, Y. (2024). How to Interpret Transient Absorption Data?: An Overview of Case Studies for Application to Organic Solar Cells. Adv. Energy Mater. *14*, 2301890. https://doi.org/10.1002/aenm.202301890.

137. Proctor, C.M., Kuik, M., and Nguyen, T.-Q. (2013). Charge carrier recombination in organic solar cells. Prog. Polym. Sci. *38*, 1941–1960. https://doi.org/10.1016/j.progpolymsci.2013.08.008.

138. Kirchartz, T., Pieters, B.E., Kirkpatrick, J., Rau, U., and Nelson, J. (2011). Recombination via tail states in polythiophene:fullerene solar cells. Phys. Rev., B *83*, 115209. https://doi.org/10.1103/PhysRevB.83.115209.

139. Kubas, A. (2021). How the Donor/Acceptor Spin States Affect the Electronic Couplings in Molecular Charge-Transfer Processes? J. Chem. Theor. Comput. *17*, 2917–2927. https://doi.org/10.1021/acs.jctc.1c00126.

140. Brédas, J.-L., Beljonne, D., Coropceanu, V., and Cornil, J. (2004). Charge-Transfer and Energy-Transfer Processes in π-Conjugated Oligomers and Polymers: A Molecular Picture. Chem. Rev. *104*, 4971–5004. https://doi.org/10.1021/cr040084k.

141. Giannini, S., Sowood, D.J.C., Cerdá, J., Frederix, S., Grüne, J., Londi, G., Marsh, T., Ghosh, P., Duchemin, I., Greenham, N.C., et al. (2024). On the role of charge transfer excitations in non-fullerene acceptors for organic photovoltaics. Mater. Today *80*, 308–326. https://doi.org/10.1016/j.mattod.2024.09.009.

142. Lakhwani, G., Rao, A., and Friend, R.H. (2014). Bimolecular Recombination in Organic Photovoltaics. Annu. Rev. Phys. Chem. *65*, 557–581. https://doi.org/10.1146/annurev-physchem-040513-103615.

143. Göhler, C., Wagenpfahl, A., and Deibel, C. (2018). Nongeminate Recombination in Organic Solar Cells. Adv. Electron. Mater. *4*, 1700505. https://doi.org/10.1002/aelm.201700505.

144. Würfel, U., Perdigón-Toro, L., Kurpiers, J., Wolff, C.M., Caprioglio, P., Rech, J.J., Zhu, J., Zhan, X., You, W., Shoaee, S., et al. (2019). Recombination between Photogenerated and Electrode-Induced Charges Dominates the Fill Factor Losses in Optimized Organic Solar Cells. J. Phys. Chem. Lett. *10*, 3473–3480. https://doi.org/10.1021/acs.jpclett.9b01175.

145. Huynh, W.U., Dittmer, J.J., Teclemariam, N., Milliron, D.J., Alivisatos, A.P., and Barnham, K.W.J. (2003). Charge transport in hybrid nanorod-polymer composite photovoltaic cells. Phys. Rev., B *67*, 115326. https://doi.org/10.1103/PhysRevB.67.115326.

146. Liu, L., Stanchina, W.E., and Li, G. (2009). Effects of semiconducting and metallic single-walled carbon nanotubes on performance of bulk heterojunction organic solar cells. Appl. Phys. Lett. *94*, 233309. https://doi.org/10.1063/1.3153514.

147. Deibel, C., and Wagenpfahl, A. (2010). Comment on "Interface state recombination in organic solar cells.". Phys. Rev., B *82*, 207301. https://doi.org/10.1103/PhysRevB.82.207301.

148. Hartnagel, P., and Kirchartz, T. (2020). Understanding the Light-Intensity Dependence of the Short-Circuit Current of Organic Solar Cells. Adv. Theor. Simul. *3*, 2000116. https://doi.org/10.1002/adts.202000116.

149. Rau, U. (2007). Reciprocity relation between photovoltaic quantum efficiency and electroluminescent emission of solar cells. Phys. Rev. B *76*, 085303. https://doi.org/10.1103/PhysRevB.76.085303.

150. Khan, S.-U.-Z., Bertrandie, J., Gui, M., Sharma, A., Alsufyani, W., Gorenflot, J.F., Laquai, F., Baran, D., and Rand, B.P. (2022). Quantifying the effect of energetic disorder on organic solar cell energy loss. Joule *6*, 2821–2834. https://doi.org/10.1016/j.joule.2022.10.012.

151. Benduhn, J., Tvingstedt, K., Piersimoni, F., Ullbrich, S., Fan, Y., Tropiano, M., McGarry, K.A., Zeika, O., Riede, M.K., Douglas, C.J., et al. (2017). Intrinsic non-radiative voltage losses in fullerene-based organic solar cells. Nat. Energy *2*, 1–6. https://doi.org/10.1038/nenergy.2017.53.

152. Azzouzi, M., Yan, J., Kirchartz, T., Liu, K., Wang, J., Wu, H., and Nelson, J. (2018). Nonradiative Energy Losses in Bulk-Heterojunction Organic Photovoltaics. Phys. Rev. X *8*, 031055. https://doi.org/10.1103/PhysRevX.8.031055.

153. Gillett, A.J., Privitera, A., Dilmurat, R., Karki, A., Qian, D., Pershin, A., Londi, G., Myers, W.K., Lee, J., Yuan, J., et al. (2021). The role of charge recombination to triplet excitons in organic solar cells. Nature *597*, 666–671. https://doi.org/10.1038/s41586-021-03840-5.

154. Liu, J., Chen, S., Qian, D., Gautam, B., Yang, G., Zhao, J., Bergqvist, J., Zhang, F., Ma, W., Ade, H., et al. (2016). Fast charge separation in a non-fullerene organic solar cell with a small driving force. Nat. Energy *1*, 1–7. https://doi.org/10.1038/nenergy.2016.89.

155. Li, W., Hendriks, K.H., Furlan, A., Wienk, M.M., and Janssen, R.A.J. (2015). High Quantum Efficiencies in Polymer Solar Cells at Energy Losses below 0.6 eV. J. Am. Chem. Soc. *137*, 2231–2234. https://doi.org/10.1021/ja5131897.

156. Eisner, F.D., Azzouzi, M., Fei, Z., Hou, X., Anthopoulos, T.D., Dennis, T.J.S., Heeney, M., and Nelson, J. (2019). Hybridization of Local Exciton and Charge-Transfer States Reduces Nonradiative Voltage Losses in Organic Solar Cells. J. Am. Chem. Soc. *141*, 6362–6374. https://doi.org/10.1021/jacs.9b01465.

157. Chen, X.-K., Coropceanu, V., and Brédas, J.-L. (2018). Assessing the nature of the charge-transfer electronic states in organic solar cells. Nat. Commun. *9*, 5295. https://doi.org/10.1038/s41467-018-07707-8.

158. Classen, A., Chochos, C.L., Lüer, L., Gregoriou, V.G., Wortmann, J., Osvet, A., Forberich, K., McCulloch, I., Heumüller, T., and Brabec, C.J. (2020). The role of exciton lifetime for charge generation in organic solar cells at negligible energy-level offsets. Nat. Energy *5*, 711–719. https://doi.org/10.1038/s41560-020-00684-7.

159. Röhr, J.A., Shi, X., Haque, S.A., Kirchartz, T., and Nelson, J. (2018). Charge Transport in Spiro-OMeTAD Investigated through Space-Charge-Limited Current Measurements. Phys. Rev. Appl. *9*, 044017. https://doi.org/10.1103/PhysRevApplied.9.044017.

160. Bristow, H., Thorley, K.J., White, A.J.P., Wadsworth, A., Babics, M., Hamid, Z., Zhang, W., Paterson, A.F., Kosco, J., Panidi, J., et al. (2019). Impact of Nonfullerene Acceptor Side Chain Variation on Transistor Mobility. Adv. Electron. Mater. *5*, 1900344. https://doi.org/10.1002/aelm.201900344.

161. Shi, X., Nádaždy, V., Perevedentsev, A., Frost, J.M., Wang, X., von Hauff, E., MacKenzie, R.C.I., and Nelson, J. (2019). Relating Chain Conformation to the Density of States and Charge Transport in Conjugated Polymers: The Role of the $\ensuremath{\beta}$-phase in Poly(9,9-dioctylfluorene). Phys. Rev. X *9*, 021038. https://doi.org/10.1103/PhysRevX.9.021038.

162. Röhr, J.A., Moia, D., Haque, S.A., Kirchartz, T., and Nelson, J. (2018). Exploring the validity and limitations of the Mott–Gurney law for charge-carrier mobility determination of semiconducting thin-films. J. Phys. Condens. Matter *30*, 105901. https://doi.org/10.1088/1361-648X/aaabad.

163. Stojanović, L., Coker, J., Giannini, S., Londi, G., Gertsen, A.S., Wenzel Andreasen, J., Yan, J., D'Avino, G., Beljonne, D., Nelson, J., et al. (2024). Disorder-Induced Transition from Transient Quantum Delocalization to Charge Carrier Hopping Conduction in a Nonfullerene Acceptor Material. Phys. Rev. X *14*, 021021. https://doi.org/10.1103/PhysRevX.14.021021.

164. Felekidis, N., Melianas, A., and Kemerink, M. (2018). Automated open-source software for charge transport analysis in single-carrier organic semiconductor diodes. Org. Electron. *61*, 318–328. https://doi.org/10.1016/j.orgel.2018.06.010.

165. Zhao, A., Le Corre, V.M., and Röhr, J.A. (2024). On the importance of varying device thickness and temperature on the outcome of space-charge-limited current measurements. Front. Electron. Mater. *4*, 1396521. https://doi.org/10.3389/femat.2024.1396521.

166. Sivula, K. (2022). Improving Charge Carrier Mobility Estimations When Using Space-Charge-Limited Current Measurements. ACS Energy Lett. *7*, 2102–2104. https://doi.org/10.1021/acsenergylett.2c01154.

167. Giannini, S., and Blumberger, J. (2022). Charge Transport in Organic Semiconductors: The Perspective from Nonadiabatic Molecular Dynamics. Acc. Chem. Res. *55*, 819–830. https://doi.org/10.1021/acs.accounts.1c00675.

168. Li, W., Ren, J., and Shuai, Z. (2021). A general charge transport picture for organic semiconductors with nonlocal electron-phonon couplings. Nat. Commun. *12*, 4260. https://doi.org/10.1038/s41467-021-24520-y.

169. Giannini, S., Di Virgilio, L., Bardini, M., Hausch, J., Geuchies, J.J., Zheng, W., Volpi, M., Elsner, J., Broch, K., Geerts, Y.H., et al. (2023). Transiently delocalized states enhance hole mobility in organic molecular semiconductors. Nat. Mater. *22*, 1361–1369. https://doi.org/10.1038/s41563-023-01664-4.

170. Wang, J., Jiang, X., Wu, H., Feng, G., Wu, H., Li, J., Yi, Y., Feng, X., Ma, Z., Li, W., et al. (2021). Increasing donor-acceptor spacing for reduced voltage loss in organic solar cells. Nat. Commun. *12*, 6679. https://doi.org/10.1038/s41467-021-26995-1.

171. Hu, Y., Cao, X., and Fan, H. (2022). Crystallization of D-A Conjugated Polymers: A Review of Recent Research. Polymers *14*, 4612. https://doi.org/10.3390/polym14214612.

172. Mei, J., and Bao, Z. (2014). Side Chain Engineering in Solution-Processable Conjugated Polymers. Chem. Mater. *26*, 604–615. https://doi.org/10.1021/cm4020805.

173. Sandberg, O.J., and Österbacka, R. (2025). Towards optimal morphology in organic solar cells? Natl. Sci. Rev. *13*, nwaf563. https://doi.org/10.1093/nsr/nwaf563.

174. Jiao, X., Ye, L., and Ade, H. (2017). Quantitative Morphology–Performance Correlations in Organic Solar Cells: Insights from Soft X-Ray Scattering. Adv. Energy Mater. *7*, 1700084. https://doi.org/10.1002/aenm.201700084.

175. Liao, H.-C., Ho, C.-C., Chang, C.-Y., Jao, M.-H., Darling, S.B., and Su, W.-F. (2013). Additives for morphology control in high-efficiency organic solar cells. Mater. Today *16*, 326–336. https://doi.org/10.1016/j.mattod.2013.08.013.

176. Topham, P.D., Parnell, A.J., and Hiorns, R.C. (2011). Block copolymer strategies for solar cell technology. J. Polym. Sci. B Polym. Phys. *49*, 1131–1156. https://doi.org/10.1002/polb.22302.

177. Vanderspikken, J., Liu, Z., Wu, X., Beckers, O., Moro, S., Quill, T.J., Liu, Q., Goossens, A., Marks, A., Weaver, K., et al. (2023). On the Importance of Chemical Precision in Organic Electronics: Fullerene Intercalation in Perfectly Alternating Conjugated Polymers. Adv. Funct. Mater. *33*, 2309403. https://doi.org/10.1002/adfm.202309403.

178. Moore, G.J., Günther, F., Yallum, K.M., Causa', M., Jungbluth, A., Réhault, J., Riede, M., Ortmann, F., and Banerji, N. (2024). Direct visualization of the charge transfer state dynamics in dilute-donor organic photovoltaic blends. Nat. Commun. *15*, 9851. https://doi.org/10.1038/s41467-024-53694-4.

179. Maimaris, M., Pettipher, A.J., Azzouzi, M., Walke, D.J., Zheng, X., Gorodetsky, A., Dong, Y., Tuladhar, P.S., Crespo, H., Nelson, J., et al. (2022). Sub-10-fs observation of bound exciton formation in organic optoelectronic devices. Nat. Commun. *13*, 4949. https://doi.org/10.1038/s41467-022-32478-8.

180. Bakulin, A.A., Rao, A., Pavelyev, V.G., van Loosdrecht, P.H.M., Pshenichnikov, M.S., Niedzialek, D., Cornil, J., Beljonne, D., and Friend, R.H. (2012). The Role of Driving Energy and Delocalized States for Charge Separation in Organic Semiconductors. Science *335*, 1340–1344. https://doi.org/10.1126/science.1217745.

181. Urbain, F., Smirnov, V., Becker, J.-P., Lambertz, A., Yang, F., Ziegler, J., Kaiser, B., Jaegermann, W., Rau, U., and Finger, F. (2016). Measuring the Competition between Bimolecular Charge Recombination and Charge Transport in Organic Solar Cells under Operating Conditions. Energy Environ. Sci. *9*, 145–154. https://doi.org/10.1039/C5EE02393A.

182. Röhr, J.A. (2018) Measurements and Modelling of Space-Charge-Limited Current Transport in Organic Single-Carrier Devices. https://doi.org/10.13140/RG.2.2.14011.46883.

183. Kirchartz, T. (2013). Influence of diffusion on space-charge-limited current measurements in organic semiconductors. Beilstein J. Nanotechnol. *4*, 180–188. https://doi.org/10.3762/bjnano.4.18.

184. Wöpke, C., Göhler, C., Saladina, M., Du, X., Nian, L., Greve, C., Zhu, C., Yallum, K.M., Hofstetter, Y.J., Becker-Koch, D., et al. (2022). Traps and transport resistance are the next frontiers for stable non-fullerene acceptor solar cells. Nat. Commun. *13*, 3786. https://doi.org/10.1038/s41467-022-31326-z.

185. Azzouzi, M., Calado, P., Telford, A.M., Eisner, F., Hou, X., Kirchartz, T., Barnes, P.R.F., and Nelson, J. (2020). Overcoming the Limitations of Transient Photovoltage Measurements for Studying Recombination in Organic Solar Cells. Sol. RRL *4*, 1900581. https://doi.org/10.1002/solr.201900581.

186. Wood, S., Blakesley, J.C., and Castro, F.A. (2018). Assessing the Validity of Transient Photovoltage Measurements and Analysis for Organic Solar Cells. Phys. Rev. Appl. *10*, 024038. https://doi.org/10.1103/PhysRevApplied.10.024038.

187. Burke, T.M., Sweetnam, S., Vandewal, K., and McGehee, M.D. (2015). Beyond Langevin Recombination: How Equilibrium Between Free Carriers and Charge Transfer States Determines the Open-Circuit Voltage of Organic Solar Cells. Adv. Energy Mater. *5*, 1500123. https://doi.org/10.1002/aenm.201500123.

188. Karki, A., Vollbrecht, J., Gillett, A.J., Selter, P., Lee, J., Peng, Z., Schopp, N., Dixon, A.L., Schrock, M., Nádaždy, V., et al. (2020). Unifying Charge Generation, Recombination, and Extraction in Low-Offset Non-Fullerene Acceptor Organic Solar Cells. Adv. Energy Mater. *10*, 2001203. https://doi.org/10.1002/aenm.202001203.

189. Zhang, B., An, N., Wu, H., Geng, Y., Sun, Y., Ma, Z., Li, W., Guo, Q., and Zhou, E. (2020). The first application of isoindigo-based polymers in non-fullerene organic solar cells. Sci. China Chem. *63*, 1262–1271. https://doi.org/10.1007/s11426-020-9777-1.

190. Li, T., Wu, Y., Zhou, J., Li, M., Wu, J., Hu, Q., Jia, B., Pan, X., Zhang, M., Tang, Z., et al. (2020). Butterfly Effects Arising from Starting Materials in Fused-Ring Electron Acceptors. J. Am. Chem. Soc. *142*, 20124–20133. https://doi.org/10.1021/jacs.0c09800.

191. Chen, S., Wang, Y., Zhang, L., Zhao, J., Chen, Y., Zhu, D., Yao, H., Zhang, G., Ma, W., Friend, R.H., et al. (2018). Efficient Nonfullerene Organic Solar Cells with Small Driving Forces for Both Hole and Electron Transfer. Adv. Mater. *30*, e1804215. https://doi.org/10.1002/adma.201804215.

192. Sun, R., Guo, J., Wu, Q., Zhang, Z., Yang, W., Guo, J., Shi, M., Zhang, Y., Kahmann, S., Ye, L., et al. (2019). A multi-objective optimization-based layer-by-layer blade-coating approach for organic solar cells: rational control of vertical stratification for high performance. Energy Environ. Sci. *12*, 3118–3132. https://doi.org/10.1039/C9EE02295C.

193. Qin, Y., Zhang, S., Xu, Y., Ye, L., Wu, Y., Kong, J., Xu, B., Yao, H., Ade, H., and Hou, J. (2019). Reduced Nonradiative Energy Loss Caused by Aggregation of Nonfullerene Acceptor in Organic Solar Cells. Adv. Energy Mater. *9*, 1901823. https://doi.org/10.1002/aenm.201901823.

194. Wang, Y., Wang, X., Lin, B., Bi, Z., Zhou, X., Naveed, H.B., Zhou, K., Yan, H., Tang, Z., and Ma, W. (2020). Achieving Balanced Crystallization Kinetics of Donor and Acceptor by Sequential-Blade Coated Double Bulk Heterojunction Organic Solar Cells. Adv. Energy Mater. *10*, 2000826. https://doi.org/10.1002/aenm.202000826.

195. Luo, Z., Liu, T., Wang, Y., Zhang, G., Sun, R., Chen, Z., Zhong, C., Wu, J., Chen, Y., Zhang, M., et al. (2019). Reduced Energy Loss Enabled by a Chlorinated Thiophene-Fused Ending-Group Small Molecular Acceptor for Efficient Nonfullerene Organic Solar Cells with 13.6% Efficiency. Adv. Energy Mater. *9*, 1900041. https://doi.org/10.1002/aenm.201900041.

196. Song, X., Gasparini, N., Ye, L., Yao, H., Hou, J., Ade, H., and Baran, D. (2018). Controlling Blend Morphology for Ultrahigh Current Density in Nonfullerene Acceptor-Based Organic Solar Cells. ACS Energy Lett. *3*, 669–676. https://doi.org/10.1021/acsenergylett.7b01266.

197. Fan, B., Du, X., Liu, F., Zhong, W., Ying, L., Xie, R., Tang, X., An, K., Xin, J., Li, N., et al. (2018). Fine-tuning of the chemical structure of photoactive materials for highly efficient organic photovoltaics. Nat. Energy *3*, 1051–1058. https://doi.org/10.1038/s41560-018-0263-4.

198. Zhao, W., Li, S., Yao, H., Zhang, S., Zhang, Y., Yang, B., and Hou, J. (2017). Molecular Optimization Enables over 13% Efficiency in Organic Solar Cells. J. Am. Chem. Soc. *139*, 7148–7151. https://doi.org/10.1021/jacs.7b02677.

199. Fei, Z., Eisner, F.D., Jiao, X., Azzouzi, M., Röhr, J.A., Han, Y., Shahid, M., Chesman, A.S.R., Easton, C.D., McNeill, C.R., et al. (2018). An Alkylated Indacenodithieno[3,2-b]thiophene-Based Nonfullerene Acceptor with High Crystallinity Exhibiting Single Junction Solar Cell Efficiencies Greater than 13% with Low Voltage Losses. Adv. Mater. *30*, 1705209. https://doi.org/10.1002/adma.201705209.

200. Huang, H., Guo, Q., Feng, S., Zhang, C., Bi, Z., Xue, W., Yang, J., Song, J., Li, C., Xu, X., et al. (2019). Noncovalently fused-ring electron acceptors with near-infrared absorption for high-performance organic solar cells. Nat. Commun. *10*, 3038. https://doi.org/10.1038/s41467-019-11001-6.

201. Yuan, J., Huang, T., Cheng, P., Zou, Y., Zhang, H., Yang, J.L., Chang, S.-Y., Zhang, Z., Huang, W., Wang, R., et al. (2019). Enabling low voltage losses and high photocurrent in fullerene-free organic photovoltaics. Nat. Commun. *10*, 570. https://doi.org/10.1038/s41467-019-08386-9.

202. Chen, H., Hu, D., Yang, Q., Gao, J., Fu, J., Yang, K., He, H., Chen, S., Kan, Z., Duan, T., et al. (2019). All-Small-Molecule Organic Solar Cells with an Ordered Liquid Crystalline Donor. Joule *3*, 3034–3047. https://doi.org/10.1016/j.joule.2019.09.009.

203. He, C., Li, Y., Liu, Y., Li, Y., Zhou, G., Li, S., Zhu, H., Lu, X., Zhang, F., Li, C.-Z., et al. (2020). Near infrared electron acceptors with a photoresponse beyond 1000 nm for highly efficient organic solar cells. J. Mater. Chem. A *8*, 18154–18161. https://doi.org/10.1039/D0TA06907H.

204. Li, X., Weng, K., Ryu, H.S., Guo, J., Zhang, X., Xia, T., Fu, H., Wei, D., Min, J., Zhang, Y., et al. (2020). Non-Fullerene Organic Solar Cells Based on Benzo[1,2-b:4,5-b′]difuran-Conjugated Polymer with 14% Efficiency. Adv. Funct. Mater. *30*, 1906809. https://doi.org/10.1002/adfm.201906809.

205. Qin, L., Liu, X., Zhang, X., Yu, J., Yang, L., Zhao, F., Huang, M., Wang, K., Wu, X., Li, Y., et al. (2020). Triplet Acceptors with a D-A Structure and Twisted Conformation for Efficient Organic Solar Cells. Angew. Chem. Int. Ed. *59*, 15043–15049. https://doi.org/10.1002/anie.202006081.

206. Wang, T., Sun, R., Wang, W., Li, H., Wu, Y., and Min, J. (2021). Highly Efficient and Stable All-Polymer Solar Cells Enabled by Near-Infrared Isomerized Polymer Acceptors. Chem. Mater. *33*, 761–773. https://doi.org/10.1021/acs.chemmater.0c04253.

207. Zhou, R., Jiang, Z., Yang, C., Yu, J., Feng, J., Adil, M.A., Deng, D., Zou, W., Zhang, J., Lu, K., et al. (2019). All-small-molecule organic solar cells with over 14% efficiency by optimizing hierarchical morphologies. Nat. Commun. *10*, 5393. https://doi.org/10.1038/s41467-019-13292-1.

208. He, C., Chen, Z., Wang, T., Shen, Z., Li, Y., Zhou, J., Yu, J., Fang, H., Li, Y., Li, S., et al. (2022). Asymmetric electron acceptor enables highly luminescent organic solar cells with certified efficiency over 18%. Nat. Commun. *13*, 2598. https://doi.org/10.1038/s41467-022-30225-7.

209. Gao, W., Fu, H., Li, Y., Lin, F., Sun, R., Wu, Z., Wu, X., Zhong, C., Min, J., Luo, J., et al. (2021). Asymmetric Acceptors Enabling Organic Solar Cells to Achieve an over 17% Efficiency: Conformation Effects on Regulating Molecular Properties and Suppressing Nonradiative Energy Loss. Adv. Energy Mater. *11*, 2003177. https://doi.org/10.1002/aenm.202003177.

210. Li, S., Zhan, L., Jin, Y., Zhou, G., Lau, T.-K., Qin, R., Shi, M., Li, C.-Z., Zhu, H., Lu, X., et al. (2020). Asymmetric Electron Acceptors for High-Efficiency and Low-Energy-Loss Organic Photovoltaics. Adv. Mater. *32*, e2001160. https://doi.org/10.1002/adma.202001160.

211. Wu, J., Fan, Q., Xiong, M., Wang, Q., Chen, K., Liu, H., Gao, M., Ye, L., Guo, X., Fang, J., et al. (2021). Carboxylate substituted pyrazine: A simple and low-cost building block for novel wide bandgap polymer donor enables 15.3% efficiency in organic solar cells. Nano Energy *82*, 105679. https://doi.org/10.1016/j.nanoen.2020.105679.

212. Sun, H., Liu, T., Yu, J., Lau, T.-K., Zhang, G., Zhang, Y., Su, M., Tang, Y., Ma, R., Liu, B., et al. (2019). A monothiophene unit incorporating both fluoro and ester substitution enabling high-performance donor polymers for non-fullerene solar cells with 16.4% efficiency. Energy Environ. Sci. *12*, 3328–3337. https://doi.org/10.1039/C9EE01890E.

213. Cui, Y., Yao, H., Zhang, J., Zhang, T., Wang, Y., Hong, L., Xian, K., Xu, B., Zhang, S., Peng, J., et al. (2019). Over 16% efficiency organic photovoltaic cells enabled by a chlorinated acceptor with increased open-circuit voltages. Nat. Commun. *10*, 2515. https://doi.org/10.1038/s41467-019-10351-5.

214. Sun, C., Pan, F., Chen, S., Wang, R., Sun, R., Shang, Z., Qiu, B., Min, J., Lv, M., Meng, L., et al. (2019). Achieving Fast Charge Separation and Low Nonradiative Recombination Loss by Rational Fluorination for High-Efficiency Polymer Solar Cells. Adv. Mater. *31*, e1905480. https://doi.org/10.1002/adma.201905480.

215. Hong, L., Yao, H., Wu, Z., Cui, Y., Zhang, T., Xu, Y., Yu, R., Liao, Q., Gao, B., Xian, K., et al. (2019). Eco-Compatible Solvent-Processed Organic Photovoltaic Cells with Over 16% Efficiency. Adv. Mater. *31*, e1903441. https://doi.org/10.1002/adma.201903441.

216. Zhang, G., Ning, H., Chen, H., Jiang, Q., Jiang, J., Han, P., Dang, L., Xu, M., Shao, M., He, F., et al. (2021). Naphthalenothiophene imide-based polymer exhibiting over 17% efficiency. Joule *5*, 931–944. https://doi.org/10.1016/j.joule.2021.02.003.

217. Qi, F., Jiang, K., Lin, F., Wu, Z., Zhang, H., Gao, W., Li, Y., Cai, Z., Woo, H.Y., Zhu, Z., et al. (2021). Over 17% Efficiency Binary Organic Solar Cells with Photoresponses Reaching 1000 nm Enabled by Selenophene-Fused Nonfullerene Acceptors. ACS Energy Lett. *6*, 9–15. https://doi.org/10.1021/acsenergylett.0c02230.

218. Chang, Y., Zhang, J., Chen, Y., Chai, G., Xu, X., Yu, L., Ma, R., Yu, H., Liu, T., Liu, P., et al. (2021). Achieving Efficient Ternary Organic Solar Cells Using Structurally Similar Non-Fullerene Acceptors with Varying Flanking Side Chains. Adv. Energy Mater. *11*, 2100079. https://doi.org/10.1002/aenm.202100079.

219. Abbas, Z., Ryu, S.U., Haris, M., Song, C.E., Lee, H.K., Lee, S.K., Shin, W.S., Park, T., and Lee, J.-C. (2022). Optimized vertical phase separation via systematic Y6 inner side-chain modulation for non-halogen solvent processed inverted organic solar cells. Nano Energy *101*, 107574. https://doi.org/10.1016/j.nanoen.2022.107574.

220. Ma, X., Wang, J., Gao, J., Hu, Z., Xu, C., Zhang, X., and Zhang, F. (2020). Achieving 17.4% Efficiency of Ternary Organic Photovoltaics with Two Well-Compatible Nonfullerene Acceptors for Minimizing Energy Loss. Adv. Energy Mater. *10*, 2001404. https://doi.org/10.1002/aenm.202001404.

221. Chai, G., Chang, Y., Zhang, J., Xu, X., Yu, L., Zou, X., Li, X., Chen, Y., Luo, S., Liu, B., et al. (2021). Fine-tuning of side-chain orientations on nonfullerene acceptors enables organic solar cells with 17.7% efficiency. Energy Environ. Sci. *14*, 3469–3479. https://doi.org/10.1039/D0EE03506H.

222. Li, C., Zhou, J., Song, J., Xu, J., Zhang, H., Zhang, X., Guo, J., Zhu, L., Wei, D., Han, G., et al. (2021). Non-fullerene acceptors with branched side chains and improved molecular packing to exceed 18% efficiency in organic solar cells. Nat. Energy *6*, 605–613. https://doi.org/10.1038/s41560-021-00820-x.

223. Zhu, L., Zhang, M., Xu, J., Li, C., Yan, J., Zhou, G., Zhong, W., Hao, T., Song, J., Xue, X., et al. (2022). Single-junction organic solar cells with over 19% efficiency enabled by a refined double-fibril network morphology. Nat. Mater. *21*, 656–663. https://doi.org/10.1038/s41563-022-01244-y.

224. Wang, J., Wang, Y., Bi, P., Chen, Z., Qiao, J., Li, J., Wang, W., Zheng, Z., Zhang, S., Hao, X., et al. (2023). Binary Organic Solar Cells with 19.2% Efficiency Enabled by Solid Additive. Adv. Mater. *35*, e2301583. https://doi.org/10.1002/adma.202301583.

225. Yu, X., Ding, P., Yang, D., Yan, P., Wang, H., Yang, S., Wu, J., Wang, Z., Sun, H., Chen, Z., et al. (2024). Self-Assembled Molecules with Asymmetric Backbone for Highly Stable Binary Organic Solar Cells with 19.7 % Efficiency. Angew. Chem. Int. Ed. *63*, e202401518. https://doi.org/10.1002/anie.202401518.

226. Guan, S., Li, Y., Xu, C., Yin, N., Xu, C., Wang, C., Wang, M., Xu, Y., Chen, Q., Wang, D., et al. (2024). Self-Assembled Interlayer Enables High-Performance Organic Photovoltaics with Power Conversion Efficiency Exceeding 20%. Adv. Mater. *36*, e2400342. https://doi.org/10.1002/adma.202400342.

227. Sun, Y., Wang, L., Guo, C., Xiao, J., Liu, C., Chen, C., Xia, W., Gan, Z., Cheng, J., Zhou, J., et al. (2024). π-Extended Nonfullerene Acceptor for Compressed Molecular Packing in Organic Solar Cells To Achieve over 20% Efficiency. J. Am. Chem. Soc. *146*, 12011–12019. https://doi.org/10.1021/jacs.4c01503.